Title
Homeostasis in the Unfolded Protein Response

Author
Pincus, David

Publication Date
2012

Peer reviewed|Thesis/dissertation

Homeostasis in the Unfolded Protein Response

by

David Pincus

DISSERTATION

Submitted in partial satisfaction of the requirements for the degree of

DOCTOR OF PHILOSOPHY

in

CELL BIOLOGY

in the

GRADUATE DIVISION

of the

UNIVERSITY OF CALIFORNIA, SAN FRANCISCO

I dedicate this thesis to my parents,

Morton and Mary Pincus

ACKNOWLEDGEMENTS

Many colleagues contributed significantly to my graduate education and maturation as a scientist. I want to thank them here.

I am grateful to my advisor Peter Walter for providing a nurturing lab that allowed me to grow and develop intellectually and technically, for showing me how to distill a story from data, for teaching me how to write, for removing obstacles from my path to discovery, for personifying the collaboration and excitement that makes UCSF what it is and – perhaps most significantly – for introducing me to Hana.

I am grateful to my advisor Hana El-Samad for her boundless time and energy, for her perfect blend of excitement and skepticism, for fostering an environment where quantitative precision and theoretical rigor are paramount, for teaching me to appreciate the breadth of interesting questions without sacrificing the depth of mechanistic understanding and for showing me how to build a lab from the ground up.

I am grateful to both Peter and Hana for their confidence in me, their constant support and encouragement and their advocacy on my behalf which has allowed me to flourish here at UCSF and has given me the opportunity to move directly to begin my own research group.

I am grateful to Wendell Lim for his support throughout graduate school, for teaching me what it takes to get a paper published and for his support and advocacy that helped get me my next position.

I am grateful to Christine Guthrie and Carol Gross for their encouragement, warmth and delight in my accomplishments. I am especially grateful to Christine for including me in her lab celebrations and for her letters of support.

I am grateful to Marc Shuman for his scientific perspective, his insights, his skepticism of systems biology and his warmth.

I am grateful to Jacob Stewart-Ornstein for co-founding the experimental wing of the El-Samad lab, for his inspiring diligence, and for the countless scientific discussions we have had and the myriad suggestions he has made that invaluably contributed to my work.

I am grateful to Brooke Gardner for cohabitating the Walter lab with me throughout graduate school, for her balance of thoughtfulness and tenacity, and for her consistent manifestation of what a good scientist looks like.

I am grateful to Michael Chevalier for his devotion to first principles, his fearless embrace of biology and for congealing our notions of how the UPR works into a mathematical formalism.

I am grateful to Claudia Rubio for teaching me how wonderful and productive a good collaboration can be.

I am grateful to Polly Fordyce for including me in her exciting work and reaffirming how synergistic *in vitro* and *in vivo* approaches can be.

I am grateful to Simon Vidal and Andres Aranda for their technical support, for allowing me to participate in their exciting projects and providing me with my first glimpse of how rewarding it can be to mentor.

I am grateful to Ben Heineke for his enthusiastic embrace of a project that seemed destined for the waste bin and his willingness to carry the torch forward.

I am grateful to Tomas Aragon and Eelco van Anken for their mentorship.

I am grateful to Shayna Lewis for her support during the preparation of this thesis. And for everything.

I am grateful to all past and current members of the Walter and El-Samad labs for all the wonderful group meetings, for the fun lab gatherings, for the funny holiday party gifts, for the off-the-cuff informal discussions, for the career and scientific advice, for useful reagents, for personal support and encouragement, for scientific rigor and for all the jokes and fun. I will miss you all dearly.

Most of this thesis has been or will be published elsewhere. The text for Chapter 1 will be published in a forthcoming Cold Spring Harbor book on the ER. The text for Chapter 2 was published in PLoS Biology in 2010. The text for Chapter 3 was published in The Journal of Cell Biology in 2011. The text for Appendix A was published in The Journal of Cell Biology in 2012. Unpublished material in Chapter 4 and Appendix B will hopefully be published soon.

ABSTRACT

The endoplasmic reticulum (ER) is the compartment in eukaryotic cells in which secreted and membrane-spanning proteins are folded, modified and assembled. These proteins are the means by which cells sense and respond to their environment and neighboring cells. Thus it is vital that these proteins fold into their appropriate structures so they can function properly. When cells are exposed to various environmental stresses, mutations or differentiation cues, the ER protein folding machinery can become overwhelmed, a condition known as ER stress. During ER stress unfolded and misfolded proteins accumulate in the ER, eliciting an intracellular signaling pathway called the unfolded protein response (UPR) that functions as a feedback loop to restore homeostasis to protein folding in the ER.

The UPR is an ancient pathway found in all organisms with an ER. The most conserved component of the UPR is Ire1, an ER-resident transmembrane protein that contains a domain in the ER lumen that senses unfolded proteins and effector kinase and RNase domains in the cytosol that initiate the response. In most organisms misfolded proteins in the ER activate Ire1 to initiate a nonconventional mRNA splicing reaction. Splicing results in the production of a transcription factor that induces UPR target genes to increase the folding capacity of the ER and thereby relieve the stress.

In the work compiled in this thesis, we find that maintaining homeostasis in the ER requires not only that Ire1 activates specifically, but also that Ire1 deactivates

efficiently. Activation and deactivation of the UPR are regulated at the level of Ire1 oligomerization on both sides of the ER membrane. Binding to unfolded proteins drives oligomerization while de-oligomerization is aided by binding to the chaperone protein BiP in the lumen of the ER (Chapter 2) and Ire1's kinase activity in the cytoplasm (Chapter 3). Unmitigated UPR signaling imposes a fitness cost on cells (Chapter 4) underscoring the need for such deactivation mechanisms. Similar deactivation mechanisms may play underappreciated roles in controlling activity in many signaling pathways and stress responses.

TABLE OF CONTENTS

FIGURES

Chapter 1

Chapter 2

Chapter 3

Chapter 4

Appendix A

Appendix B

Chapter 1

Introduction: ER Stress Sensing in the Unfolded Protein Response

ER Stress Sensing in the Unfolded Protein Response

Brooke M. Gardner[1], David Pincus[1], Katja Gotthardt[1], Ciara M. Gallagher[1], and Peter Walter[1,2,*]

[1] Department of Biochemistry and Biophysics, University of California, San Francisco 94122

[2] Howard Hughes Medical Institute, University of California, San Francisco 94122

[*] Corresponding author: peter@walterlab.ucsf.edu (415) 476-4636

Contact Information:

Brooke M. Gardner: brooke.gardner@ucsf.edu, (415) 476 5676

David Pincus: david.pincus@ucsf.edu, (415) 476 5676

Katja Gotthardt: katja.gotthardt@ucsf.edu, (415) 476 5676

Ciara M. Gallagher: ciara.gallagher@ucsf.edu, (415) 476 5676

Abstract

Secretory and transmembrane proteins enter the endoplasmic reticulum (ER) as unfolded proteins and exit as either folded proteins in transit to their target organelles or as misfolded proteins targeted for degradation. The Unfolded Protein Response (UPR) maintains the protein-folding homeostasis within the ER, ensuring that the protein-folding capacity of the ER meets the load of client proteins. Activation of the UPR depends on three ER stress sensor proteins, Ire1, PERK, and ATF6. While the consequences of activation are well understood, how these sensors detect ER stress remains unclear. Recent evidence suggests that yeast Ire1 directly binds to unfolded proteins, which induces its oligomerization and activation. BiP dissociation from Ire1 regulates this oligomeric equilibrium, ultimately modulating Ire1's sensitivity and duration of activation. The mechanistic principles of ER stress sensing are the focus of this review.

Introduction

Secreted and transmembrane proteins enter the secretory pathway by translocation into the endoplasmic reticulum (ER). These newly synthesized polypeptides must properly fold before being transported to their target organelles. Proteins that do not properly fold within a certain time are targeted for ER Associated Degradation (ERAD), which efficiently retro-translocates them from the ER into the cytosol for degradation via the ubiquitin-proteasome system (Smith et al. 2011). To support proper protein folding and prevent aggregation in the ER lumen, an environment with a high protein concentration (~100 mg/ml), numerous ER-resident chaperones and folding enzymes assist maturation by signal-peptide cleavage, glycosylation, and disulfide bond formation (Araki and Nagata 2011). Chaperones in particular are involved in every aspect of ER quality control. The most abundant and best-characterized ER-resident chaperone is BiP/Grp78 (immunoglobulin heavy chain binding protein/glucose-regulated protein 78), an Hsp70 family ATPase involved in numerous functions, including translocating nascent polypeptides, facilitating *de novo* protein folding and assembly, targeting misfolded proteins to ERAD machinery, and maintaining calcium homeostasis (Hendershot 2004; Otero et al. 2010). To sustain protein-folding homeostasis in the ER, the cell must balance the ER protein folding load with sufficient ER protein folding machinery, particularly chaperones such as BiP.

Multiple physiological and pathological conditions can interfere with ER quality

control and lead to an accumulation of misfolded proteins in the ER. Such an increase of unfolded proteins is termed "ER stress" and can have deleterious consequences for the cell. To cope with ER stress and maintain protein homeostasis eukaryotic cells have evolved the Unfolded Protein Response (UPR). The UPR coordinates the increase in ER folding capacity through a broad transcriptional upregulation of ER folding, lipid biosynthesis, and ERAD machinery (Travers et al. 2000) with a decrease in folding load through selective mRNA degradation and translational repression (Harding et al. 1999; Hollien and Weissman 2006; Hollien et al. 2009). The UPR is therefore cytoprotective, allowing cells to adapt to developmental and environmental conditions that impinge on ER protein folding. During severe and prolonged ER stress, however, the UPR can become cytotoxic rather than cytoprotective, inducing apoptosis (Lin et al. 2007). ER stress-induced apoptosis is an important pathogenic factor in a number of widespread diseases, including diabetes, neurodegenerative diseases, atherosclerosis and renal disease (Tabas and Ron 2011). Because of the UPR's central role in determining cell fate, there have been multiple studies to identify small molecules modulators to exploit the UPR for therapeutic benefit (Fribley et al. 2011; Papandreou et al. 2011; Volkmann et al. 2011; Cross et al. 2012; Mimura et al. 2012).

Three ER Stress Sensors Initiate the UPR

In metazoans, three parallel pathways employing unique signal transduction

mechanisms collectively comprise the UPR. In each branch, an ER-resident integral membrane protein, Ire1 (inositol requiring enzyme 1), PERK (protein kinase RNA (PKR)-like ER kinase), or ATF6 (activating transcription factor 6) senses abnormal conditions in the ER lumen and transmits the information across the membrane into the cytosol where a series of transcription factors carry information to the nucleus (Figure 1) (Walter and Ron 2011). The three branches collaborate to upregulate protein folding machinery and decrease the burden of unfolded proteins. In this review, we highlight recent mechanistic insights into how ER stress is detected in yeast and subsequently discuss the implications for ER stress sensing in metazoan cells.

Ire1

Ire1 is the only ER stress sensor present in all eukaryotes and therefore reflects the most ancient and most conserved branch of the UPR (Mori 2009). As a type I transmembrane protein, Ire1 contains an N-terminal ER lumenal domain and C-terminal cytoplasmic kinase and RNase domains. In the presence of ER stress, Ire1 forms higher-order oligomeric assemblies triggered by self-association of the ER lumenal domain (Ire1-LD). ER stress-dependent Ire1 oligomerization can be visualized microscopically as foci *in vivo* (Kimata et al. 2007; Aragon et al. 2009; Li et al. 2010; Pincus et al. 2010) and is required for downstream activation of its cytosolic kinase and RNase.

Although oligomerization driven *trans*-autophosphorylation is a common stereotype of cell signaling, Ire1 does not signal downstream via phosphorylation. Rather, a conformational change that occurs upon nucleotide binding acts as a molecular switch to activate Ire1's RNase domain (Papa et al. 2003; Aragon et al. 2009; Korennykh et al. 2009). Once activated, Ire1's RNase specifically cleaves its mRNA substrate, *HAC1* mRNA (homolog of ATF/CREB1) in yeast or *XBP1* mRNA (X-box binding protein1) (Cox and Walter 1996; Yoshida et al. 2001) in metazoan cells to initiate an unconventional splicing reaction. After Ire1 removes the intron, the severed exons are ligated by tRNA ligase in yeast and an unknown ligase in metazoan cells, and the mature mRNA is translated to produce a potent bZIP transcription factor that upregulates genes encoding ER quality control components (Sidrauski et al. 1996; Travers et al. 2000; Yoshida et al. 2001).

The enzymatic activity of the purified kinase/RNase domain of Ire1 is highly cooperative, indicating that full RNase activity is only obtained upon assembly of more than two Ire1 molecules (Korennykh et al. 2009; Li et al. 2010). Crystal structures of the yeast kinase/RNase domains suggest that Ire1 first associates into back-to-back dimers, followed by assembly into higher-order oligomers that stabilize the RNase active site through oligomer-specific protein/protein interfaces (Lee et al. 2008; Korennykh et al. 2009). This higher-order assembly is facilitated by both the oligomerization initiated by the lumenal domain and the active, nucleotide-bound conformation of the kinase. Ire1 mutants impaired in nucleotide binding lose RNase activity, while mutants impaired in phospho-transfer, but retaining

nucleotide binding, maintain RNase activity (Shamu and Walter 1996; Chawla et al. 2011; Rubio et al. 2011).

To date, Ire1 remains the only validated substrate of its kinase domain. Although only nucleotide binding and not phosphorylation is required for *HAC1* mRNA cleavage, the absence of phosphorylation does affect the kinetics of the UPR, leading to prolonged *HAC1* mRNA splicing and delayed disassembly of Ire1 foci (Chawla et al. 2011; Rubio et al. 2011). These results suggest that phosphorylation plays a role in deactivation of Ire1 by destabilizing Ire1 oligomers, perhaps through electrostatic repulsion from the high local concentration of negatively charged phosphate groups (Rubio et al. 2011). Initial phosphorylation events, however, may promote oligomer formation (Lee et al. 2008; Korennykh et al. 2009). The deactivation of Ire1 signaling is important for physiology since sustained *HAC1* mRNA splicing impairs cell survival (Chawla et al. 2011; Rubio et al. 2011). Phosphorylation may play an expanded role in metazoan cells where adaptor protein docking to phosphorylation sites may mediate branching of the signaling pathway. For example, interactions between phosphorylated IRE1 and the adaptor protein TRAF2 ultimately lead to JNK (Jun amino-terminal kinase) activation, whose sustained activity induces pro-apoptotic signaling (Urano et al. 2000).

While *HAC1* mRNA is the only known RNA substrate of yeast Ire1 (Niwa et al. 2005), Ire1 not only mediates *XBP1* mRNA splicing but also the rapid degradation of a subset of mRNAs in metazoan cells (Hollien and Weissman 2006). This pathway,

termed Regulated Ire1-Dependent Decay (RIDD), cleaves mRNAs encoding membrane and secreted proteins and may consequently decrease the protein influx into the ER. Substrate specificity of this more promiscuous Ire1-mediated cleavage and decay appears to be mediated by both localization of the mRNA to the ER membrane and low stringency consensus sites. Intriguingly, *in vivo* experiments show that the specific *XBP1* mRNA cleavage and RIDD modes of RNase activity can be uncoupled. In mammalian cells, an ATP competitive analog (1NM-PP1) can specifically activate a drug-sensitized Ire1 mutant, but this method of activation only induces *XBP1* mRNA splicing but not RIDD (Han et al. 2009; Hollien et al. 2009). It remains to be shown whether and how Ire1 switches between XBP1-specific and RIDD modes of activity. The state of oligomerization may determine the stringency of the RNase for substrate recognition.

PERK

PERK is a type I transmembrane protein present in metazoans that partially resembles Ire1. PERK's lumenal stress-sensing domain is structurally and functionally related to Ire1's, though the sequence identity is low, and PERK also contains a cytosolic kinase domain that undergoes *trans*-autophosphorylation in response to ER stress. Unlike Ire1, however, PERK also phosphorylates the eukaryotic translation initiation factor eIF2α. Phosphorylation of eIF2α results in a reduction of general protein synthesis and thus a decrease in the load of proteins entering the ER. Under such conditions, mRNAs containing inhibitory upstream

open reading frames in their 5'-untranslated region are preferentially translated (Jackson et al. 2010). One such mRNA encodes the transcription factor ATF4 that activates downstream UPR target genes, including GADD34 (growth arrest and DNA damage-inducible 34) and CHOP (transcription factor C/EBP homologous protein) (Harding et al. 2000; Scheuner et al. 2001). GADD34 encodes the regulatory subunit of the protein phosphatase PP1C complex that dephosphorylates eIF2α (Novoa et al. 2001), comprising a negative feedback loop to reverse the translational attenuation mediated by PERK. The downstream transcription factor CHOP activates genes involved in apoptosis (Wang et al. 1998; Zinszner et al. 1998). Thus, the PERK branch first mediates a pro-survival response, which switches into a pro-apoptotic response upon prolonged ER stress (reference to David Ron's paper in this volume).

ATF6

ATF6 is an additional sensor in metazoan cells responsible for ER stress-induced ER expansion and upregulation of chaperones, foldases and components of the ERAD pathway (Adachi et al. 2008; Bommiasamy et al. 2009). Unlike Ire1 and PERK, ATF6 is a type II transmembrane protein with a C-terminal stress sensing lumenal domain and an N-terminal bZip transcription factor domain. In response to ER stress, ATF6 transits from the ER to the Golgi, where it is proteolyzed sequentially by the site-1 and site-2 proteases (S1P and S2P) to release its N-terminal transcription factor domain from the membrane (Haze et al. 1999). The released N-terminus (ATF6-N) translocates to the nucleus where it binds to the ER stress response element (ERSE) and activates transcription of UPR target genes (Yoshida et al. 1998).

The Challenge of Detecting ER Stress

Conceptually there are many possibilities for how these three sensors could monitor ER stress: redox potential, calcium homeostasis, membrane aberrancy, concentration of unfolded proteins, or availability of folding machinery. In all cases, however, ER stress sensing must be delicately tuned to avoid hypersensitivity to small fluctuations in normal conditions but also respond quickly to legitimate ER stress. In this review, we highlight recent mechanistic insights into how yeast Ire1 detects ER stress and subsequently discuss the implications for ER stress sensing in metazoans.

The UPR was first proposed to explain the observation that over-expression of a misfolded protein led to upregulation of the chaperones BiP and Grp94 (Kozutsumi et al. 1988). Since ER stress dependent BiP upregulation operationally defined the UPR, BiP dissociation from Ire1 was originally proposed to be the primary regulatory step for UPR activation. In this model, BiP controls its own expression and ER stress is monitored by the concentration of free chaperone. (Ng et al. 1992; Shamu et al. 1994). Recent evidence, however, favors an alternative mechanism for ER stress sensing: direct binding to unfolded proteins. The combination of the crystal structure of Ire1 lumenal domain accompanied by biochemical evidence that Ire1 binds misfolded proteins *in vivo* and short peptide proxies *in vitr*o provides compelling evidence that Ire1 can sense ER stress by directly monitoring the concentration of unfolded proteins (Credle et al. 2005; Zhou et al. 2006; Gardner and Walter 2011). Therefore, the higher-order oligomerization of Ire1, which is

required for downstream activation, is influenced by two factors: binding to unfolded proteins, which shifts Ire1 towards an active, oligomeric state, and binding to BiP, which stabilizes Ire1 in the inactive, monomeric state (Figure 2A). While BiP buffers UPR activity and helps turn Ire1 off, direct binding to unfolded proteins switches Ire1 on.

BiP Dissociation is Not the Switch for Ire1 Activation

Three observations led to the original proposal that Ire1 monitors levels of free BiP in the ER and induces the UPR as a feedback mechanism to restore BiP levels during ER stress. First, BiP overexpression diminished UPR signaling; second, decreasing the concentration of BiP in the ER activated the UPR; and third, accumulated misfolded proteins in the ER that do not interact with BiP failed to induce the UPR (Hardwick et al. 1990; Dorner et al. 1992; Ng et al. 1992; Kohno et al. 1993). Analogous to how cytoplasmic chaperone hsp70 regulates Heat Shock Factor (HSF1) in eukaryotic cells – upon heat shock hsp70 is titrated away from HSF1 – it was proposed that BiP binding sequesters Ire1 in an inactive state (Abravaya et al. 1992; Shamu et al. 1994). In ER stress conditions, accumulated unfolded proteins in the ER would saturate the free pool of chaperones, titrating BiP away from Ire1 to activate UPR signaling.

BiP titration as a switch of Ire1 activation gained further support when it was shown that BiP binds to Ire1, PERK and ATF6 in unstressed cells and dissociates from the UPR sensors during acute ER stress (Bertolotti et al. 2000; Okamura et al. 2000;

Shen et al. 2002). The effect of BiP mutations on Ire1 activity were also consistent with a role for BiP as a negative regulator of Ire1 activity. BiP mutants that constitutively bound Ire1 hindered Ire1 activation during ER stress, suggesting that BiP release is required for activation. BiP mutants defective in Ire1 binding either showed constitutive activation of Ire1 (Kimata et al. 2003) or showed an inability to negatively regulate Ire1 (Todd-Corlett et al. 2007). However, since BiP is essential for protein translocation and folding in the ER, BiP mutants are plagued with pleiotropic effects and cause varying degrees of constitutive ER stress. Thus, it is difficult to decipher whether the effect of BiP mutants on Ire1 activation results from the change in association with Ire1 or altered conditions in the ER.

By contrast, a mutational analysis of Ire1's lumenal domain in yeast mapped the BiP binding site to the juxtamembrane segment (Kimata et al. 2004). Although removal of this region abolished ER stress-regulated BiP binding, the Ire1 mutant remained inactive in the absence of ER stress and retained its stress-dependent activation (Figure 2B). Though this Ire1 mutant was hyper-responsive to heat shock and ethanol, it became evident that BiP is not the primary regulator of Ire1 activity.

Structural Hints of Direct Binding to Unfolded Proteins

An alternative view of Ire1 activation posits that a ligand produced by the accumulation of unfolded proteins directly binds and activates Ire1 (Shamu et al. 1994). There was little evidence for ligand mediated Ire1 activation until the crystal structure of the lumenal domain of Ire1 (Ire1-LD) from *S. cerevisiae* revealed that the dimer of Ire1-LD forms a deep groove, suggesting a ligand-binding site (Figure

3A) (Credle et al. 2005). The architecture of this groove –a floor of β-sheets with α-helical walls – resembles the peptide-binding groove of major histocompatibility complexes (MHC) (Figure 4A and C). Because of this similarity, it was proposed that unfolded proteins are Ire1-activating ligands.

Although no ligand was co-crystallized with yeast Ire1-LD, this structure featuring an open and obvious groove is thought to represent the active form of Ire1 (Figure 4A). In support of this notion, Ire1 forms oligomers at two interfaces within the crystal lattice (Figure 3C) (Credle et al. 2005). Interface 1 buries 2,380 $Å^2$ of solvent-accessible surface and is formed by hydrogen bonding and hydrophobic interactions between two central, anti-parallel β-sheets. The dimer created at Interface 1 forms the putative peptide-binding groove (Figure 3A, 4A). Interface 2 relates these dimers in a back-to-back fashion, burying 2,117 $Å^2$ (Figure 3C). Mutations within either of these interfaces prevent Ire1 foci formation, *HAC1* mRNA splicing, and activation of UPR target genes, indicating the functional importance of oligomerization through these interfaces *in vivo* (Credle et al. 2005; Aragon et al. 2009). Ligand binding across the proposed groove would directly stabilize the dimer formed at Interface 1, as well as the conformation required for oligomerization through Interface 2.

Biochemical Evidence of Unfolded Protein Binding to Ire1

There is increasing biochemical evidence to support the structure-based view that unfolded proteins are Ire1-activating ligands. Purified yeast Ire1-LD inhibits the aggregation of unfolded proteins *in vitro*, potentially by binding and shielding

regions that would otherwise cause aggregation (Kimata et al. 2007). Ire1 also co-immunoprecipitates with a model misfolded protein known to activate the UPR (carboxypeptidase Y, CPY*) (Gardner and Walter 2011; Promlek et al. 2011). Further co-immunoprecipitation experiments suggest that the interaction between Ire1 and CPY* depends on the formation of the proposed ligand-binding groove: mutations disrupting Interface 1 and residues within the groove abolish the interaction between Ire1 and CPY*, while mutations in Interface 2, which only disrupt oligomerization, do not affect the interaction between Ire1 and CPY*.

Furthermore, analysis of Ire1-LD binding to peptides derived from CPY* demonstrated that there are discrete Ire1 binding sites within CPY* (Gardner and Walter 2011). These results suggest that Ire1 ligands are unstructured proteins with sufficient flexibility to sample the binding groove and that multiple ligands can be displayed as part of a single unfolded protein. Moreover, Ire1 discriminates amongst peptide sequences and displays clear amino acid preferences. Systematic mutational analysis of a binding peptide revealed that yeast Ire1-LD preferentially binds to regions containing basic and hydrophobic residues. Although similar sequence preferences are also displayed by some chaperones, a comparison of peptides bound by BiP and Ire1 revealed that they each bind a separate, but overlapping set of peptides (Gardner and Walter 2011). This indicates that BiP and Ire1 do not always compete for ligands and that BiP saturation is not required for Ire1 activation.

Insights into the Mechanism of Peptide-Binding

As of yet, no experiments verify the groove as the ligand-binding site within Ire1-LD. Notably, however, residues on the β-sheet floor whose side-chains point into the groove are more conserved than adjacent ones that point away. Mutations of three of these conserved residues, M229A, F285A, Y301A, inhibit the activation of Ire1 *in vivo*, prevent co-immunoprecipitation with CPY*, and diminish binding to unfolded proteins and peptides in solution, strongly indicating that the groove is important for ligand-binding (Credle et al. 2005; Kimata et al. 2007; Gardner and Walter 2011; Promlek et al. 2011). Moreover, *in silico* docking shows that a peptide ligand seeks out the groove as a highly preferred binding site in Ire1-LD (Gardner, Korennykh, and Walter, unpublished).

Similar to DnaK and MHC molecules, Ire1 must bind a variety of ligands while remaining selective for unfolded proteins (DnaK, Ire1) or extended peptides (MHC). DnaK and MHCII, which have both been crystallized with ligands (Figure 4C, D), may provide insight into how Ire1 binds a variety of unfolded proteins within the same binding pocket. Sidechains of DnaK and MHC II form extensive hydrogen bond networks with the backbone of the ligand, ensuring binding to extended polypeptides with little stringency for ligand character. The limited specificity for ligand residues arises from pockets with variable volume, charge, and available stacking interactions. Deeper pockets specific to large hydrophobic side-chains anchor the peptide, while shallower pockets can accommodate a wider range of residues (Stern et al. 1994; Murthy and Stern 1997)

Ire1 could combine all three of these characteristics to bind unfolded proteins: hydrogen bonding to the polypeptide backbone, electrostatic interactions, and the burial of anchor residues in deep pockets. Indeed, Ire1 displays side-chains across the groove capable of hydrogen bonding to the polypeptide backbone. Ire1's preference for basic residues may be mediated by two acidic residues (E172, D176) along the sides of the groove that are highly conserved among fungi or through acidic residues in an unstructured loop (aa 380-387). Finally, the proposed ligand-binding groove of Ire1 contains deep pockets on either end that could bind specific side-chains and anchor ligand-binding (Figure 4A). These pockets are particularly deep and contain several chambers that may select for specific adjacent side-chains, perhaps basic and hydrophobic residues.

Ligand-Binding Triggers Ire1 Oligomerization

As mentioned previously, the oligomerization of Ire1-LD activates the cytosolic kinase domain and highly cooperative RNase domain (Korennykh et al. 2009). Analytical ultracentrifugation experiments in the presence of a short peptide with a high affinity for Ire1 revealed that peptide binding alters the oligomeric state of Ire1-LD, causing higher-order oligomerization (Figure 2C). By mutating Interface 2, the peptide-induced oligomerization can be limited to dimerization (Gardner and Walter 2011). These experiments show that binding to a short peptide, a proxy for an unfolded protein, stabilizes the dimer of Ire1 in an oligomerization competent state, therefore driving Ire1 activation.

The Equilibrium Model of UPR Activation

The regulatory contribution of BiP binding and unfolded protein binding can be viewed as opposing forces on Ire1's oligomeric equilibrium (Figure 2A). While ligand-induced oligomerization activates Ire1, BiP association stabilizes the inactive, monomeric form of Ire1 preventing Ire1 from hyper-responding to low levels of ER stress (Korennykh et al. 2009; Pincus et al. 2010; Gardner and Walter 2011). Computational simulations of this equilibrium model remarkably recapitulate the observed dynamics of the UPR in yeast and illustrate the importance of BiP regulation. In the absence of BiP binding, Ire1 molecules are poised closer to the activation threshold, but are not constitutively active without further stimulus. Moreover – as predicted by the computational model (Figure 2D)– in the absence of BiP binding, Ire1 displayed delayed deactivation and de-oligomerization kinetics when ER stress was removed (Figure 2E) (Pincus et al. 2010). Therefore, the combination of buffering by BiP and cooperative activation of Ire1 achieves an appropriate sensitivity to ER stress while maintaining a robust and speedy response to ER stress.

Other Regulation of Ire1 Activation

BiP and unfolded proteins may not be the only factors to influence Ire1 activation. Additional layers of regulation could arise through alternate inputs detected either by Ire1-LD or other domains. Several studies of Ire1 in which the LD was removed and replaced with a leucine zipper show that Ire1 still responds to ER stress, although the response is delayed and less robust (Liu et al. 2000; Promlek et al. 2011). While the mechanism of this activation is unclear, it has been proposed that

Ire1's transmembrane domain is sensitive to aberrations in the ER membrane. Furthermore, biochemical and structural studies of the yeast cytoplasmic domain of Ire1 identified a small ligand-binding pocket on Ire1 cytosolic face that binds quercetin, a naturally occurring flavonol, and stabilizes the active RNase dimer (Wiseman et al. 2010). Presumably any mechanism of stabilizing Ire1 oligomers, including limited membrane diffusion or increased affinity at cytoplasmic interfaces, could contribute to Ire1 activation.

ER Stress Sensing by Metazoan UPR Sensors

ER stress sensing by the three metazoan sensors, IRE1, PERK, and ATF6, is less understood. During ER stress, all three sensor proteins undergo a change in oligomerization state, which is accompanied by BiP dissociation. IRE1 and PERK oligomerize to activate their cytosolic domains, while ATF6 de-oligomerizes in response to ER stress. We predict that the principles of yeast Ire1 activation are maintained for the homologous metazoan sensors, IRE1 and PERK. The mechanism of ATF6 activation remains elusive, and although it may also be buffered by BiP binding, its downstream activation is more analogous to that of SREBP than Ire1 or PERK.

IRE1 and PERK

The secondary structure homology between yeast Ire1 and metazoan IRE1 and PERK indicates that they may have similar activation mechanisms in which they directly bind unfolded proteins but are also regulated by BiP association. Indeed, PERK and Ire1 lumenal domains from different species are experimentally

interchangeable and can substitute for yeast Ire1-LD (Bertolotti et al. 2000; Liu et al. 2000). Similar to yeast Ire1, PERK and IRE1 residues required for disulfide bond formation and glycosylation are dispensable for ER stress sensing (Ma et al. 2002; Liu et al. 2003; Oikawa et al. 2005; Oikawa et al. 2009). BiP binds to both IRE1 and PERK in the juxtamembrane region and dissociates during ER stress when IRE1 and PERK form higher-order complexes (Bertolotti et al. 2000; Liu et al. 2000). For IRE1, this higher-order oligomerization has been observed *in vivo* as foci formation and the cooperativity of the endoribonuclease of human IRE1 indicates that it is required for robust Ire1 activation (Li et al. 2010). Mutants of IRE1 and PERK in which the BiP interaction is impaired show higher basal level activation (Ma et al. 2002; Oikawa et al. 2009). No further phosphorylation of PERK was observed during ER stress (Ma et al. 2002), however, the importance of BiP dissociation from endogenous PERK requires further characterization. In the case of IRE1, the BiP-binding impaired mutant retained significant stress-dependent induction, indicating that BiP binding and dissociation is not the only layer of IRE1 regulation.

The crystal structure of human IRE1-LD is remarkably similar to that of yeast Ire1-LD with a few key differences (Figure 3B) (Zhou et al. 2006). The core structure of a dimer forming a putative ligand-binding groove with a β-sheet platform and α-helical walls is conserved. However, although a groove is still present, it is not as deep as the yeast counterpart because the α-helices are closer together and block the continuous, deep groove across the dimer (Figure 3B, 4B). Because of this, it was suggested that human IRE1-LD is unlikely to bind unfolded proteins(Zhou et al.

2006), even though the remaining shallow groove contains deep pockets that could still bind anchor residues as a ligand arches over the helices.

Given the overall conservation of the Ire1-LD structure, we find it more likely that these differences represent distinct conformational steps in the same pathway of Ire1 activation. Perhaps the yeast structure is an open, oligomeric, active conformation, and the human structure is a closed, dimeric, inactive conformation. Indeed, Interface 2, which is required for oligomerization and activity of yeast Ire1-LD, is not observed in the human structure, consistent with it being an inactive conformation. The formation of Interface 2 between a β-sheet and an α-helical turn region (arrows, Figure 3C and 3D) is sterically hindered by the long helix αB in the human structure, which forms a new, smaller interface that has not been tested *in vivo*. The αB-helix corresponds to an unresolved region in the yeast LD structure, while an α-helical turn region involved in Interface 2 is alternately unstructured in the human structure. These changes may suggest the conformational change observed upon ligand binding.

If PERK and IRE1 do indeed bind unfolded proteins, it will be interesting to see how the altering characteristics of residues within the groove may have redefined their ligand preference. Specialization of the recognition code illustrated by yeast Ire1 would allow some sensors to be "blind" to certain unfolded proteins, yet acutely sensitive to others. On the other hand, sensors could have evolved to be particularly sensitive to certain markers of ER stress or "canary" proteins. Hypothetically,

pathogens or developmental programs could also exploit this binding specificity in higher organisms.

ATF6

The lumenal domain of ATF6 bears no sequence homology to those of Ire1 or PERK, and its activation is strikingly different, relying upon a change in subcellular localization and intramembrane proteolysis. Analogous to Ire1 and PERK, ATF6 activation is associated with both a change in oligomerization state and BiP dissociation. Unlike Ire1 and PERK, ATF6 is an oligomer in the ER of unstressed cells (Nadanaka et al. 2007). Conversion from an oligomer to a monomer may be important for activation as the oligomer is not found in the Golgi and, when compared to the monomer, is a poor substrate for S1P cleavage. De-oligomerization is not sufficient for ATF6 activation, however, since mutation of both conserved cysteines, which mediate oligomerization, did not lead to constitutive trafficking of ATF6 to the Golgi (Nadanaka et al. 2007). Upon ER stress BiP dissociates from the lumenal domain of ATF6 (Shen et al. 2002; Shen et al. 2005). BiP dissociation is not sufficient for activation as deletion of most of the lumenal domain, and therefore BiP binding, did not lead to constitutive trafficking of ATF6.

Mechanistically, the activation of ATF6 in response to ER stress is more analogous to Sterol Response Element Binding Protein (SREBP), which also transits to the Golgi where its N terminal transcription factor is released by S1P and S2P-mediated proteolysis. SREBP's transit to the ER is regulated by the interaction between two binding proteins, SCAP (SREBP cleavage activating protein), which acts as a positive

transport factor, and INSIG (Insulin Induced Gene), which acts as a retention factor by masking the COPII sorting signal in SCAP (Sun et al. 2007). The interaction between SCAP and INSIG is regulated by cholesterol – the absence of cholesterol induces a conformational change in SCAP leading to its dissociation from INSIG (Adams et al. 2004; Feramisco et al. 2005). Therefore, it is SCAP and not SREBP that senses cholesterol levels in the membrane. While SCAP is not required (Ye et al. 2000), it remains to be seen if activation of ATF6 during ER stress requires a specific interacting partner or whether ATF6 lumenal domain functions as an intrinsic stress sensor.

Concluding Remarks

In conclusion, there is increasing evidence that direct binding to unfolded proteins triggers Ire1 activation in *S. cerevesiae* by inducing a conformational change to promote oligomerization. BiP dissociation from Ire1 fine-tunes this oligomeric equilibrium, regulating the sensitivity and duration of UPR activation. The mechanics of Ire1 binding to unfolded proteins requires further research to detail both ligand specificity and conformational changes. Furthermore, it remains unclear if these principles of Ire1 activation are upheld in metazoan sensors. Structural homology suggests that the mechanism of IRE1 and PERK activation have been conserved, though they may have specialized to detect different types of unfolded proteins or integrate other characteristics of ER stress. Differentiated cells are met with different types of challenges to their protein homeostasis, and it may be beneficial to cells predictably challenged by a developmental program to respond differently than those challenged by unpredictable environmental stress. We anticipate that the ER stress sensing mechanisms of metazoan cells are precisely tuned to accommodate the specialized needs of the organism. A detailed understanding of these mechanisms could direct the design of small molecule modulators to specifically modulate entire branches of the UPR for therapeutic benefit.

Figure Legends

Figure 1. **The three branches of the UPR.** In metazoans, three parallel signaling pathways comprise the UPR. ER-resident transmembrane sensor proteins, Ire1, PERK and ATF6, activate signaling in each UPR branch. Upon activation (the specific mechanism by which each sensor detects ER stress is the focus of this review), each sensor elicits unique downstream responses. Ire1's active cytosolic RNase domain cleaves an intron out of an mRNA, leading to the production of a potent transcriptional activator that induces genes to increase the folding capacity of the ER (XBP1 in metazoans, Hac1 in budding yeast). The active RNase also cleaves ER-localized messages, leading to their degradation, to reduce the load of unfolded proteins entering the ER. PERK's active cytosolic kinase domain phosphorylates the translation initiation factor eIF2α, thereby inhibiting global translation and reducing the load of newly synthesized proteins entering the ER. While generally inhibiting translation, eIF2α phosphorylation allows specific messages with inhibitory leader sequences to be preferentially translated. One of these messages encodes ATF4, a transcriptional activator that induces a cascade that ultimately produces pro-apoptotic factors. Active ATF6 translocates to the Golgi where it is proteolytically processed to release its N-terminal transcriptional activator domain that induces genes to increase the folding capacity in the ER.

Figure 2. **Unfolded proteins are the switch that activates Ire1 while BiP binding regulates the sensitivity and duration of the response.**

A) Free energy model for Ire1. Ire1 is in equilibrium between monomeric and oligomeric states. Binding to BiP stabilizes the monomeric state by providing a sink to buffer the amount of free Ire1. Binding to unfolded proteins stabilizes the oligomeric state by overcoming the activation barrier for Ire1 oligomerization.

B) BiP dissociation from Ire1 is not sufficient to activate Ire1 (reprinted from (Pincus et al. 2010) Upper panel: Quantification of co-immunoprecipitation experiments showing that wild-type Ire1 binds to BiP in the absence of ER-stress, and dissociates from much of the bound BiP in the presence of ER stress. A mutant of Ire1 lacking the ER juxtamembrane segment (Ire1-bipless) binds to BiP in the absence of stress only to the degree that wild type Ire1 binds to BiP in the presence of stress. In ER stress conditions, Ire1-bipless shows no change in its association with BiP. Lower panel: Northern blot measuring splicing of *HAC1* mRNA showing that, despite its lack of ER-stress dependent BiP dissociation, the RNase of Ire1-bipless is not constitutively active and remains ER-stress inducible.

C) Peptide binding triggers Ire1-LD oligomerization *in vitro* (reprinted from (Gardner and Walter 2011). Analytical ultracentrifugation of recombinant Ire1-LD in the presence and absence of a peptide proxy for an unfolded protein shows that Ire1-LD redistributes into large oligomeric assemblies in the presence of peptide.

D) Mathematical model simulation predicts that Ire1-bipless would display delayed deactivation kinetics compared to wild type Ire1 once ER stress is removed (reprinted from (Pincus et al. 2010).

E) Experimental verification that Ire1-bipless deactivates less efficiently than wild type Ire1 once ER stress is removed (reprinted from (Pincus et al. 2010). FRET measurements between Ire1 molecules reveals that de-oligomerization is impaired in the Ire1-bipless mutant.

Figure 3. Crystal structure of yeast and human Ire1 indicate how Ire1 oligomerizes. A) The S. cerevisiae Ire1-LD dimer formed at Interface 1 creates a putative ligand-binding groove (PDB: 2BE1). The groove is formed by a floor of β-sheets and two α-helical walls. Each monomer is colored red to blue from N to C terminus. Compare to Figure 4A for a surface representation. B) The H. sapiens Ire1-LD dimer formed at Interface 1 has similar architecture to yeast Ire1-LD, though the α-helical walls narrow the putative ligand binding groove (PDB: 2HZ6). Each monomer is colored red to blue from N to C terminus. Compare to Figure 4B for a surface representation. C) Two groove forming dimers of yeast Ire1-LD oligomerize through Interface 2 in the crystal lattice. An α-helical turn region (small arrow) interacts with a β-sheet (large arrow) to mediate this interaction. Residues that have been mutated and shown to impair UPR activation are colored red. D) Two groove forming dimers of human Ire1-LD interact through a novel Interface 2 in the crystal lattice. The interaction between the β-sheet (large arrow) and the now unstructured α-helical turn region (small arrow) that formed Interface 2 in the yeast Ire1-LD is now interrupted by a the long helix αB. Figures were made using PyMOL (Schrodinger 2010).

Figure 4. Crystal structures of Ire1 reveal a putative ligand-binding groove similar to those of MHC and DnaK. Surface models of the structures of (A) the yeast Ire1-LD, (B) the human Ire1-LD, (C) MHCII peptide binding domain crystallized with a peptide ligand (magenta; PDB: 1DLH), and (D) DnaK substrate binding domain crystallized with a peptide ligand (magenta; PDB: 1DKX). All structures are colored white to blue by depth looking down on the proposed or proven ligand-binding groove. Capped side views show a cross-section of the ligand-binding groove to illustrate the pockets available to bind anchor residues.

Acknowledgements

Peter Walter is an investigator of the Howard Hughes Medical Institute. Molecular graphics and analyses were performed either with The PyMOL Molecular Graphics System, Version 1.5.0.4 Schrödinger, LLC or with the UCSF Chimera package. Chimera is developed by the Resource for Biocomputing, Visualization, and Informatics at the University of California, San Francisco, with support from the National Institutes of Health (National Center for Research Resources grant 2P41RR001081, National Institute of General Medical Sciences grant 9P41GM103311).

References

Abravaya K, Myers MP, Murphy SP, Morimoto RI. 1992. The human heat shock protein hsp70 interacts with HSF, the transcription factor that regulates heat shock gene expression. *Genes Dev* **6**: 1153-1164.

Adachi Y, Yamamoto K, Okada T, Yoshida H, Harada A, Mori K. 2008. ATF6 Is a Transcription Factor Specializing in the Regulation of Quality Control Proteins in the Endoplasmic Reticulum. *Cell Struct Funct* **33**: 75-89.

Adams CM, Reitz J, De Brabander JK, Feramisco JD, Li L, Brown MS, Goldstein JL. 2004. Cholesterol and 25-hydroxycholesterol inhibit activation of SREBPs by different mechanisms, both involving SCAP and insigs. *J Biol Chem* **279**: 52772-52780.

Aragon T, van Anken E, Pincus D, Serafimova IM, Korennykh AV, Rubio CA, Walter P. 2009. Messenger RNA targeting to endoplasmic reticulum stress signalling sites. *Nature* **457**: 736-740.

Araki K, Nagata K. 2011. Protein folding and quality control in the ER. *Cold Spring Harb Perspect Biol* **3**: a007526.

Bertolotti A, Zhang Y, Hendershot LM, Harding HP, Ron D. 2000. Dynamic interaction of BiP and ER stress transducers in the unfolded-protein response. *Nat Cell Biol* **2**: 326-332.

Bommiasamy H, Back SH, Fagone P, Lee K, Meshinchi S, Vink E, Sriburi R, Frank M, Jackowski S, Kaufman RJ et al. 2009. ATF6 alpha induces XBP1-independent expansion of the endoplasmic reticulum. *J Cell Sci* **122**: 1626-1636.

Chawla A, Chakrabarti S, Ghosh G, Niwa M. 2011. Attenuation of yeast UPR is essential for survival and is mediated by IRE1 kinase. *J Cell Biol* **193**: 41-50.

Cox JS, Walter P. 1996. A novel mechanism for regulating activity of a transcription factor that controls the unfolded protein response. *Cell* **87**: 391-404.

Credle JJ, Finer-Moore JS, Papa FR, Stroud RM, Walter P. 2005. On the mechanism of sensing unfolded protein in the endoplasmic reticulum. *Proc Natl Acad Sci U S A* **102**: 18773-18784.

Cross BC, Bond PJ, Sadowski PG, Jha BK, Zak J, Goodman JM, Silverman RH, Neubert TA, Baxendale IR, Ron D et al. 2012. The molecular basis for selective inhibition of unconventional mRNA splicing by an IRE1-binding small molecule. *Proc Natl Acad Sci U S A* **109**: E869-878.

Dorner AJ, Wasley LC, Kaufman RJ. 1992. Overexpression of GRP78 mitigates stress induction of glucose regulated proteins and blocks secretion of selective proteins in Chinese hamster ovary cells. *EMBO J* **11**: 1563-1571.

Feramisco JD, Radhakrishnan A, Ikeda Y, Reitz J, Brown MS, Goldstein JL. 2005. Intramembrane aspartic acid in SCAP protein governs cholesterol-induced conformational change. *P Natl Acad Sci USA* **102**: 3242-3247.

Fribley AM, Cruz PG, Miller JR, Callaghan MU, Cai P, Narula N, Neubig RR, Showalter HD, Larsen SD, Kirchhoff PD et al. 2011. Complementary cell-based high-throughput screens identify novel modulators of the unfolded protein response. *J Biomol Screen* **16**: 825-835.

Gardner BM, Walter P. 2011. Unfolded proteins are Ire1-activating ligands that directly induce the unfolded protein response. *Science* **333**: 1891-1894.

Han D, Lerner AG, Vande Walle L, Upton JP, Xu W, Hagen A, Backes BJ, Oakes SA, Papa FR. 2009. IRE1alpha kinase activation modes control alternate endoribonuclease outputs to determine divergent cell fates. *Cell* **138**: 562-575.

Harding HP, Novoa I, Zhang Y, Zeng H, Wek R, Schapira M, Ron D. 2000. Regulated translation initiation controls stress-induced gene expression in mammalian cells. *Mol Cell* **6**: 1099-1108.

Harding HP, Zhang YH, Ron D. 1999. Protein translation and folding are coupled by an endoplasmic-reticulum-resident kinase. *Nature* **397**: 271-274.

Hardwick KG, Lewis MJ, Semenza J, Dean N, Pelham HR. 1990. ERD1, a yeast gene required for the retention of luminal endoplasmic reticulum proteins, affects glycoprotein processing in the Golgi apparatus. *EMBO J* **9**: 623-630.

Haze K, Yoshida H, Yanagi H, Yura T, Mori K. 1999. Mammalian transcription factor ATF6 is synthesized as a transmembrane protein and activated by proteolysis in response to endoplasmic reticulum stress. *Molecular Biology of the Cell* **10**: 3787-3799.

Hendershot LM. 2004. The ER function BiP is a master regulator of ER function. *Mt Sinai J Med* **71**: 289-297.

Hollien J, Lin JH, Li H, Stevens N, Walter P, Weissman JS. 2009. Regulated Ire1-dependent decay of messenger RNAs in mammalian cells. *J Cell Biol* **186**: 323-331.

Hollien J, Weissman JS. 2006. Decay of endoplasmic reticulum-localized mRNAs during the unfolded protein response. *Science* **313**: 104-107.

Jackson RJ, Hellen CU, Pestova TV. 2010. The mechanism of eukaryotic translation initiation and principles of its regulation. *Nat Rev Mol Cell Biol* **11**: 113-127.

Kimata Y, Ishiwata-Kimata Y, Ito T, Hirata A, Suzuki T, Oikawa D, Takeuchi M, Kohno K. 2007. Two regulatory steps of ER-stress sensor Ire1 involving its cluster formation and interaction with unfolded proteins. *J Cell Biol* **179**: 75-86.

Kimata Y, Kimata YI, Shimizu Y, Abe H, Farcasanu IC, Takeuchi M, Rose MD, Kohno K. 2003. Genetic evidence for a role of BiP/Kar2 that regulates Ire1 in response to accumulation of unfolded proteins. *Mol Biol Cell* **14**: 2559-2569.

Kimata Y, Oikawa D, Shimizu Y, Ishiwata-Kimata Y, Kohno K. 2004. A role for BiP as an adjustor for the endoplasmic reticulum stress-sensing protein Ire1. *J Cell Biol* **167**: 445-456.

Kohno K, Normington K, Sambrook J, Gething MJ, Mori K. 1993. The promoter region of the yeast KAR2 (BiP) gene contains a regulatory domain that responds to the presence of unfolded proteins in the endoplasmic reticulum. *Mol Cell Biol* **13**: 877-890.

Korennykh AV, Egea PF, Korostelev AA, Finer-Moore J, Zhang C, Shokat KM, Stroud RM, Walter P. 2009. The unfolded protein response signals through high-order assembly of Ire1. *Nature* **457**: 687-693.

Kozutsumi Y, Segal M, Normington K, Gething MJ, Sambrook J. 1988. The presence of malfolded proteins in the endoplasmic reticulum signals the induction of glucose-regulated proteins. *Nature* **332**: 462-464.

Lee KP, Dey M, Neculai D, Cao C, Dever TE, Sicheri F. 2008. Structure of the dual enzyme Ire1 reveals the basis for catalysis and regulation in nonconventional RNA splicing. *Cell* **132**: 89-100.

Li H, Korennykh AV, Behrman SL, Walter P. 2010. Mammalian endoplasmic reticulum stress sensor IRE1 signals by dynamic clustering. *Proc Natl Acad Sci U S A* **107**: 16113-16118.

Lin JH, Li H, Yasumura D, Cohen HR, Zhang C, Panning B, Shokat KM, Lavail MM, Walter P. 2007. IRE1 signaling affects cell fate during the unfolded protein response. *Science* **318**: 944-949.

Liu CY, Schroder M, Kaufman RJ. 2000. Ligand-independent dimerization activates the stress response kinases IRE1 and PERK in the lumen of the endoplasmic reticulum. *J Biol Chem* **275**: 24881-24885.

Liu CY, Xu Z, Kaufman RJ. 2003. Structure and intermolecular interactions of the luminal dimerization domain of human IRE1alpha. *J Biol Chem* **278**: 17680-17687.

Ma K, Vattem KM, Wek RC. 2002. Dimerization and release of molecular chaperone inhibition facilitate activation of eukaryotic initiation factor-2 kinase in response to endoplasmic reticulum stress. *J Biol Chem* **277**: 18728-18735.

Mimura N, Fulciniti M, Gorgun G, Tai YT, Cirstea D, Santo L, Hu Y, Fabre C, Minami J, Ohguchi H et al. 2012. Blockade of XBP1 splicing by inhibition of IRE1alpha is a promising therapeutic option in multiple myeloma. *Blood* **119**: 5772-5781.

Mori K. 2009. Signalling pathways in the unfolded protein response: development from yeast to mammals. *J Biochem* **146**: 743-750.

Murthy VL, Stern LJ. 1997. The class II MHC protein HLA-DR1 in complex with an endogenous peptide: implications for the structural basis of the specificity of peptide binding. *Structure* **5**: 1385-1396.

Nadanaka S, Okada T, Yoshida H, Mori K. 2007. Role of disulfide bridges formed in the luminal domain of ATF6 in sensing endoplasmic reticulum stress. *Mol Cell Biol* **27**: 1027-1043.

Ng DT, Watowich SS, Lamb RA. 1992. Analysis in vivo of GRP78-BiP/substrate interactions and their role in induction of the GRP78-BiP gene. *Mol Biol Cell* **3**: 143-155.

Niwa M, Patil CK, DeRisi J, Walter P. 2005. Genome-scale approaches for discovering novel nonconventional splicing substrates of the Ire1 nuclease. *Genome Biol* **6**: R3.

Novoa I, Zeng H, Harding HP, Ron D. 2001. Feedback inhibition of the unfolded protein response by GADD34-mediated dephosphorylation of eIF2alpha. *J Cell Biol* **153**: 1011-1022.

Oikawa D, Kimata Y, Kohno K, Iwawaki T. 2009. Activation of mammalian IRE1alpha upon ER stress depends on dissociation of BiP rather than on direct interaction with unfolded proteins. *Exp Cell Res* **315**: 2496-2504.

Oikawa D, Kimata Y, Takeuchi M, Kohno K. 2005. An essential dimer-forming subregion of the endoplasmic reticulum stress sensor Ire1. *Biochem J* **391**: 135-142.

Okamura K, Kimata Y, Higashio H, Tsuru A, Kohno K. 2000. Dissociation of Kar2p/BiP from an ER sensory molecule, Ire1p, triggers the unfolded protein response in yeast. *Biochem Biophys Res Commun* **279**: 445-450.

Otero JH, Lizak B, Hendershot LM. 2010. Life and death of a BiP substrate. *Semin Cell Dev Biol* **21**: 472-478.

Papa FR, Zhang C, Shokat K, Walter P. 2003. Bypassing a kinase activity with an ATP-competitive drug. *Science* **302**: 1533-1537.

Papandreou I, Denko NC, Olson M, Van Melckebeke H, Lust S, Tam A, Solow-Cordero DE, Bouley DM, Offner F, Niwa M et al. 2011. Identification of an Ire1alpha endonuclease specific inhibitor with cytotoxic activity against human multiple myeloma. *Blood* **117**: 1311-1314.

Pincus D, Chevalier MW, Aragon T, van Anken E, Vidal SE, El-Samad H, Walter P. 2010. BiP binding to the ER-stress sensor Ire1 tunes the homeostatic behavior of the unfolded protein response. *PLoS Biol* **8**: e1000415.

Promlek T, Ishiwata-Kimata Y, Shido M, Sakuramoto M, Kohno K, Kimata Y. 2011. Membrane aberrancy and unfolded proteins activate the endoplasmic reticulum stress sensor Ire1 in different ways. *Mol Biol Cell* **22**: 3520-3532.

Rubio C, Pincus D, Korennykh A, Schuck S, El-Samad H, Walter P. 2011. Homeostatic adaptation to endoplasmic reticulum stress depends on Ire1 kinase activity. *J Cell Biol* **193**: 171-184.

Scheuner D, Song B, McEwen E, Liu C, Laybutt R, Gillespie P, Saunders T, Bonner-Weir S, Kaufman RJ. 2001. Translational control is required for the unfolded protein response and in vivo glucose homeostasis. *Mol Cell* **7**: 1165-1176.

Schrodinger, LLC. 2010. The PyMOL Molecular Graphics System, Version 1.3r1.

Shamu CE, Cox JS, Walter P. 1994. The unfolded-protein-response pathway in yeast. *Trends Cell Biol* **4**: 56-60.

Shamu CE, Walter P. 1996. Oligomerization and phosphorylation of the Ire1p kinase during intracellular signaling from the endoplasmic reticulum to the nucleus. *EMBO J* **15**: 3028-3039.

Shen JS, Chen X, Hendershot L, Prywes R. 2002. ER stress regulation of ATF6 localization by dissociation of BiP/GRP78 binding and unmasking of golgi localization signals. *Dev Cell* **3**: 99-111.

Shen JS, Snapp EL, Lippincott-Schwartz J, Prywes R. 2005. Stable binding of ATF6 to BiP in the endoplasmic reticulum stress response. *Mol Cell Biol* **25**: 921-932.

Sidrauski C, Cox JS, Walter P. 1996. tRNA ligase is required for regulated mRNA splicing in the unfolded protein response. *Cell* **87**: 405-413.

Smith MH, Ploegh HL, Weissman JS. 2011. Road to ruin: targeting proteins for degradation in the endoplasmic reticulum. *Science* **334**: 1086-1090.

Stern LJ, Brown JH, Jardetzky TS, Gorga JC, Urban RG, Strominger JL, Wiley DC. 1994. Crystal structure of the human class II MHC protein HLA-DR1 complexed with an influenza virus peptide. *Nature* **368**: 215-221.

Sun LP, Seemann J, Goldstein JL, Brown MS. 2007. Sterol-regulated transport of SREBPs from endoplasmic reticulum to Golgi: Insig renders sorting signal in Scap inaccessible to COPII proteins. *P Natl Acad Sci USA* **104**: 6519-6526.

Tabas I, Ron D. 2011. Integrating the mechanisms of apoptosis induced by endoplasmic reticulum stress. *Nat Cell Biol* **13**: 184-190.

Todd-Corlett A, Jones E, Seghers C, Gething MJ. 2007. Lobe IB of the ATPase domain of Kar2p/BiP interacts with Ire1p to negatively regulate the unfolded protein response in Saccharomyces cerevisiae. *J Mol Biol* **367**: 770-787.

Travers KJ, Patil CK, Wodicka L, Lockhart DJ, Weissman JS, Walter P. 2000. Functional and genomic analyses reveal an essential coordination between the unfolded protein response and ER-associated degradation. *Cell* **101**: 249-258.

Urano F, Wang X, Bertolotti A, Zhang Y, Chung P, Harding HP, Ron D. 2000. Coupling of stress in the ER to activation of JNK protein kinases by transmembrane protein kinase IRE1. *Science* **287**: 664-666.

Volkmann K, Lucas JL, Vuga D, Wang X, Brumm D, Stiles C, Kriebel D, Der-Sarkissian A, Krishnan K, Schweitzer C et al. 2011. Potent and selective inhibitors of the inositol-requiring enzyme 1 endoribonuclease. *J Biol Chem* **286**: 12743-12755.

Walter P, Ron D. 2011. The unfolded protein response: from stress pathway to homeostatic regulation. *Science* **334**: 1081-1086.

Wang XZ, Kuroda M, Sok J, Batchvarova N, Kimmel R, Chung P, Zinszner H, Ron D. 1998. Identification of novel stress-induced genes downstream of chop. *EMBO J* **17**: 3619-3630.

Wiseman RL, Zhang YH, Lee KPK, Harding HP, Haynes CM, Price J, Sicheri F, Ron D. 2010. Flavonol Activation Defines an Unanticipated Ligand-Binding Site in the Kinase-RNase Domain of IRE1. *Mol Cell* **38**: 291-304.

Ye J, Rawson RB, Komuro R, Chen X, Dave UP, Prywes R, Brown MS, Goldstein JL. 2000. ER stress induces cleavage of membrane-bound ATF6 by the same proteases that process SREBPs. *Mol Cell* **6**: 1355-1364.

Yoshida H, Haze K, Yanagi H, Yura T, Mori K. 1998. Identification of the cis-acting endoplasmic reticulum stress response element responsible for transcriptional induction of mammalian glucose-regulated proteins - Involvement of basic leucine zipper transcription factors. *J Biol Chem* **273**: 33741-33749.

Yoshida H, Matsui T, Yamamoto A, Okada T, Mori K. 2001. XBP1 mRNA is induced by ATF6 and spliced by IRE1 in response to ER stress to produce a highly active transcription factor. *Cell* **107**: 881-891.

Zhou J, Liu CY, Back SH, Clark RL, Peisach D, Xu Z, Kaufman RJ. 2006. The crystal structure of human IRE1 luminal domain reveals a conserved dimerization interface required for activation of the unfolded protein response. *Proc Natl Acad Sci U S A* **103**: 14343-14348.

Zinszner H, Kuroda M, Wang X, Batchvarova N, Lightfoot RT, Remotti H, Stevens JL, Ron D. 1998. CHOP is implicated in programmed cell death in response to impaired function of the endoplasmic reticulum. *Genes Dev* **12**: 982-995.

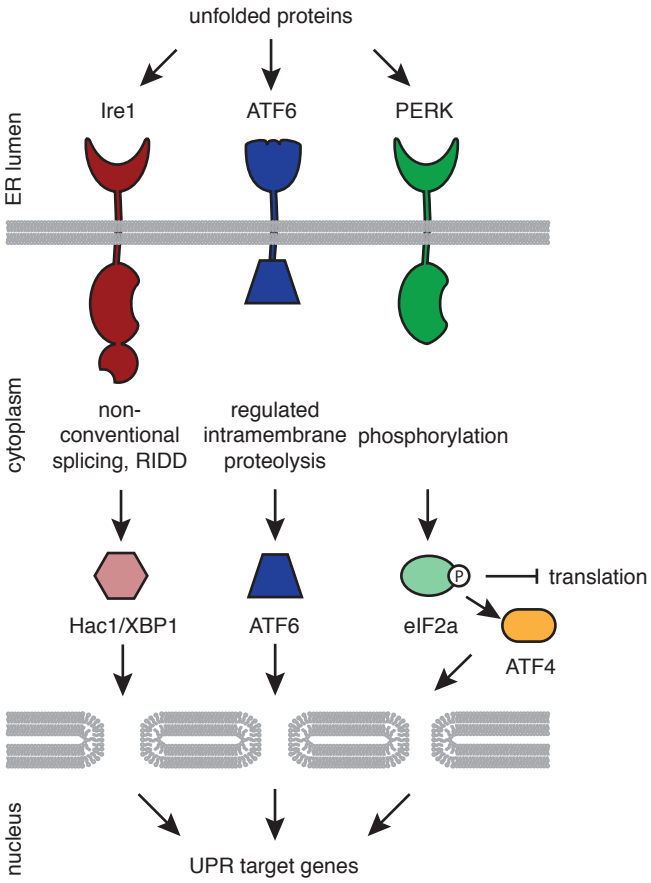
unfolded proteins
Ire1
ATF6
PERK
ER lumen
cytoplasm
non-
conventional
splicing, RIDD
regulated
intramembrane
proteolysis
phosphorylation
translation
Hac1/XBP1
ATF6
eIF2a
ATF4
nucleus
UPR target genes

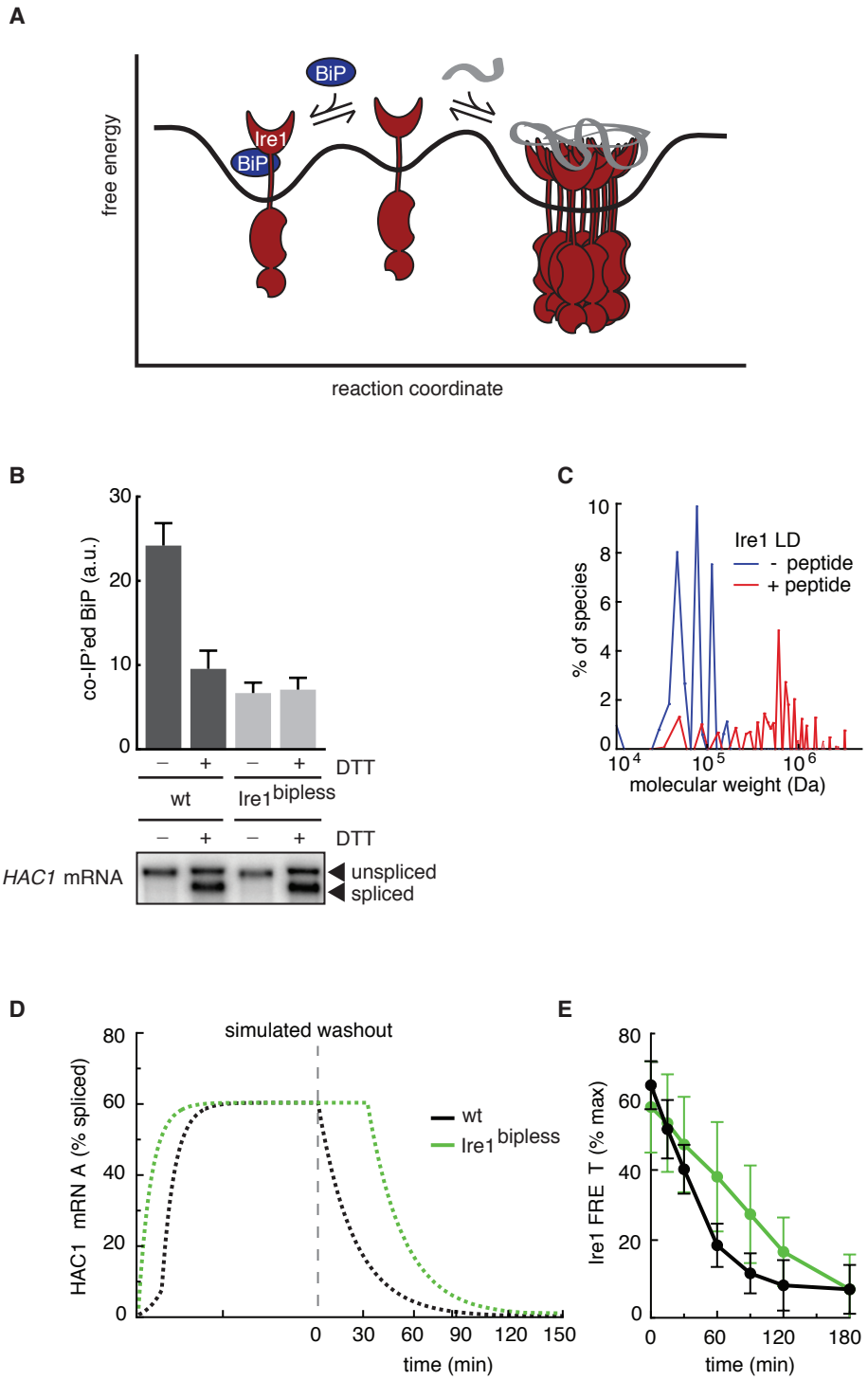
A
BiP
Ire1
BiP
free energy
reaction coordinate
B
co-IP'ed BiP (a.u.)
30
20
10
0
– + – +
DTT
wt
Ire1bipless
– + – +
DTT
HAC1 mRNA
unspliced
spliced
C
% of species
10
8
6
4
2
0
Ire1 LD
- peptide
+ peptide
10 4
10 5
10 6
molecular weight (Da)
D
simulated washout
HAC1 mRN A (% spliced)
80
60
40
20
0
wt
Ire1 bipless
0 30 60 90 120 150
time (min)
E
Ire1 FRE T (% max)
80
60
40
20
0
0 60 120 180
time (min)

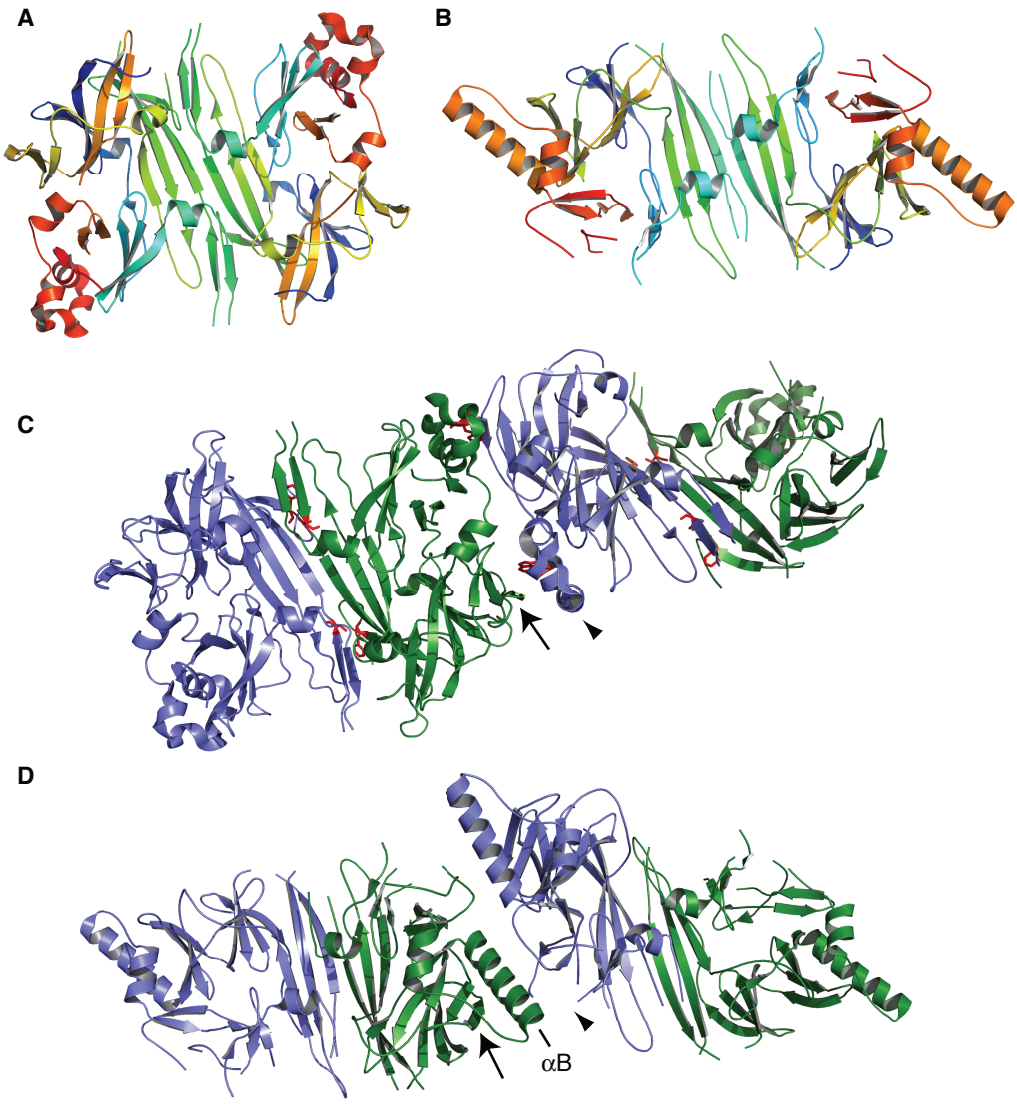
A
B
C
D
αB

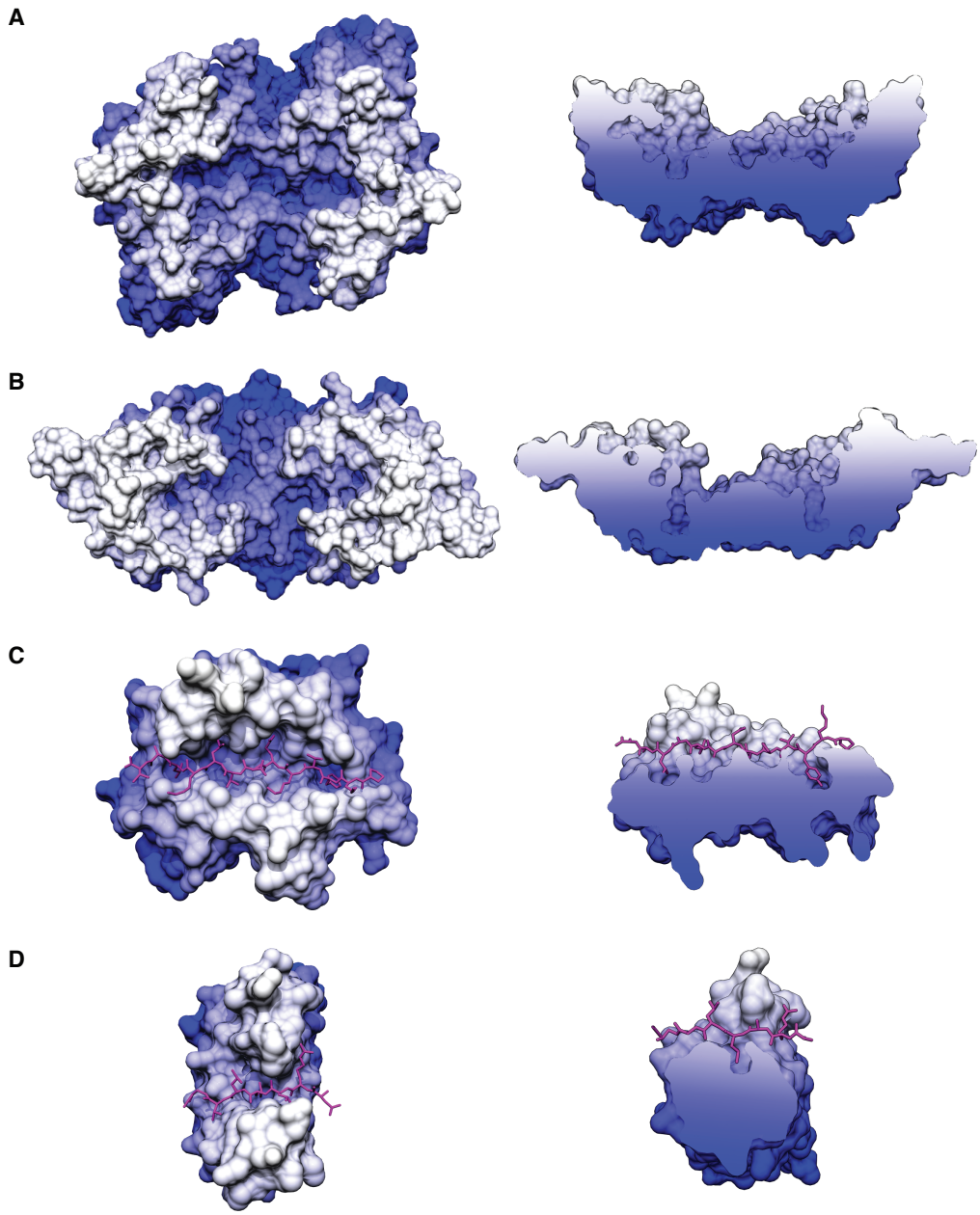
A
B
C
D

Chapter 2

BiP Binding to the ER-Stress Sensor Ire1 Tunes the Homeostatic Behavior of the Unfolded Protein Response

BiP Binding to the ER-Stress Sensor Ire1 Tunes the Homeostatic Behavior of the Unfolded Protein Response

David Pincus[1,2], Michael W. Chevalier[1], Tomás Aragón[1,2¤a], Eelco van Anken[1,2¤b], Simon E. Vidal[1], Hana El-Samad[1]*, Peter Walter[1,2]

1 Department of Biochemistry and Biophysics, University of California at San Francisco, San Francisco, California, United States of America, **2** Howard Hughes Medical Institute, University of California at San Francisco, San Francisco, California, Unites States of America

Abstract

The unfolded protein response (UPR) is an intracellular signaling pathway that counteracts variable stresses that impair protein folding in the endoplasmic reticulum (ER). As such, the UPR is thought to be a homeostat that finely tunes ER protein folding capacity and ER abundance according to need. The mechanism by which the ER stress sensor Ire1 is activated by unfolded proteins and the role that the ER chaperone protein BiP plays in Ire1 regulation have remained unclear. Here we show that the UPR matches its output to the magnitude of the stress by regulating the duration of Ire1 signaling. BiP binding to Ire1 serves to desensitize Ire1 to low levels of stress and promotes its deactivation when favorable folding conditions are restored to the ER. We propose that, mechanistically, BiP achieves these functions by sequestering inactive Ire1 molecules, thereby providing a barrier to oligomerization and activation, and a stabilizing interaction that facilitates de-oligomerization and deactivation. Thus BiP binding to or release from Ire1 is not instrumental for switching the UPR on and off as previously posed. By contrast, BiP provides a buffer for inactive Ire1 molecules that ensures an appropriate response to restore protein folding homeostasis to the ER by modulating the sensitivity and dynamics of Ire1 activity.

Citation: Pincus D, Chevalier MW, Aragón T, van Anken E, Vidal SE, et al. (2010) BiP Binding to the ER-Stress Sensor Ire1 Tunes the Homeostatic Behavior of the Unfolded Protein Response. PLoS Biol 8(7): e1000415. doi:10.1371/journal.pbio.1000415

Academic Editor: Jeffrey W. Kelly, Scripps Research Institute, United States of America

Received February 9, 2010; **Accepted** May 27, 2010; **Published** July 6, 2010

Funding: DP is supported by a graduate fellowship from the NSF; HES is supported by the NSF, NIH, NCI, the Packard foundation, and Sandler family foundation. PW is an Investigator of the HHMI. This work was partially funded by NCI award U54CA143836 to HES. The funders had no role in study design, data collection and analysis, decision to publish, or preparation of the manuscript.

Competing Interests: The authors have declared that no competing interests exist.

Abbreviations: DTT, dithiothreitol; ER, endoplasmic reticulum; FRET, fluorescence resonance energy transfer; GFP, green fluorescent protein; PDI, protein disulfide isomerase; SR, splicing reporter; TR, transcriptional reporter; UPR, unfolded protein response

* E-mail: helsamad@biochem.ucsf.edu

¤a Current address: Department of Hepatology and Gene Therapy, Center for Applied Medical Research, Pamplona, Spain
¤b Current address: Division of Genetics and Cell Biology, San Raffaele Scientific Institute, Milan, Italy

Introduction

The secreted and membrane-spanning proteins that eukaryotic cells use to sense and respond to their environments and to communicate with other cells are functional only when they attain their proper three-dimensional structures. Folding of these proteins takes place in the endoplasmic reticulum (ER), aided by molecular chaperones. Degradation pathways help to discard misfolded proteins. When cells experience environmental stresses, nutrient depletion, or certain differentiation cues, the ER folding and degradation machineries can become overwhelmed and the cell risks accumulating and secreting malfunctional and potentially harmful proteins [1]. Such conditions of ER stress activate the unfolded protein response (UPR) [2], resulting in an expanded ER [3,4] and increased expression of genes encoding ER chaperones, ER associated degradation machinery, and other components of the secretory pathway [5]. As such, the UPR provides a feedback loop that helps cells maintain high fidelity in protein folding and assembly.

The UPR plays a fundamental role in maintaining cellular homeostasis and is therefore at the center of many normal physiological responses and pathologies. For example, when the severity of ER stress exceeds the capacity of the UPR to restore homeostasis, mammalian cells commit to apoptosis [2]. Furthermore, the UPR is activated in many cancer cells [6,7,8] as well as during familial protein-folding and neurodegenerative diseases [9,10]. Deficiencies in UPR signaling can also lead to diabetes [11]. Thus, the UPR constitutes an important control module whose core signaling machinery, which is conserved from yeast to humans, proves critical for cell physiology.

Misfolded secretory proteins accumulate in the ER lumen. The UPR is initiated in that compartment when the transmembrane sensor molecule Ire1 self-associates and activates its cytoplasmic endoribonuclease domain [12,13,14,15]. Activated Ire1 transmits the signal by removing a non-conventional intron from its mRNA substrates, *HAC1* mRNA in yeast and XBP1 mRNA in metazoans, which upon subsequent ligation are translated to produce potent transcriptional activators of UPR target genes [16,17,18]. Since the Hac1 protein is short-lived (half-life of ~2 min) [18,19], Ire1 activity is the key determinant of the magnitude and duration of the UPR.

Despite early clues for Ire1's role as a central UPR regulator, the mechanism by which it senses unfolded proteins remains disputed. One model proposes that Ire1 activity is mainly

Author Summary

Secreted and membrane-spanning proteins constitute one of every three proteins produced by a eukaryotic cell. Many of these proteins initially fold and assemble in the endoplasmic reticulum (ER). A variety of physiological and environmental conditions can increase the demands on the ER, overwhelming the ER protein folding machinery. To restore homeostasis in response to ER stress, cells activate an intracellular signaling pathway called the unfolded protein response (UPR) that adjusts the folding capacity of the ER according to need. Its failure impairs cell viability and has been implicated in numerous disease states. In this study, we quantitatively interrogate the homeostatic capacity of the UPR. We arrive at a mechanistic model for how the ER stress sensor Ire1 cooperates with its binding partner BiP, a highly redundant ER chaperone, to fine-tune UPR activity. Moving between a predictive computational model and experiments, we show that BiP release from Ire1 is not the switch that activates Ire1; rather, BiP modulates Ire1 activation and deactivation dynamics. BiP binding to Ire1 and its dissociation in an ER stress-dependent manner buffers the system against mild stresses. Furthermore, BiP binding accelerates Ire1 deactivation when stress is removed. We conclude that BiP binding to Ire1 serves to fine-tune the dynamic behavior of the UPR by modulating its sensitivity and shutoff kinetics. This function of the interaction between Ire1 and BiP may be a general paradigm for other systems in which oligomer formation and disassembly must be finely regulated.

regulated by the ER-resident chaperone BiP (Kar2 in yeast). In this model, BiP inhibits Ire1 activity by binding to it in the absence of stress. During stress, BiP is titrated away by unfolded proteins, leaving Ire1 free to oligomerize and activate. This model was suggested because immunoprecipitation experiments showed that Ire1 interacts with BiP in unstressed cells and dissociates from BiP under ER stress conditions [20,21,22]. Site directed mutagenesis of BiP yielded mutants that do not bind to Ire1 [23], but since they failed to support growth when expressed as the only copy of BiP, they are difficult to interpret mechanistically in view of the many pleiotropic functions of BiP. By contrast, mutants of Ire1 lacking the juxtamembrane segment of its lumenal domain that is responsible for BiP binding retained regulation: mutant Ire1 was inactive in the absence of ER stress and activated in its presence [15,22,24,25], thus suggesting that BiP release and rebinding are not causal for switching Ire1 on and off.

An alternative model of Ire1 regulation postulates that unfolded proteins bind to the lumenal domain of Ire1, triggering Ire1 self-association and activation of its cytoplasmic effector domains. Support for such activation of Ire1 by direct binding to unfolded proteins stems from structural studies of the Ire1 lumenal domain that revealed a putative peptide binding groove [24]. Mutational probing experiments demonstrated that the residues pointing into the groove are required for signaling [24].

Recently a hybrid, two-step model for UPR regulation has been proposed in which both BiP and unfolded proteins regulate Ire1: initial dissociation of BiP from Ire1 drives its oligomerization, while subsequent binding to unfolded proteins leads to its activation [15]. This model posits that BiP regulates Ire1 oligomerization, yet oligomerization is not sufficient for Ire1 activation. However, in vitro experiments demonstrated that the oligomerization state of the cytoplasmic domains of Ire1 determines the rate of enzymatic activity [12].

Thus, while genetic and biochemical analyses of the UPR have been immensely successful in elucidating many aspects of the UPR's unusual signal transduction mechanism, a coherent model of Ire1 regulation and the involvement of BiP has remained elusive. In this work, we study the UPR as a coordinated homeostatic system by carrying out measurements of the time dynamics of the pathway across a wide range of ER stress levels. Using population-based assays of UPR activity complemented with dynamic dose-resolved flow cytometry and a predictive computational model, we dissect the role of BiP in modulating the sensitivity and duration of the UPR. Specifically, by comparing the wild type UPR to a strain bearing a mutant version of Ire1 that lacks the UPR-specific BiP interaction motif, we show that BiP prevents Ire1 from activating in response to low levels of stress and that it aids in Ire1 deactivation once the stress has been alleviated. Using a single cell Ire1 FRET assay, we provide evidence suggesting that BiP performs these functions by sequestering inactive Ire1 molecules. By buffering Ire1, BiP ensures that only appropriate levels of stress trigger the UPR and that the duration of UPR induction matches the magnitude of the stress. These data position BiP as a modulator of the dynamic properties of the UPR.

Results

The Unfolded Protein Sensor Ire1 Undergoes Activation and Deactivation

Most UPR studies to date have been carried out under saturating conditions, where induction of protein folding damage surpasses the homeostatic capacity of the UPR and hence remains unmitigated. To position the experimental system in a physiological regime where cells proliferate efficiently when the UPR functions adequately, we probed the response to depletion of the metabolite inositol [26]. In the absence of inositol in the growth media, Ire1 is required for cells to induce the expression of genes required for inositol synthesis as part of the UPR transcriptional program [27]. To monitor UPR induction dynamics following this stimulus, we depleted inositol in a yeast culture and assayed for Ire1 activity as reflected by the splicing of *HAC1* mRNA observed on Northern blots (Figure 1A, see Methods). After a lag phase—presumably the time required to exhaust residual inositol stores—*HAC1* mRNA splicing reached a maximal level by 120 min, and then declined during an adaptation phase to recover near basal levels by 240 min. Population growth slowed during the induction phase but was restored upon recovery (Figure S1A). Thus, the UPR indeed functions as a homeostat in response to inositol depletion: the lack of inositol triggers activation of the biosynthetic pathway via Ire1, which initially overshoots and then settles at a new basal level that meets the cells' needs to grow under the new conditions. In this example, our detection of *HAC1* mRNA splicing was not sensitive enough to detect a difference between the starting condition and the new basal level. However, blotting for the UPR target *INO1* mRNA, which encodes inositol 1-phosphate synthase required for *de novo* inositol synthesis, demonstrated that the readjusted level at the 240 min time point was elevated compared to the un-induced system (Figure 1A, right panel), as was the expression of a UPR reporter (Figure S1B).

To determine whether similar adaptation also occurs after Ire1 activation in response to other modes of UPR induction, we treated cells with DTT, a reducing agent that counteracts disulfide bond formation and thereby induces protein misfolding in the ER. Disulfide bonds are formed through a relay in which ER client proteins are initially oxidized by protein disulfide isomerase (PDI). PDI is in turn oxidized by the FAD-dependent oxidase Ero1, which is finally oxidized by molecular oxygen [28].

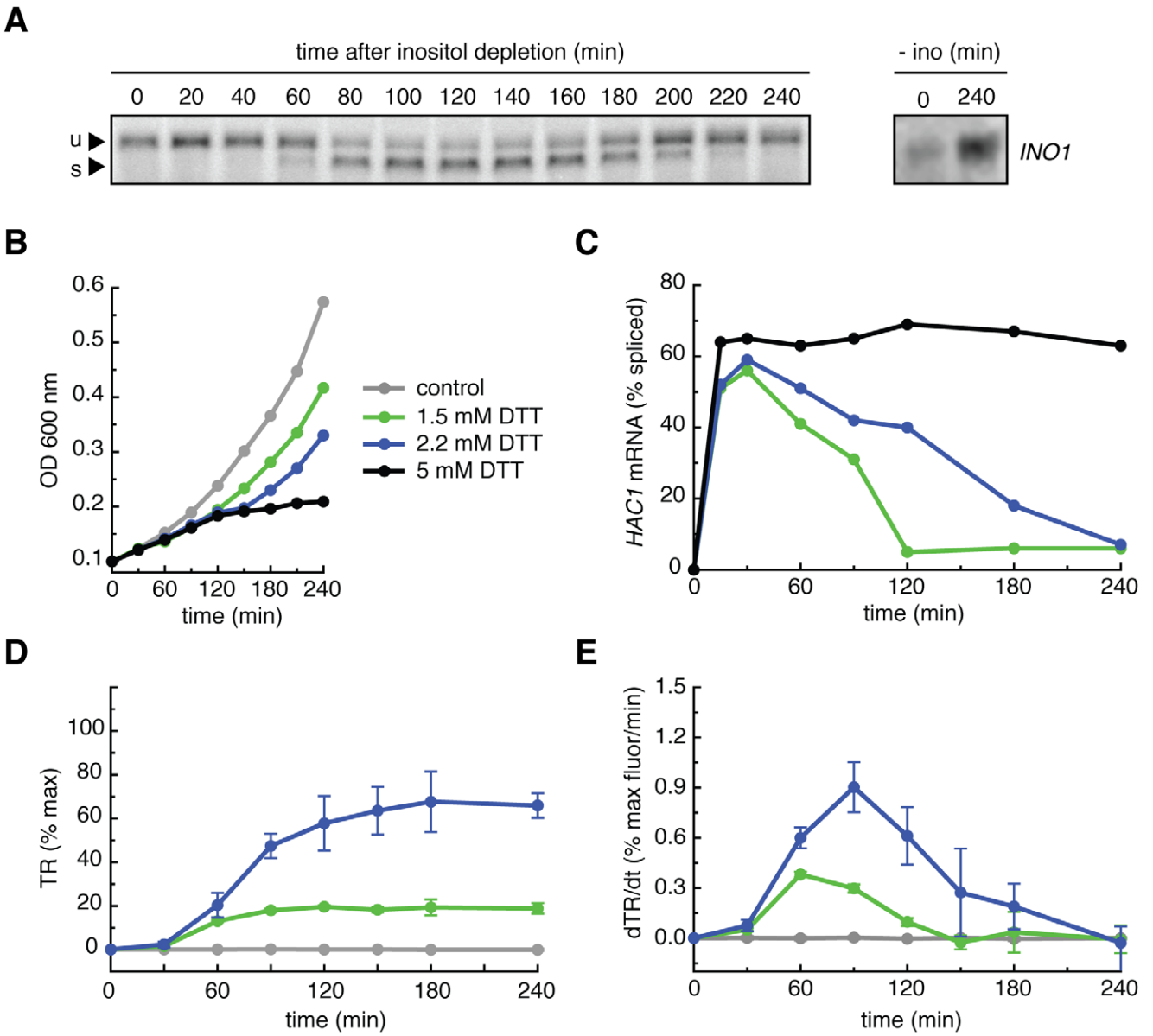

Figure 1. Transient Ire1 activation in non-lethal ER stress conditions. (A) After depletion of inositol from the growth media, wild type yeast cells were sampled from a master culture every 20 min, and total RNA was purified and subjected to Northern blot analysis using a probe for the first exon of *HAC1* mRNA. After a lag phase, *HAC1* mRNA splicing displayed activation and deactivation phases. u, unspliced *HAC1* mRNA; s, spliced *HAC1* mRNA. Right panel: wild type cells 0 min and 240 min after inositol depletion and probed for the *INO1* mRNA. (B) Cell growth was monitored over time in wild type cells treated with 5 mM, 2.2 mM, 1.5 mM, and 0 mM DTT by measuring the OD_{600}. Cells treated with 5 mM DTT cease to divide, while cells treated with 2.2 mM or 1.5 mM DTT continue to grow. (C) Wild type cells were treated with 5 mM, 2.2 mM, or 1.5 mM DTT and sampled over time. After Northern blot analysis, the percentage of spliced *HAC1* mRNA was quantified (blots are shown in the supplement). Cells treated with 5 mM DTT displayed sustained maximal splicing, while cells treated with 2.2 mM or 1.5 mM displayed transient *HAC1* mRNA splicing: the same activation and deactivation phases as the response to the depletion of inositol. (D) Wild type cells were constructed bearing a transcriptional reporter (TR) consisting of four repeats of a UPR-responsive DNA element controlling the expression of GFP. These cells were treated with 2.2 mM, 1.5 mM, or 0 mM DTT, sampled over time, and subjected to flow cytometry to quantify the GFP fluorescence. The TR was induced to dose-dependent plateaus due to the >8 h half life of GFP. % max is defined as the GFP fluorescence in cells treated with 5 mM DTT for 4 h. (E) When plotted as the rate of GFP produced per minute, the TR displayed the same activation and deactivation phases as spliced *HAC1* mRNA. Transient Ire1 activation leads to transient transcriptional activation. % max as defined in (D).
doi:10.1371/journal.pbio.1000415.g001

Both *PDI* and *ERO1* are UPR target genes, but since Ero1 directly passes the electrons to molecular oxygen, its abundance limits oxidative capacity. Thus, we reasoned that for moderate amounts of DTT, UPR-mediated induction of *ERO1* would compensate for the increased demand for oxidation, allowing Ire1 to deactivate.

To test this, we treated cells with a range of DTT concentrations. Cells treated with 5 mM DTT no longer proliferated, indicating the presence of a maximal ER stress beyond which cells can no longer compensate effectively even in the presence of a maximally active UPR (Figure 1B, black). By contrast, cells treated with 2.2 mM or 1.5 mM DTT continued to

Table 1. Plasmids used in this study.

Plasmid	Description	Marker
pDEP005	SR, pRS305-Phac1-h5′-GFP-h3′	LEU2
pDEP007	Ire1-GFP, wt IRE1-GFP in pRS305	LEU2
pDEP010	Ire1-mCherry, wt IRE1 in pRS306	URA3
pDEP017	TR, pRS304-4×UPRE-GFP	TRP1
pDEP044	2 μ plasmid, wt IRE1 in pRS423	HIS3
pDEP045	2 μ plasmid, Ire1bipless in pRS423	HIS3
pDEP049	$Ire1^{bipless}$, pRS306-PIre1-$Ire1^{bipless}$	URA3
pDEP053	$Ire1^{bipless}$-GFP, pRS306-PIre1-$Ire1^{bipless}$-GFP	URA3
pDEP060	$Ire1^{biipless}$-mCherrry, pRS305-Ire1bipless-mCherry	LEU2

doi:10.1371/journal.pbio.1000415.t001

proliferate, albeit at rates decreased from control cells (Figure 1B, purple and green). To investigate whether these growth phenotypes correlated with the activation and deactivation of the UPR, we monitored Ire1 activation by measuring *HAC1* mRNA splicing as above (Figure S2). Consistent with the observed growth arrest, Ire1 activation was maximal and sustained in 5 mM DTT (Figure 1C, black): *HAC1* mRNA was spliced to its full extent 30 min after DTT addition and splicing was maintained at this high level for the duration of the experiment. By contrast, in cells treated with doses of 2.2 mM or 1.5 mM DTT, Ire1 deactivation occurred in 4 h and 2 h, respectively (Figure 1C, blue and green). Therefore, under non-saturating DTT conditions, cells show the same transient Ire1 activity that characterized the response to inositol depletion. Furthermore, the duration of that transient response increased along with the magnitude of the stress.

To ascertain that the Ire1 activation and deactivation phases are reflective of the regulation of UPR target genes, we measured the expression of a synthetic UPR-regulated GFP transcriptional reporter (TR) over time in cells treated with 1.5 or 2.2 mM DTT (Figure 1D, E, see Methods). In these cells, the TR was induced to dose-dependent plateaus after a lag of approximately 30 min. The lag is consistent with the time required for transcription, translation, and GFP chromophore maturation, while the plateaus reflect the accumulation of the long-lived GFP reporter protein (half-life >8 h). Induction of a natural UPR target promoter, *ERO1*, closely matched the response from the synthetic TR (Figure S3). Therefore, the expression of UPR target genes at any given time is reflected by the rate of GFP production, rather than its abundance. When plotted as a function of the rate of GFP production (dTR/dt; Figure 1E), the TR exhibited activation and deactivation phases at 1.5 and 2.2 mM DTT that mirrored the dynamics of upstream *HAC1* mRNA splicing (compare Figure 1C and 1E).

Taken together, the data shown in Figure 1 indicate that under different inducing stimuli, the UPR undergoes induction and adaptation phases that are reflected in the transient splicing activity of its sensor Ire1. Ire1 activity, in turn, is faithfully transmitted to the system's transcriptional output.

$Ire1^{bipless}$ Is Stress-Inducible But Can Organize in Small Foci in the Absence of Stress

To assess whether the activation and adaptation properties of Ire1 are dependent on BiP binding and dissociation, we expressed a mutant form of Ire1, $Ire1^{bipless}$, lacking a 51 amino acid segment ($Ire1^{\Delta 475-526,GKSG}$) that contains the BiP binding site (see Methods, Tables 1, 2). While similar to the $Ire1^{\Delta V}$ mutant described in [22], $Ire1^{bipless}$ retains 10 amino acids defined in the crystal structure of the core lumenal domain [24] that were deleted in $Ire1^{\Delta V}$. As previously reported, wild type Ire1 associated with BiP in a co-immunoprecipitation assay in the absence of ER stress (Figure 2A, B) but the association diminished when cells were treated for 1 h with 5 mM DTT (Figure 2A, B). By contrast, no change in the association of $Ire1^{bipless}$ and BiP was observed between stressed and unstressed cells (Figure 2A, B). The residual binding of BiP to $Ire1^{bipless}$ is likely due to non-specific absorption of the notoriously sticky chaperone (Figure 2A, B). As the amount does not change between UPR-induced and uninduced cells, this residual interaction does not reflect a physiologically important regulatory interaction.

Table 2. Yeast strains used in this study.

Yeast Strain	Description	Markers Used
YDP001	wild type, CRY1, w303a derivative	none
YDP002	Δire1, CRY1 Δire1::KAN	KANr
YDP003	wt SR, CRY1 SR::LEU	LEU
YDP005	wt TR, CRY1 TR::TRP	TRP
YDP007	Ire1-GFP, Δire1, Ire1-GFP::LEU	LEU
YDP010	Ire1-mCherry, Δire1, Ire1-mCherry::URA	URA
YDP012	FRET, Δire1, Ire1-GFP::LEU, Ire1-mCherry::URA	LEU, URA
YDP015	Δhac1, Δhac1::TRP	TRP
YDP016	Δhac SR, Δhac1::TRP, SR::LEU	LEU, TRP
YDP020	$Ire1^{bipless}$, Δire1::KAN, $Ire1^{bipless}$::URA	KANr, URA
YDP021	$Ire1^{bipless}$ SR, Δire1::KAN, $Ire1^{bipless}$::URA, SR::LEU	KANr, URA, LEU
YDP025	$Ire1^{bipless}$-GFP, Δire1::KAN, $Ire1^{bipless}$-GFP::URA	KANr, URA
YDP030	$Ire1^{bipless}$-mCherry Δire1::KAN, $Ire1^{bipless}$-mCherry::LEU	KANr, LEU
YDP036	$Ire1^{bipless}$ FRET, Δire1::KAN, $Ire1^{bipless}$-GFP::URA,	KANr, URA, LEU
	Ire1bipless-mCherry::LEU	

doi:10.1371/journal.pbio.1000415.t002

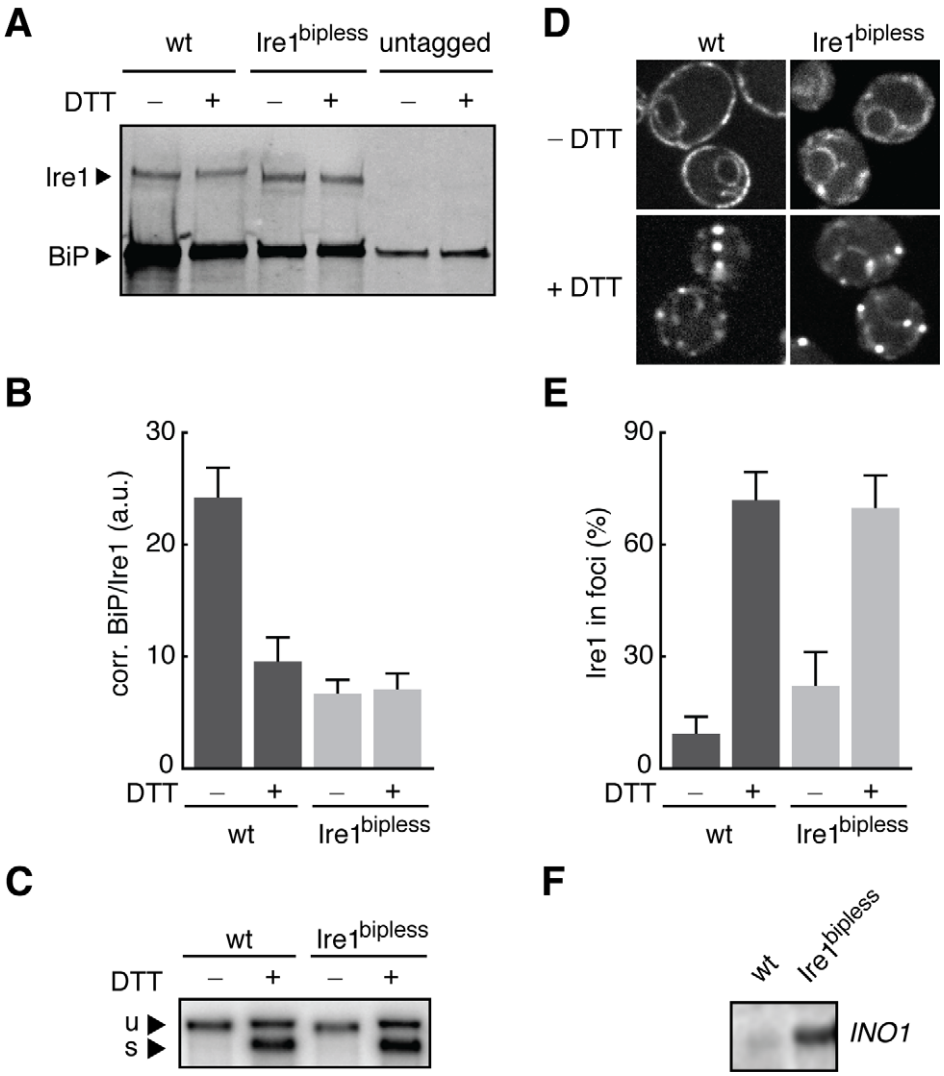

Figure 2. Ire1^{bipless} is stress-activated with no change to its association with BiP. (A) Ire1^{bipless} is a mutant of Ire1 lacking 51 amino acids containing the BiP interaction motif (Δ475–526). Cells bearing HA-tagged alleles of wild type Ire1 or Ire1^{bipless} were harvested before and after treatment with 5 mM DTT for 1 h. Cells were lysed and Ire1 and Ire1^{bipless} were immuno-precipitated with anti-HA agarose beads. The proteins eluted from the beads were resolved by SDS-PAGE, transferred to PVDF, co-incubated with anti-HA and anti-BiP antibodies followed by fluorophore-conjugated secondary antibodies, and scanned on the Li-Cor imager. BiP decreased its association with wild type Ire1 after treatment with DTT, while BiP did not change its association with Ire1^{bipless} after DTT treatment. Some BiP binds nonspecifically. (B) Three independent immunoprecipitation experiments were quantified after scanning with the Li-Cor. The ratio of BiP/Ire1, after subtraction of the nonspecific BiP signal as measured in the *Ire1*Δ cells, shows that BiP dissociates from wild type Ire1 in response to DTT, that Ire1^{bipless} binds to less BiP in the absence of stress than wild type Ire1 binds in the presence of DTT, and that Ire1^{bipless} does not change its association with BiP after treatment with DTT. (C) Cells bearing wild type Ire1 or Ire1^{bipless} were harvested before and after treatment with 5 mM DTT for 1 h, total RNA was purified, subjected to Northern blot analysis, and probed for *HAC1* mRNA. Wild type and Ire1^{bipless} displayed no differences in splicing: no *HAC1* mRNA was spliced in the absence of DTT and splicing was equally induced after treatment with DTT. (D) GFP-tagged alleles of wild type Ire1 and Ire1^{bipless} were expressed and imaged in the presence and absence of DTT. GFP domains are inserted between the transmembrane domain and the linker of the kinase domain on the cytoplasmic side of Ire1, as in [13]. Wild type Ire1 displays a diffuse perinuclear and cortical ER localization in the absence of stress and forms bright clusters after treatment of 5 mM DTT for 1 h. Ire1^{bipless} displays similar perinuclear and cortical localization in the absence of stress, but with small clusters in some cells. After DTT treatment, Ire1^{bipless} forms clusters like the wild type. (E) Quantification of Ire1 clustering shows that Ire1^{bipless} forms more foci in the absence of stress than wild type, but forms clusters equal to the wild type after treatment with 5 mM DTT for 1 h. (F) Wild type and ire^{bipless} cells in the absence of stress probed for basal expression of *INO1* mRNA expression.
doi:10.1371/journal.pbio.1000415.g002

To determine whether the diminished association between Ire1^{bipless} and BiP impacts Ire1 activation, we measured *HAC1* mRNA splicing in wild type cells and cells expressing Ire1^{bipless} grown in the presence and absence of 5mM DTT for 1 h (Figure 2C). In both wild type and Ire1^{bipless} cells, no detectable *HAC1* mRNA was spliced in the absence of stress, and splicing was identically induced in the two strains after treatment with DTT. These data refute any model that poses modulation of the BiP•Ire1 association as the exclusive regulator of Ire1 activity.

Next, we investigated the subcellular localization of Ire1^{bipless} in the presence and absence of ER stress. In response to ER stress, wild type Ire1 oligomerizes in clusters in the ER membrane that appear as discrete foci in fluorescence microscopy images [14,15]. Similar to wild type GFP-tagged Ire1, GFP-tagged Ire1^{bipless}

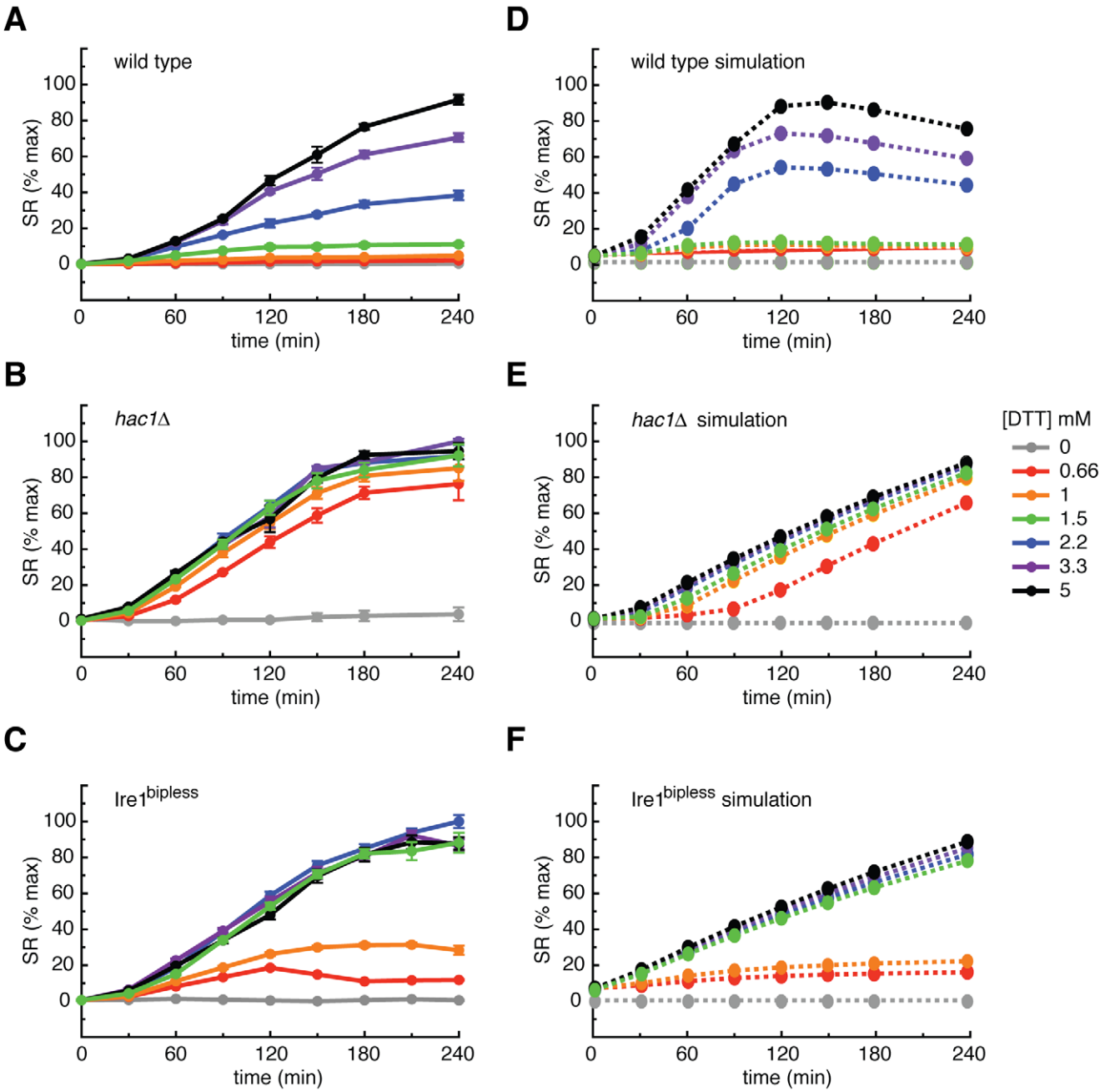

Figure 3. Experimental and simulated DTT titration time courses in wild type, *hac1*Δ, and Ire1^{bipless} cells. (A) Wild type cells expressing the GFP splicing reporter (SR) were treated with doses of DTT spanning the active concentration range, sampled over time, and their fluorescence was measured by flow cytometry. The SR, like the TR, reached dose-dependent plateaus due to the >8 h half life of GFP. (B) *hac1*Δ cells expressing the SR were treated as above. *hac1*Δ cells were hypersensitive to DTT and saturate the reporter at all experimental doses. (C) Ire1^{bipless} cells expressing the SR were treated as above and showed increased sensitivity to DTT compared to the wild type, responding to 0.66 mM DTT and saturating at 1.5 mM DTT. (D) Simulations of the "wild type" model. The architecture of the model, described in the text and depicted in Figure 4A, includes BiP binding to Ire1 and negative feedback. When the model includes a cooperative Ire1 deactivation term (described in text), it recapitulated the wild type DTT titration time course. (E) Simulations of the "*hac1*Δ" in which the negative feedback terms have been removed captured the hypersensitivity observed experimentally. (F) Simulations of the "Ire1^{bipless}" model in which the Ire1/BiP interaction terms have been removed revealed the increased DTT sensitivity compared to the wild type.
doi:10.1371/journal.pbio.1000415.g003

displayed cortical and perinuclear ER localization in the absence of stress and formed bright foci in cells treated for 1 h with 5 mM DTT (Figure 2D). Quantification revealed that Ire1^{bipless} formed foci of equal magnitude to the wild type protein upon UPR induction. In unstressed cells, however, Ire1^{bipless} displayed a 2-fold increase in the level of clustering compared to wild type Ire1 (Figure 2E), and the foci exhibited considerable cell-to-cell variability (Figure S4, see Discussion).

The increased clustering of Ire1^{bipless} did not apparently lead to activation, since a Northern blot of total RNA from cells bearing

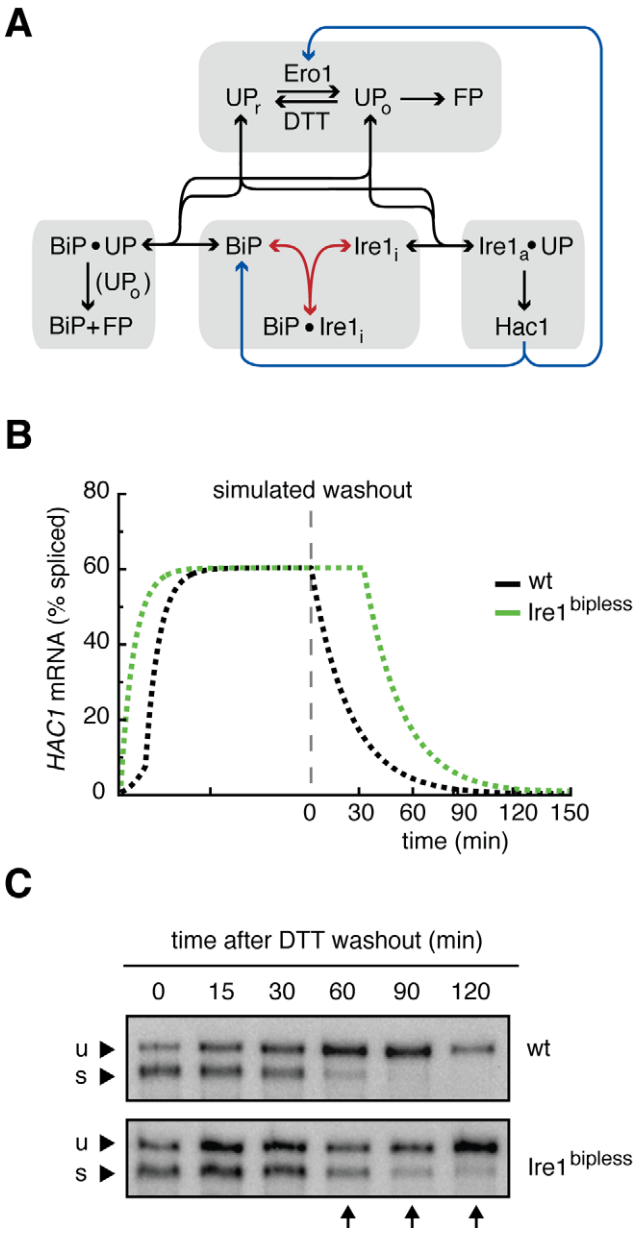

Figure 4. Model architecture, prediction and experimental validation. (A) The molecular interactions that comprise the model. See the supplement for complete modeling details. Ire1 can exist in three states: (1) inactive monomer (Ire1$_i$, middle lower box), (2) inactive in complex with BiP (Ire1$_i$•BiP, middle lower box), and (3) active in complex with an unfolded protein (Ire1$_a$•UP, lower right box). Either reduced (UP$_r$) or oxidized (UP$_o$) can bind to and activate Ire1, but UP$_o$s quickly become folded proteins (FP, upper box and lower left box). The amount of UP$_r$s and UP$_o$s is determined by the flux of unfolded proteins and the red/ox potential, defined here as the ratio of Ero1/DTT. Active Ire1 in complex with unfolded proteins produces the Hac1 transcription factor, which induces the production of Ero1 and BiP. BiP can also exist in three states: (1) monomer (BiP, middle lower box), (2) bound to Ire1$_i$ (BiP•Ire1$_i$), and (3) in complex with unfolded proteins (BiP•UP). BiP can bind to both UP$_r$ and UP$_o$, but only aids in the folding of UP$_o$ (bottom left box). The blue arrows indicate the feedback terms that are removed in the "*hac1*Δ" model, and the red arrows indicate the Ire1/BiP interaction terms that are removed in the "Ire1^{bipless}" model. (B) Simulations "wild type" and "Ire1^{bipless}" cells treated with 5 mM DTT for 100 min and then the DTT is suddenly removed predict a deactivation delay for Ire1^{bipless} cells: "wild type" cells immediately began to deactivate while Ire1^{bipless} continued activity for ~30 min after DTT withdrawal. (C) Wild type and Ire1^{bipless} were treated with 5 mM DTT for 1 h, filtered, washed, and resuspended in fresh media lacking DTT and sampled over time. Samples were assayed for *HAC1* mRNA splicing by Northern blot to measure Ire1 activity. Consistent with the simulations, wild type cells deactivated after 90 min while Ire1^{bipless} cells deactivated after 180 min.
doi:10.1371/journal.pbio.1000415.g004

Ire1^{bipless} did not show detectable amounts of spliced *HAC1* mRNA in the absence of stress (Figure 2C). We considered it possible that splicing occurred at a level below the detection limit of the Northern blot assay. This reasoning is supported by Northern blots for *INO1* mRNA, which is a more sensitive indicator of UPR induction as demonstrated above (Figure 1A, right). Indeed, *INO1* mRNA was significantly elevated in cells expressing Ire1^{bipless} as compared to cells expressing wild type Ire1 under non-inducing conditions (Figure 2F). Furthermore, there is a notable increase in the basal signal from a UPR reporter in unstressed Ire1^{bipless} cells (Figure S5). Thus, UPR signaling in Ire1^{bipless} cells is leaky.

Ire1^{bipless} Cells Are Sensitized to Low Levels of ER Stress

The propensity of Ire1^{bipless} to form small clusters in the absence of stress prompted us to ask if cells bearing Ire1^{bipless} would be more sensitive than wild type to low levels of stress. To test this notion, we expressed a GFP splicing reporter (SR), in which the first exon of the *HAC1* open reading frame is replaced by GFP (Figure S6A). The *HAC1* intron represses translation of the mRNA, so GFP is only produced once active Ire1 removes the intron. Using flow cytometry, the SR allowed us to precisely quantify Ire1 activity over time in wild type and Ire1^{bipless} cells. The SR did not compete with endogenous *HAC1* mRNA for Ire1 when wild type cells were treated with 5 mM DTT for 1 h (Figure S6B), and similar to the TR, the GFP encoded by the SR decayed with a half-life of >8 h.

When wild type cells expressing the SR were treated with increasing concentrations of DTT, the SR was induced to dose-dependent plateaus (Figure 3A), and the rate of GFP production displayed the peak and decline behavior characteristic of the splicing of endogenous *HAC1* mRNA (dSR/dt; Figure S7A). Consistent with the data shown in Figure 1, cells expressing wild type Ire1 were insensitive to DTT at concentrations below 1.5 mM as apparent from the absence of SR induction. By contrast, *hac1*Δ cells were hypersensitive to DTT: they induced the SR to near maximal levels at all doses (Figure 3B), and the rate of GFP production remained high until the reporter saturated (Figure S7B). In the absence of *HAC1*, Ire1 activation fails to initiate a transcriptional response, and the stress is never alleviated.

Interestingly, Ire1^{bipless} cells showed an intermediate SR phenotype. Ire1^{bipless} cells were more sensitive to DTT than wild type cells, becoming activated at 0.66 mM DTT and saturated at 1.5 mM DTT (Figures 3C, S7C). These data are consistent with the notion that increased clustering in Ire1^{bipless} cells in the absence of DTT is coupled with sensitization, which allows activation at low levels of stress.

A Computational Model of Ire1 Regulation Recapitulates the Enhanced Sensitivity of the UPR in Ire1^{bipless} Cells

To validate that our data are consistent with a model of Ire1 regulation that includes interactions with unfolded proteins and BiP and to provide hypotheses for how BiP could specifically contribute to Ire1 regulation, we built a computational model of the UPR with the following assumptions (see Text S1). Ire1 can

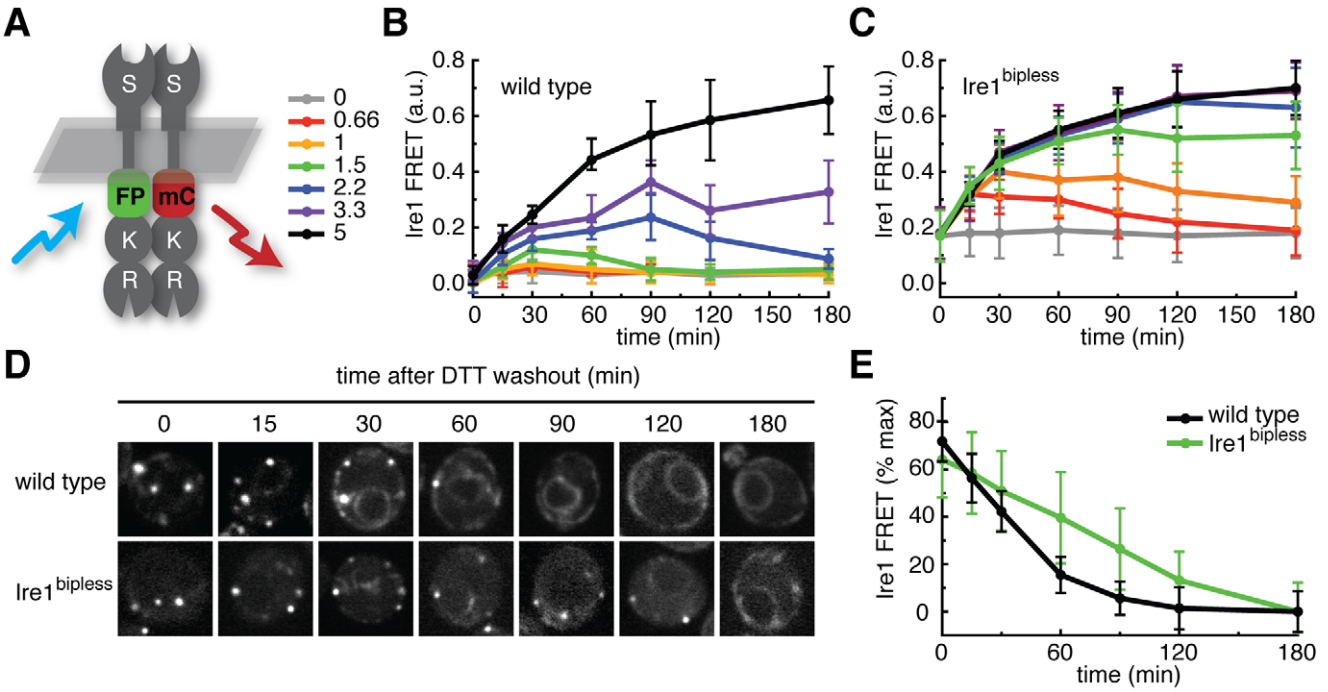

Figure 5. FRET measurements of wild type Ire1 and Ire1^{bipless}. (A) Cartoon of Ire1 FRET. GFP- and mCherry-tagged versions of Ire1 or Ire1^{bipless} were co-expressed and cells were imaged by confocal microscopy. GFP and mCherry domains are inserted between the transmembrane domain and the kinase linker on the cytoplasmic side of Ire1, as in [13]. When exposed to blue light (488 nm) the GFP is excited, and if it is within a few nm of mCherry, it can excite mCherry instead of emitting green light. This transferred energy is emitted by mCherry as red light and can be measured as a FRET signal. (B) DTT titration time course measured by FRET in wild type cells. Ire1 displayed transient oligomerization after treatment with 2.2 mM or 1.5 mM DTT, and sustained oligomerization in response to 5 mM DTT. Doses are indicated in (C). (C) DTT titration time course measured by FRET in Ire1^{bipless} cells. Ire1^{bipless} displayed sustained oligomerization after treatment with 2.2 mM or 1.5 mM DTT, and transient activation after treatment with 0.66 and 0.99 mM DTT. (D) Cells expressing FRET pairs of wild type Ire1 (top panels) or Ire1^{bipless} (bottom panels) were treated with 5 mM DTT for 1 h and subsequently washed, resuspended in fresh media, and imaged by confocal microscopy. (E) Quantification of FRET signal from DTT washout experiment. Wild type Ire1 de-oligomerized completely by 90 min, while Ire1^{bipless} did not fully de-oligomerize for 180 min.
doi:10.1371/journal.pbio.1000415.g005

exist in one of three states: (i) as a free inactive monomer, (ii) as an inactive complex bound to BiP, or (iii) as an active complex bound to an unfolded protein (Figure 4A). Further, free BiP can bind to unfolded proteins and either productively aid in their folding or nonproductively dissociate. Unfolded proteins are either reduced or oxidized depending on the redox potential of the ER and must be oxidized in order to fold. In the model, the redox potential is set by the ratio of DTT to Ero1. When bound to an unfolded protein, the active Ire1 complex initiates the production of the Hac1 transcription factor, which in turn increases the production of BiP and Ero1 to close the UPR feedback loop. To explicitly model the measured experimental output (GFP fluorescence), the active Ire1 complex was set to trigger the production of a simulated SR in addition to producing Hac1. We extracted available model parameters from the literature and fitted remaining parameters to a subset of the experimental data (Figure S8, see Supporting Information for details). Using this "wild type" model as a baseline for comparison, we generated a "*hac1*Δ" model in which no induced production of BiP or Ero1 exists and an "Ire1^{bipless}" model in which the interaction between Ire1 and BiP is disabled (Figure 4A).

The functional form of the dissociation of the active Ire1/unfolded protein complex was a modeling choice. Significantly, a model in which this dissociation was assumed to be linear did not reproduce the difference between the wild type and Ire1^{bipless} when the SR time courses were simulated (Figure S9). Instead, a nonlinear, cooperative dissociation function of the active Ire1-unfolded protein complex was required to recapitulate the data; i.e., the dissociation rate of the active Ire1-unfolded protein complex must decrease in proportion to the concentration of the active oligomeric complex raised to a power greater than one. Given that Ire1 signals by clustering into foci, this nonlinear dissociation function can be thought of as a consequence of having to disassemble a cooperative enzyme complex (Figure S10, see Discussion). When simulated with such nonlinear dissociation of the active Ire1 complex, the model robustly recapitulated the DTT titration time course results in wild type, *hac1*Δ, and Ire1^{bipless} cells (Figure 3D–F). When the SR time course was simulated with the wild type Ire1 model, doses of DTT of 1.5 mM and below produced less than 10% activity, 2.2 mM DTT produced an approximately half-maximal response, 3.3 mM DTT produced a response of approximately 75% of the maximum, and 5 mM DTT produced a near saturating response (Figure 3D). By contrast, simulation of the *hac1*Δ model produced near saturating responses to all doses, recapitulating the hypersensitivity measured in vivo (Figure 3E). Furthermore, simulation of the Ire1^{bipless} model yielded an intermediate phenotype in which 0.66 mM DTT produced 15% activity, and doses of 1.5 mM DTT and above saturated the response (Figure 3F). Importantly, this agreement between the model simulations and experimental data was an emergent property of the functional interactions in the system, which arose independently of the choice of parameter values (Figures S11, S12).

In Silico Modeling Predicts a Role for BiP in Ire1 Deactivation Kinetics

In addition to accounting for the increased sensitivity of Ire1^{bipless} compared to the wild type in the DTT titration time course experiments, our computational model predicted that Ire1^{bipless} should exhibit delayed shutoff dynamics compared to the wild type after DTT is removed (Figure 4B).

This prediction can be rationalized in intuitive terms. When DTT is removed, disulfide bonds can form and proteins can mature. Thus the concentration of the ligand for Ire1 activation starts to decrease, and individual Ire1 molecules dissociate from the active oligomer. When wild type Ire1 dissociates, it can either rejoin the signaling complex (through interaction with an unfolded protein), or it can bind to BiP. Therefore, Ire1 deactivation proceeds rapidly since the inactive free form can be sequestered away by binding to BiP. In contrast, Ire1^{bipless} lacks the ability to interact with BiP. Thus, while DTT removal will still prompt the dissociation of Ire1 from the active oligomer as the concentration of unfolded proteins decreases, the inability of Ire1^{bipless} to bind to BiP increases the probability that an inactive Ire1^{bipless} monomer will be recaptured by an unfolded protein and reactivate. As a result, Ire1^{bipless} deactivation would proceed more slowly than that of wild type Ire1.

To test this prediction experimentally, we performed a DTT washout experiment in which wild type and Ire1^{bipless} cells were treated with 5 mM DTT for 1 h to fully activate Ire1 in both strains. Subsequently, DTT was removed by filtration, cells were washed and resuspended in fresh media, and samples were collected over time to assay for *HAC1* mRNA splicing by Northern blot (Figure 4C). Additional samples of wild type cells were collected to assay for the association of Ire1 and BiP by immunoprecipitation (Figure S13). Confirming the model predictions, we found that while Ire1 deactivated after 60 min in the wild type, Ire1^{bipless} retained activity for 120 min. As expected, Ire1 deactivation correlated with re-association with BiP (Figure S13). These results point to a role for BiP binding in promoting Ire1 deactivation once stress has been alleviated.

FRET Measurements of Ire1 Oligomers Reveal a Mechanistic Role for BiP in Ire1 Deactivation

To pursue the mechanism through which Ire1 deactivation proceeds, we hypothesized that, since Ire1 signals through assemblies of high-order oligomers, BiP binding may sequester breakaway Ire1 monomers, therefore promoting de-oligomerization of active Ire1 complexes. If this were the case, Ire1^{bipless} cells should exhibit slower disappearance of Ire1 oligomers than wild type cells upon removal of stress.

To directly test this hypothesis, we co-expressed GFP- and mCherry-tagged versions of Ire1 or Ire1^{bipless} and employed a microscopy-based fluorescence resonance energy transfer (FRET) assay [29] to quantify Ire1 self-association (Figures 5A, S14, see Methods). In an otherwise wild type scenario, the FRET signal displayed a broad dynamic range, from 0.01 a.u. (s.e.m. = 0.02, $n = 36$) in untreated cells in which the Ire1 fluorescence displayed a diffuse ER localization to 0.73 a.u. (s.e.m. = 0.06, $n = 41$) in cells treated with 5 mM DTT for 4 h, in which Ire1 is maximally clustered into foci (Figure S6B). In Ire1^{bipless} cells, the basal FRET signal in the absence of DTT was elevated to 0.17 a.u. (s.e.m. = 0.09, $n = 53$), but the maximum FRET signal in the presence of DTT (0.71 a.u., s.e.m. = 0.08, $n = 32$) was comparable to wild type. As expected, wild type cells displayed transient increases in FRET signal that returned to baseline levels over the course of the experiment after treatment with 2.2 or 1.5 mM DTT (Figure 5B, C). In contrast, Ire1^{bipless} cells were sensitized and displayed transient increases in FRET signal only when treated with 0.66 mM or 0.99 mM DTT but showed persistent strong FRET signal when treated with 1.5 mM or 2.2 mM DTT. These data recapitulate the role of BiP in buffering the Ire1 to low levels of stress (Figure 3).

To assess the role of BiP in the de-oligomerization of Ire1, we performed a DTT washout experiment and measured Ire1 FRET over time in wild type and Ire1^{bipless} cells (Figure 5D, E). After treatment of both strains with 5 mM DTT for 1 h, we washed the cells in fresh media lacking DTT and imaged the cells over time. Consistent with the deactivation kinetics of wild type and Ire1^{bipless} cells as measured by Northern blot, wild type Ire1 de-oligomerization proceeded rapidly and the FRET signal returned to baseline after 60 min. By contrast, the Ire1^{bipless} FRET signal remained higher than basal levels at 120 min. Taken together, these data indicate that BiP binding to Ire1 contributes to the efficient de-oligomerization of active Ire1 complexes.

Discussion

In this work, we investigated the homeostatic properties of the UPR in response to a range of physiological stress levels. Using time-resolved measurements of the induction and adaptation kinetics of the wild type UPR and a mutant UPR in which the sensor molecule Ire1 is not modulated by the chaperone BiP, we established a model for dynamic UPR regulation. In this model, Ire1 is principally activated when unfolded proteins bind to it directly. In a dynamic equilibrium, binding to unfolded proteins pulls Ire1 into oligomeric clusters and away from the chaperone BiP. Oligomerization, which occurs as a direct consequence of unfolded protein binding to Ire1's lumenal domain, is necessary and sufficient for Ire1 activation, and as such is the central control point in the UPR. Rather than regulating the first step of Ire1 activation, BiP provides superimposed modulation of the UPR's dynamic properties. Specifically, BiP assumes a dual role in which it simultaneously acts as a buffer to reduce the system's sensitivity to low stress levels and as a timer to tune the response time to the magnitude of stress by assisting in Ire1 deactivation once homeostasis is restored to the ER. The model establishes the UPR as a dynamic system whose capacity is adjusted to efficiently counteract a large spectrum of stress magnitudes and suggests a long-sought role for BiP binding to Ire1.

The UPR Is a Homeostat

When cells experience protein folding stress in the ER, the UPR is activated to increase the ER's folding capacity. For manageable stress magnitudes, the UPR is capable of restoring folding homeostasis. However, if the magnitude of the stress surpasses the capacity of the UPR, yeast cells sustain maximal Ire1 signaling and cease to proliferate (Figure 1B, C). Within the physiological regime of ER stress, the response of Ire1 to moderate DTT inputs (1.5 mM and 2.2 mM DTT, Figure 1C) displayed transient activation dynamics, followed by adaptation to near basal levels. Interestingly, the duration of Ire1 activity—not the maximal amplitude of its activity—correlated with the magnitude of the stress. Since the Hac1 transcription factor is short-lived, the length of the Ire1 activation pulse should determine the duration of UPR target gene activation by Hac1 [18,19]. This in turn determines the volume of the ER and the concentration of ER chaperones, components of the degradation machinery, and other cytoprotective proteins that are produced to combat the stress. This mode of signal regulation in which the duration of the output matches the magnitude of the input is known in engineering as "pulse-width

modulation." It is widely employed to reduce noise in engineered control systems by transforming an analog signal (amplitude) into a digital all-or-none pulse of varying length [30].

Although in principle real-time information about the folding status of the cell could be conveyed exclusively through the interaction of unfolded proteins with Ire1 to determine the duration of UPR induction, we find that BiP plays an important role in modulating the length of the Ire1 activation pulse (Figures S6A,C, 5B,C). Perhaps this modulating role of BiP reflects the necessity for precise tuning of the Ire1 pulse beyond what can be achieved through Ire1 and unfolded proteins alone. Interestingly, it was recently shown that a mutant of mammalian Ire1α shares salient properties with Ire1^{bipless}: it does not bind to BiP, retains ER stress inducibility, and displays increased basal activity [31]. Therefore, it seems likely that the role of BiP in buffering Ire1 oligomerization is conserved in mammalian cells. Moreover, as the transmembrane kinase PERK, which in metazoan cells functions in a parallel UPR signaling branch to Ire1, shares close sequence homology to Ire1's lumenal domain, lessons learned for Ire1 modulation by BiP are likely to also apply to PERK regulation.

Precise tuning, and subsequently the buffering role of BiP, becomes all the more important since the UPR is linked to crucial cell fate decisions such as commitment to apoptosis [32]. The decision to commit to apoptosis might depend directly on the time of exposure to stress or on a thresholding mechanism through which either the extent of cellular damage or UPR machinery are assessed. Both scenarios would translate into an enhanced commitment to apoptosis in the absence of BiP modulation of Ire1.

BiP Buffers Ire1's Switch-Like Activity

As detailed above, precision homeostasis in the UPR requires the pathway-specific interaction of Ire1 and BiP. Disruption of this interaction in vivo leads to increased sensitivity to low levels of stress ("leakiness"), coupled to slower deactivation of Ire1 once stress is removed (Figure 4C). By using FRET to measure Ire1 self-association, we found that BiP performs these functions by aiding Ire1 de-oligomerization (Figure 5C–E). In vitro, Ire1 functions as a cooperative enzyme with a Hill coefficient >8, and the active species are large oligomers [12]. This high cooperativity could translate in vivo to a switch-like response of Ire1 to small changes in the concentration of unfolded proteins. For example, it follows from basic principles of enzyme kinetics that if Ire1 signals in clusters of 16 molecules, a mere 35% increase in unfolded proteins would cause Ire1 to go from 10% to 90% active. In this light, BiP's role as a binding partner that desensitizes Ire1 can be viewed as a gatekeeper that prevents triggering of the Ire1 activation switch following small or transient fluctuations in the local concentration of unfolded proteins. By doing so, BiP works to ensure that Ire1 is only activated when the stress is sufficient to warrant a response, thus improving information quality in the signaling pathway [33].

It is formally possible that in addition to loss of its UPR-specific BiP interaction Ire1^{bipless} retains its ER-stress dependent activation, yet displays altered activation dynamics due to non-native conformational interactions. However, since Ire1^{bipless} oligomerizes and activates in a ligand-specific manner to the same extent as wild type Ire1, we contend that in the simplest scenario, Ire1^{bipless}, like the previous "bipless" mutant Ire1$^{\Delta V}$ [22,25], is a structurally sound molecule that is activated by the same mechanism that activates wild type Ire1.

Though similar to Ire1^{bipless}, Ire1$^{\Delta V}$ was not shown to be hypersensitive to DTT or to deactivate after washout with delayed kinetics [22]. However, Ire1$^{\Delta V}$ did display hypersensitivity to heat shock and delayed deactivation kinetics in response to ethanol [22]. While the discrepancies between Ire1^{bipless} and Ire1$^{\Delta V}$ may be due to differences in experimental resolution, the elevated response of Ire1$^{\Delta V}$ to heat shock and ethanol is consistent with the notion that BiP buffers Ire1 to these mild ER stresses.

Ire1 Regulation Reconstituted in Silico Holds Clues to the Mechanisms of Ire1 Modulation by BiP

Our study of the intricate UPR dynamics was guided by a computational model which was able to recapitulate our data and generate useful predictions. In the model, BiP serves as a buffer to the pool of inactive Ire1. By binding to free Ire1, BiP sequesters the inactive form of Ire1 and both prevents activation at low levels of stress and promotes deactivation once the stress has been overcome (Figures 3D–F, 4B).

This mechanism of Ire1 activation in our model contrasts with the two-step Ire1 activation model [15], in which unfolded proteins first trigger BiP dissociation from Ire1 to induce oligomerization, and subsequently bind to the oligomers to activate signaling. As opposed to separating oligomerization and activation into two steps, our model treats unfolded protein binding as the single activating step; Ire1 is in dynamic equilibrium with BiP and unfolded proteins, and its unfolded protein bound state is active. Thus, BiP dissociation, rather than triggering oligomerization, yields monomeric Ire1, which can then either bind to an unfolded protein and activate or re-bind to BiP. We note that the small Ire1^{bipless} foci that formed in the absence of stress resulted in increased expression of *INO1* mRNA and increased basal levels of UPR reporter fluorescence (Figures 1A, S5). Thus, we never observed inactive foci, in support of our model that oligomerization and activation occur in the same step.

In addition to this different mechanism of Ire1 activation, our model also proposes a mechanism for Ire1 deactivation. Since BiP and unfolded proteins compete for Ire1, BiP serves as a buffer that allows rapid deactivation of Ire1 as the concentration of unfolded proteins decreases. Finally, in contrast to the static picture of Ire1 activation presented in the two-step model, we present a time-resolved, quantitative model that accurately portrays Ire1 activation in response to any dose of DTT over time in its activation and adaptation phases.

While the computational model reflects our current understanding of Ire1 regulation, it is likely to be an oversimplification. Next generation models could easily improve the verisimilitude by including additional ER processes that are not currently represented in the model (such as glycosylation, ERAD, and BiP's ATP hydrolysis cycle) or better constraining the model parameters by targeted measurements. Yet even with increasing mechanistic detail the requirement for cooperative Ire1 deactivation is likely to persist (Figure S9). This feature, modeled as decreasing Hill function of active Ire1 molecules, is consistent with the notion that Ire1 signals through assemblies of high-order oligomers. As Ire1 oligomers grow in size or number, the percentage of Ire1 molecules that have the ability to be deactivated decreases as many molecules become captured inside macromolecular assemblies. Such cooperativity in Ire1 deactivation can be depicted intuitively as a simple steric consequence of Ire1 oligomerization (Figure S10).

Interestingly, this cooperativity can also be invoked to interpret the increased variability in foci formation in the Ire1^{bipless} mutant cells (Figures S4 and S15). BiP's role can be thought of as a vehicle to help Ire1 traverse the threshold-like inactivation curve. In a wild type cell where focus formation might initiate stochastically, the presence of BiP can accelerate the dissociation of the foci. However, in an Ire1^{bipless} mutant, any stochastically formed focus would be stable for a longer time (Figure 5C–E). If focus

dissolution is an all-or-none process, an extreme scenario is one where Ire1 focus formation in wild type and Ire1^{bipless} cells occurs as a pulse train whose low frequency of activation is the same in both populations. However, the duration of each pulse would be longer in Ire1^{bipless} than in wild type cells. This simplified scenario would result in modest differences in foci formation as averaged over the population since the activation probability is itself low. It would nonetheless result in large variations around this average exhibited by individual cells. According to this view, BiP buffering would ensure that activated Ire1 signaling centers assume a more homogeneous size, providing for a consistent input/output relationship and consistent deactivation kinetics. As such, BiP buffering fine-tunes the UPR by filtering noise from the signal transmission process, thereby increasing the information content of the signal and improving the cell's homeostatic control of the ER.

This mode of regulation by which a free pool of a protein is buffered by chaperones may be a widely used mechanism in biology. For example, many kinases interact with cytosolic chaperones, and kinase signaling receptors that oligomerize during activation may hence be buffered similarly. Moreover, dynamic protein assemblies, such as clathrin coats or SNARE complexes, utilize chaperone interactions to aid disassembly [34,35]. Insights gained from our understanding of the functional consequences of the interaction between BiP and Ire1 may therefore be generally applicable to many other systems, in which protein oligomers have to form and be broken down again in a highly controlled manner.

Methods

Strains and Cell Growth

Reporter constructs and mutant alleles are genomically integrated into wild type or mutant strains. All experiments were conducted in complete, synthetic media (2×SDC: yeast nitrogen base, glucose, complete amino acids).

Reporter Constructs

TR (transcriptional reporter). The TR is GFP under the control of a crippled *cyc1* promoter, containing 4 repeats of a UPR-responsive cis element (4×UPRE).

SR (splicing reporter). The SR is a reporter of Ire1 endonuclease activity. It is expressed from the native *HAC1* promoter and identical to the *HAC1* mRNA except that the first exon has been replaced by that of GFP. The intron, splice sites, and untranslated regions are identical to the *HAC1* mRNA.

Ire1 imaging and FRET reporters. All fluorophore-tagged versions of Ire1 and Ire1^{bipless} have the fluorescent protein (GFP or mCherry) inserted between the transmembrane domain and the cytoplasmic linker that connects the kinase domain to the transmembrane domain, as in [13].

HA-Tagged Constructs. Ire1 and Ire1^{bipless} were c-terminally HA-tagged for immunoprecipitation and immunodetection.

Construction of Ire1^{bipless} and Expression in Yeast Cells

Ire1^{bipless} is an allele of Ire1 that lacks the 51 amino acid juxtamembrane segment of the lumenal domain. This region is not in the crystal structure of the lumenal domain (Credle et al. [24]). Amino acids 475–526 of Ire1 were removed by 2-step PCR cloning and replaced with a 4 amino acid linker (Gly-Lys-Ser-Gly) on an episomal yeast plasmid (pRS315). The resulting positive, sequenced clone (*Ire1^{bipless}*) was sub-cloned onto integrative plasmids (pRS305, pRS306), transformed into *Ire1*Δ cells (YDP002), and shown to complement for growth in the absence of inositol. Imaging constructs of Ire1^{bipless} (GFP- and mCherry-tagged) were created by sub-cloning from the sequenced plasmid into the integrative wild type Ire1-GFP and Ire1-mCherry plasmids used for the FRET experiments. All experiments except the immunoprecipitations were conducted with genomically integrated Ire1^{bipless} constructs.

Northern Blot Analysis

We cultured cells in 2×SDC media to $OD_{600} = 0.4$, collected 50 ml per sample, washed cells in 1 ml 2×SDC and stored pellets at −80°C. Total RNA was extracted by resuspending cells in AE buffer (50 mM NaOAc, pH 5.2, 10 mM EDTA in DEPC-treated water), adding SDS to 1% and acid phenol (pH ~4) (Fisher) to 50%, and heating at 65°C for 10 min. After spinning out the cell remains, we added chloroform and separated by centrifuging in phase-lock tubes (5 Prime). We precipitated the RNA with ethanol, washed with ethanol, and finally dissolved in 50 µl DEPC water.

RNA samples were quantified by spectrophotometry, added to loading buffer (1×E/formamide/formaldehyde/ethidium bromide/bromphenol blue), and heated at 55°C for 15 min. Samples were cooled on ice for 5 min and loaded. The gel is 1.5% agarose/20% formaldehyde/1×E and is run for 270 min at 100 V. Gels were transferred to nitrocellulose by wicking in 10× SSC for 24 h, and RNA crosslinked with 150 J. Blots were pre-hybridized in Church buffer for 3 h at 65°C, and hybridized overnight with random primer-generated probes from a *HAC1* PCR product that incorporated α-^{32}P-CTP using GE ready-to-go beads. Blots were washed in 2× SSC, sealed in plastic, exposed to phosphor-imager screens overnight, imaged with the storm scanner, and quantified with ImageQuant software.

Titration Time Courses and Flow Cytometry

We cultured cells bearing the SR or TR at 30°C in 2× SDC in 96 well deep well plates in an Innova plate shaker at 900 rpm. DTT stocks were made fresh from powder stored at 4°C for each experiment, and always 1 M in 10 ml. From this stock kept on ice, we prepared fresh 5× working stocks to start the experiment by diluting DTT in 1 step into 2× SDC to 37.5 mM (5×7.5 mM) in 10 ml. This 37.5 mM working stock was serially diluted by 1.5-fold increments (6 ml + 3 ml SDC) 10 times to span the range 0.13–7.5 mM. Every 2 h throughout the experiment, we repeated the full dilution series from the 1 M stock, making 1× dilution stocks in 2× SDC. To start the experiment, 200 µl of each 5× stock was added to 800 µl cells in the 96 well plates at time 0. The cells were incubated and shook at 30°C and were sampled every 30 min by 12-channel pipetting 75 µl of each culture into a 96 well microtiter plate. 5 µl of each 75 µl was subjected to flow cytometry analysis using a BD LSR-II equipped with a high throughput sampler, a 488 nm 100 mW laser, FITC emission filter, and FACS DIVA software to compile .fcs files. .fcs files were analyzed in MatLab and/or FloJo. No cuts or gates were applied to cell distributions. Median FITC-A values were calculated for each dose-time point and plotted in ProFit. Errors are calculated from the standard deviation of the median for 3 biological replicates.

Ire1 FRET Assay and Confocal Microscopy

We constructed the experimental FRET strain by co-expressing Ire1-GFP and Ire1-mCherry in the same cell from the endogenous *IRE1* promoter integrated in the genome of an *Ire1*Δ strain and constructed bleed-through control strains by expressing either Ire1-GFP or Ire1-mCherry integrated alone in the deletion strain. FRET assays were performed using a Yokogawa CSU-22 spinning disc confocal on a Nikon TE-2000 inverted microscope equipped

with 150 mW 488 and 562 nm lasers. Cells bearing the reporters were grown in 2× SDC to mid log phase, diluted to $OD_{600} = 0.1$, gently sonicated, and 80 µl added to 96 well glass bottom plates coated with concanavalin-A. Cells were allowed to settle for 20 min before imaging. DTT dilutions were prepared as 5× working stocks as in the titration time course experiments, and 20 µl added to wells at time 0.

Cells were imaged at each time point with 3×3 s exposures: 488 excitation/590 emission (GCh), 562 ex/590 em (ChCh), 488 ex/520 em (GG). Images were processed by first identifying cell boundaries and assigning the 16-bit fluorescence images to individual cells using the open-source cell-id software. Background was calculated by the mean intensity of areas in each fluorescent image not assigned to cells and subtracted from the cellular mean intensities to obtain corrected single cell values for GG, ChCh, and GCh.

The GCh value is a conglomerate of true FRET signal and fluorescent channel bleed-through from the individual fluorophores. The average GCh values from the single-fluorophore control strains were subtracted from the experimental strain GCh values to obtain final corrected values. FRET was calculated for each cell with the formula: F = GCh/(GG*ChCh)^0.5.

For each time point at each dose, we obtained images of three different fields of cells, collecting a total of 30–60 cells per dose per time point. Mean values were plotted in ProFit and error bars represent the standard error of the mean.

Immunoprecipitation and Western Blot Analysis

Cells bearing C-terminally HA-tagged Ire1 or $Ire1^{bipless}$ expressed from the *IRE1* promoter on 2 micron plasmids were cultured, collected, and stored in the same manner as for the Northern blot analysis. Cell pellets were thawed on ice, resuspended in 1 ml IP buffer (50 mM Tris-HCl, pH 8.0, 150 mM NaCl, 1% Triton X-100, protease inhibitors), and subjected to bead-beating (5×1 min, with 2 min on ice between iterations). Beads and cell debris were centrifuged and the cell free lysate was incubated with anti-HA conjugated agarose beads for 2 h at 4°C. Beads were spun, washed 5× with 1 ml IP buffer, and boiled in SDS-PAGE loading buffer.

Samples were run on BioRad ready-gels (4%–15% acrylamide, Tris/glycine/SDS) for 90 min at 35 mA. The proteins were subsequently transferred to Millipore Immobilon PVDF membranes at 220 mA for 45 min. Blots were blocked in 1% casein in TBS (10 mM Tris, 150 mM NaCl) for 30 min, followed by incubation with primary antibodies overnight. The rabbit polyclonal anti-Kar2 was used at 1:5000 dilution, and the mouse anti-HA was used at 1:2000. The next morning, the blots were washed 3× for 10 min with TBS, and then incubated with Li-Cor fluorescently-coupled secondary antibodies, goat anti-mouse 680 and 800, at 1:10,000 dilution for 30 min. Blots were again washed 3× for 10 min with TBS, scanned with the Li-Cor infrared scanner, and processed with the Odyssey software package.

DTT Washout Experiments

Wild type and $Ire1^{bipless}$ were cultured to $OD_{600} = 0.4$ in 400 ml 2×SDC at 30°. Cultures were brought to 500 ml and treated with 5 mM DTT for 1 h. Cells were sampled, filtered onto nitrocellulose membranes with 1 µm pores, washed with 100 ml 2×SDC, and then resuspended in 500 ml 2×SDC and returned to 30° incubation and sampled as indicated. For the FRET washout experiment, 1 ml cultures were spun, washed, resuspended, and imaged.

Supporting Information

Figure S1 Cell growth and UPR target gene expression in the absence of inositol. (A) Inositol was depleted from a yeast culture and growth was monitored over time by optical density. Compared to a logarithmically growing control strain, cells depleted of inositol display a transient growth lag followed by a return to exponential growth. (B) Expression of the TR (see text) measured over time following inositol depletion. The reporter fluorescence continues to increase after the splicing of *HAC1* mRNA has returned to baseline (Figure 1A) and remains elevated.
Found at: doi:10.1371/journal.pbio.1000415.s001 (0.23 MB TIF)

Figure S2 Northern blot time courses of *HAC1* mRNA in cells treated with (A) 1.5, (B) 2.2, and (C) 5 mM DTT.
Found at: doi:10.1371/journal.pbio.1000415.s002 (0.31 MB TIF)

Figure S3 Titration time course of *ERO1* promoter driving expression of GFP. Cells bearing chromosomally integrated *pERO1-GFP* were treated with various doses of DTT and measured over time by flow cytometry. The response from the *ERO1* promoter closely matches the TR and SR.
Found at: doi:10.1371/journal.pbio.1000415.s003 (0.16 MB TIF)

Figure S4 Cell-to-cell variation of $Ire1^{bipless}$. (A) 20 images of individual cells bearing wild type GFP tagged Ire1. The signal is homogenously distributed in the ER. (B) 20 images of individual cells bearing GFP tagged $Ire1^{bipless}$. The signal is diffused in the ER in some cells and clustered to varying degrees in other cells. This increased variation compared to the wild type may indicate that low levels of *HAC1* mRNA splicing may occur in the absence of ER stress, but that this is below the limit of detection by Northern blot once the population has been averaged.
Found at: doi:10.1371/journal.pbio.1000415.s004 (1.58 MB TIF)

Figure S5 Absolute SR fluorescence in wild type, Δ*hac1*, and $Ire1^{bipless}$ cells. Median values of SR fluorescence in unstressed (−) and cells treated with 5 mM DTT for 3 h (+). Error bars represent the standard deviation of three experiments.
Found at: doi:10.1371/journal.pbio.1000415.s005 (0.11 MB TIF)

Figure S6 A single cell reporter of the splicing reaction. (A) Schematic of the splicing reporter (SR) depicting the unspliced mRNA. The SR consists of a GFP-encoding exon, and the intron, splice sites, and untranslated regions identical to the *HAC1* mRNA. (B) Expression of the SR from the *HAC1* promoter does not compete with the endogenous *HAC1* mRNA for Ire1 under ER stress conditions.
Found at: doi:10.1371/journal.pbio.1000415.s006 (0.12 MB DOC)

Figure S7 Rates of SR production across DTT titration time courses. (A) Wild type cells show transient activation at 1.5 and 2.2 mM. (B) *hac1*Δ cells are fully activated until the reporter saturates at all doses. (C) $Ire1^{bipless}$ cells are fully activated at 1.5 and 2.2 mM DTT, and show transient activation at 0.66 and 0.99 mM DTT.
Found at: doi:10.1371/journal.pbio.1000415.s007 (0.29 MB TIF)

Figure S8 Target gene induction function. (A) Function describing the transcriptional induction of UPR target genes, like for most other model parameters, was fit to experimental data found in the literature.
Found at: doi:10.1371/journal.pbio.1000415.s008 (0.30 MB TIF)

Figure S9 Nonlinearity is required to recapitulate the difference between wild type and $Ire1^{bipless}$ cells in a computational model of the UPR. (A) Simulated DTT dose response of "wild type," "*hac1*Δ," and "$Ire1^{bipless}$" models

including a nonlinear term describing the dissociation of the active Ire1-unfolded protein complex. The hypersensitivity of *hac1*Δ and the intermediate sensitivity of Ire1^{bipless} are recapitulated. (B) Simulated washout experiment including nonlinearity matches experimental data. (C) Simulated DTT dose response of "wild type," "*hac1*Δ," and "Ire1^{bipless}" models including only linear terms. No significant difference between wild type and Ire1^{bipless} is predicted. (D) Simulated washout experiment with all linear terms does not recapitulate the experimental results.
Found at: doi:10.1371/journal.pbio.1000415.s009 (0.55 MB TIF)

Figure S10 Heuristic model for the nonlinearity of Ire1 deactivation. (A) Top-down view of an active Ire1 oligomer. The molecules in the middle of the oligomer do not have the chance to dissociate from the oligomer and are hence kinetically trapped in the active mode. This results in the cooperative deactivation of active Ire1 complexes. (B) The deactivation function of the active Ire1-unfolded protein complex is a nonlinear hill function of the concentration of the active complex.
Found at: doi:10.1371/journal.pbio.1000415.s010 (0.32 MB TIF)

Figure S11 Model predictions are robust to variation of floating parameters. Sensitivity of model results to parameter variations about the best fit (solid curves). Simulations of the washout experiment were run over a range of parameter. Results are shown for three. Black curves are wild type, and green curves are Ire1^{bipless}. (A) S_u is source (rate of UP import). (B) a_{up} is ratio of affinities of Ire1 and BiP for unfolded proteins. (C) R is affinity of BiP for free Ire1.
Found at: doi:10.1371/journal.pbio.1000415.s011 (0.40 MB TIF)

Figure S12 Model predictions are robust to variation in literature-derived parameters. (A) In silico dose responses of "wild type," "*hac1*Δ," and "Ire1^{bipless}" models with the folding time (S_u) varied. The dose response simulations are robust to changes in the folding time of proteins in the ER. (B) The deactivation delay of Ire1^{bipless} following simulated washout is robust to changes in folding time (S_u) of proteins in the ER. (C) The deactivation delay of Ire1^{bipless} following simulated DTT washout is robust to changes in the cellular diffusion constant. (D) Variation in the number of Ire1 molecules should affect the deactivation kinetics of Ire1^{bipless} more than wild type.
Found at: doi:10.1371/journal.pbio.1000415.s012 (0.63 MB TIF)

Figure S13 BiP re-associates with Ire1 with kinetics that match Ire1 deactivation following DTT washout. (A) Cells bearing HA-tagged, wild type Ire1 were treated with 5 mM DTT for 1 h. DTT was washed by filtration and cells were collected over time. Ire1 was immuno-precipitated from lysates, and precipitates were immuno-blotted with antibodies against Ire1 (anti-HA) and BiP (anti-Kar2) (see Methods). (B) The ratio of BiP to Ire1 in each lane above. BiP re-associates with Ire1 to the level of unstressed cells.
Found at: doi:10.1371/journal.pbio.1000415.s013 (0.89 MB TIF)

Figure S14 Characterization and quantification of Ire1 FRET reporter. (A) Expression of the FRET reporter allows cells to splice *HAC1* mRNA as well as wild type. (B) Images of Ire1-GFP, Ire1-mCherry, and raw Ire1 FRET from unstressed cells and cells treated with 5 mM DTT for 180 min. (C) Example images of fluorescence bleed through images in stressed and unstressed cells. Bleed through was subtracted from the raw FRET signal as a function of dose and time. (D). Single cells were defined and FRET from single cells was quantified using Cell ID 1.4 [27].
Found at: doi:10.1371/journal.pbio.1000415.s014 (2.55 MB TIF)

Figure S15 Ire1^{bipless} cells display increased cell-to-cell variation in the absence of stress. Histograms of wild type and Ire1^{bipless} cells expressing the splicing and transcriptional reporters in the absence of stress. Different color histograms represent separate experiments. Inset number are the standard deviation divided by the mean (CV). Ire1^{bipless} cells have increased variation compared to the wild type despite the increased mean.
Found at: doi:10.1371/journal.pbio.1000415.s015 (0.50 MB TIF)

Text S1 Computational model and methods.
Found at: doi:10.1371/journal.pbio.1000415.s016 (0.12 MB PDF)

Acknowledgments

We would like to thank Alexei Korennykh, Jacob Stewart-Ornstein, Lizabeth Gomes, Cole Dovey, Richard Yu, Gustavo Pesce, and the Walter and El-Samad labs for valuable scientific discussions.

Author Contributions

The author(s) have made the following declarations about their contributions: Conceived and designed the experiments: DP TA EVA HES PW. Performed the experiments: DP MWC SEV. Analyzed the data: DP MWC HES PW. Contributed reagents/materials/analysis tools: DP MWC TA EVA. Wrote the paper: DP HES PW.

References

1. Ron D, Walter P (2007) Signal integration in the endoplasmic reticulum unfolded protein response. Nat Rev Mol Cell Biol 8: 519–529.
2. Bernales S, Papa FR, Walter P (2006) Intracellular signaling by the unfolded protein response. Annu Rev Cell Dev Biol 22: 487–508.
3. Bernales S, McDonald KL, Walter P (2006) Autophagy counterbalances endoplasmic reticulum expansion during the unfolded protein response. PLoS Biol 4: e423. doi:10.1371/journal.pbio.0040423.
4. Shuck S, Prinz WA, Thorn KS, Voss C, Walter P (2009) Membrane expansion alleviates endoplasmic reticulum stress independent of the unfolded protein response. J Cell Biol 187: 525–536.
5. Travers KJ, Patil CK, Wodicka L, Lockhart DJ, Weissman JS, et al. (2000) Functional and genomic analyses reveal an essential coordination between the unfolded protein response and ER-associated degradation. Cell 101: 249–258.
6. So AY, de la Fuente E, Walter P, Shuman M, Bernales S (2009) The unfolded protein response during prostate cancer development. Cancer Metastasis Rev 28: 219–223.
7. Lin JH, Walter P, Yen TS (2008) Endoplasmic reticulum stress in disease pathogenesis. Annu Rev Pathol 3: 399–425.
8. Ma Y, Hendershot LM (2004) The role of the unfolded protein response in tumour development: friend or foe? Nat Rev Cancer 4: 966–977.
9. Schroder M, Kaufman RJ (2005) The mammalian unfolded protein response. Annu Rev Biochem 74: 739–789.
10. Matus S, Lisbona F, Torres M, Leon C, Thielen P, et al. (2008) The stress rheostat: an interplay between the unfolded protein response (UPR) and autophagy in neurodegeneration. Curr Mol Med 8: 157–172.
11. Scheuner D, Kaufman RJ (2008) The unfolded protein response: a pathway that links insulin demand with beta-cell failure and diabetes. Endocr Rev 29: 317–333.
12. Korennykh AV, Egea PF, Korostelev AA, Finer-Moore J, Zhang C, et al. (2009) The unfolded protein response signals through high-order assembly of Ire1. Nature 457: 687–693.
13. Shamu CE, Walter P (1996) Oligomerization and phosphorylation of the Ire1p kinase during intracellular signaling from the endoplasmic reticulum to the nucleus. EMBO J 15: 3028–3039.
14. Aragon T, van Anken E, Pincus D, Serafimova IM, Korennykh AV, et al. (2009) Messenger RNA targeting to endoplasmic reticulum stress signalling sites. Nature 457: 736–740.
15. Kimata Y, Ishiwata-Kimata Y, Ito T, Hirata A, Suzuki T, et al. (2007) Two regulatory steps of ER-stress sensor Ire1 involving its cluster formation and interaction with unfolded proteins. J Cell Biol 179: 75–86.
16. Cox JS, Walter P (1996) A novel mechanism for regulating activity of a transcription factor that controls the unfolded protein response. Cell 87: 391–404.
17. Sidrauski C, Cox JS, Walter P (1996) tRNA ligase is required for regulated mRNA splicing in the unfolded protein response. Cell 87: 405–413.

18. Kawahara T, Yanagi H, Yura T, Mori K (1997) Endoplasmic reticulum stress-induced mRNA splicing permits synthesis of transcription factor Hac1p/Ern4p that activates the unfolded protein response. Mol Biol Cell 8: 1845–1862.
19. Chapman RE, Walter P (1997) Translational attenuation mediated by an mRNA intron. Curr Biol 7: 850–859.
20. Bertolotti A, Zhang Y, Hendershot LM, Harding HP, Ron D (2000) Dynamic interaction of BiP and ER stress transducers in the unfolded-protein response. Nat Cell Biol 2: 326–332.
21. Okamura K, Kimata Y, Higashio H, Tsuru A, Kohno K (2000) Dissociation of Kar2p/BiP from an ER sensory molecule, Ire1p, triggers the unfolded protein response in yeast. Biochem Biophys Res Commun 279: 445–450.
22. Kimata Y, Oikawa D, Shimizu Y, Ishiwata-Kimata Y, Kohno K (2004) A role for BiP as an adjustor for the endoplasmic reticulum stress-sensing protein Ire1. J Cell Biol 167: 445–456.
23. Todd-Corlett A, Jones E, Seghers C, Gething M-J, (2007) Lobe IB of the ATPase domain of Kar2p/BiP interacts with Ire1p to regultate the unfolded prtotein response in *Saccharomyces cerevisiae*. J Mol Bio 367: 770–787.
24. Credle JJ, Finer-Moore JS, Papa FR, Stroud RM, Walter P (2005) On the mechanism of sensing unfolded protein in the endoplasmic reticulum. Proc Natl Acad Sci U S A 102: 18773–18784.
25. Oikawa D, Kimata Y, Kohno K (2007) Self-association and BiP dissociation are not sufficient for activation of the ER stress sensor Ire1. J Cell Sci 120: 1681–1688.
26. Cox JS, Shamu CE, Walter P (1993) Transcriptional induction of genes encoding endoplasmic reticulum resident proteins requires a transmembrane protein kinase. Cell 73: 1197–1206.
27. Jesch SA, Zhao X, Wells MT, Henry SA (2005) Genome-wide analysis reveals inositol, not choline, as the major effector of Ino2p-Ino4p and unfolded protein response target gene expression in yeast. J Biol Chem 280: 9106–9118.
28. Tu BP, Weissman JS (2004) Oxidative protein folding in eukaryotes: mechanisms and consequences. J Cell Biol 164: 341–346.
29. Chernomoretz A, Bush A, Yu R, Gordon A, Colman-Lerner A (2008) Using Cell-ID 1.4 with R for microscope-based cytometry. Curr Protoc Mol Biol Chapter 14: Unit 14 18.
30. Behar M, Hao N, Dohlman HG, Elston TC (2008) Dose-to-duration encoding and signaling beyond saturation in intracellular signaling networks. PLoS Comput Biol 4: e1000197. doi:10.1371/journal.pcbi.1000197.
31. Oikawa D, Kimata Y, Kohno K, Iwawaki T (2009) Activation of mammalian IRE1α upon ER stress depends on dissociation of BiP rather than on direct interaction with unfolded proteins. Exp Cell Res 315: 2496–2504.
32. Lin JH, Li H, Yasumura D, Cohen HR, Zhang C, et al. (2007) IRE1 signaling affects cell fate during the unfolded protein response. Science 318: 944–949.
33. Yu RC, Pesce CG, Colman-Lerner A, Lok L, Pincus D, et al. (2008) Negative feedback that improves information transmission in yeast signalling. Nature 456: 755–761.
34. Rothman JE, Schmid SL (1986) Enzymatic recycling of clathrin from coated vesicles. Cell 46: 5–9.
35. Sollner T, Bennett MK, Whiteheart SW, Scheller RH, Rothman JE (1993) A protein assembly-disassembly pathway in vitro that may correspond to sequential steps of synaptic vesicle docking, activation, and fusion. Cell 75: 409–418.

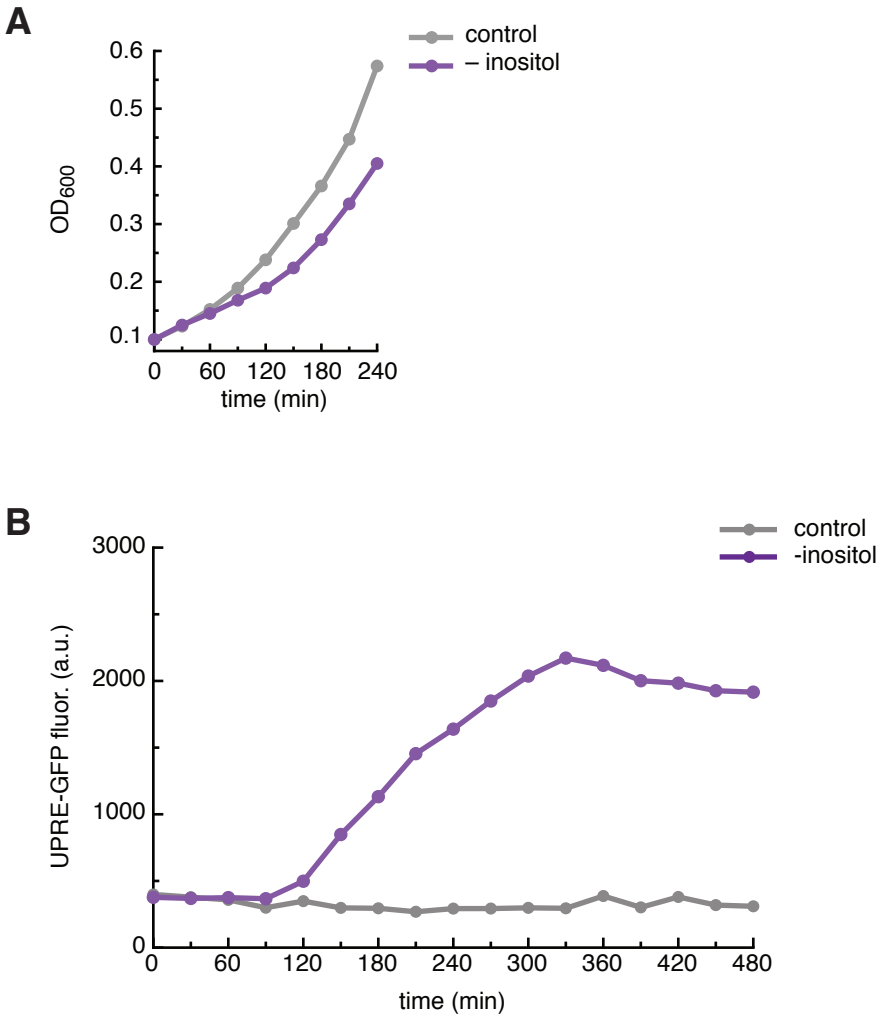
A
control
– inositol
0.6
0.5
0.4
0.3
0.2
0.1
OD600
0
60
120
180
240
time (min)
B
control
-inositol
3000
2000
1000
0
UPRE-GFP fluor. (a.u.)
0
60
120
180
240
300
360
420
480
time (min)

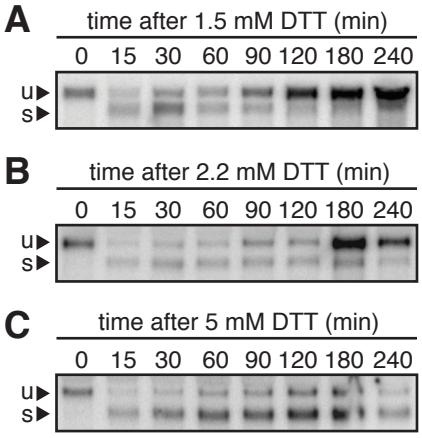
A
time after 1.5 mM DTT (min)
0 15 30 60 90 120 180 240
u
s
B
time after 2.2 mM DTT (min)
0 15 30 60 90 120 180 240
u
s
C
time after 5 mM DTT (min)
0 15 30 60 90 120 180 240
u
s

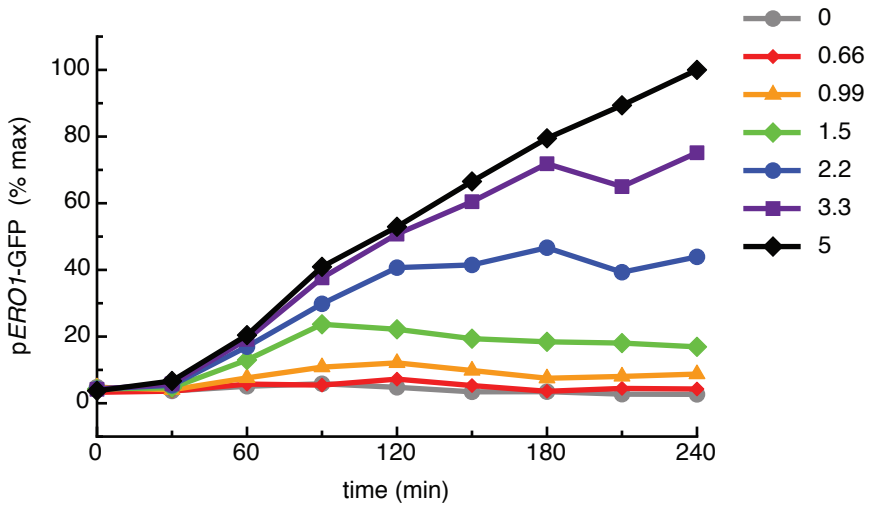
pERO1-GFP (% max)
100
80
60
40
20
0
0
60
120
180
240
time (min)
0
0.66
0.99
1.5
2.2
3.3
5

A

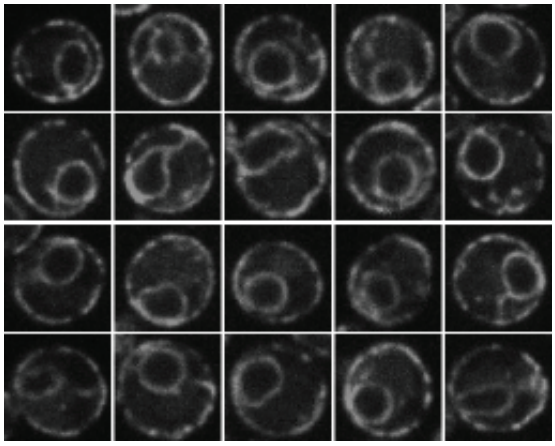

B

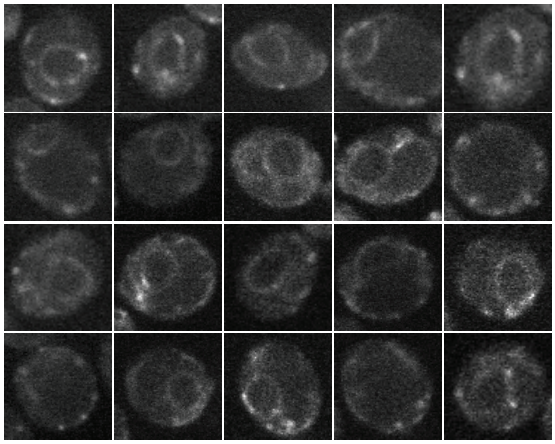

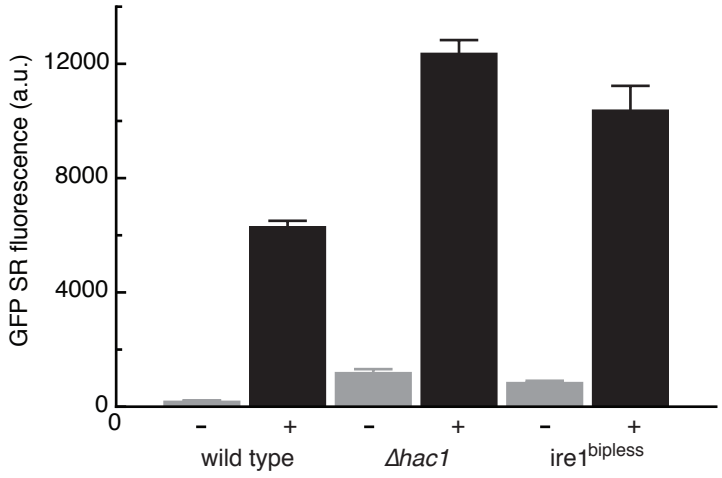
GFP SR fluorescence (a.u.)
12000
8000
4000
0
0
-
+
-
+
-
+
wild type
Δhac1
ire1bipless

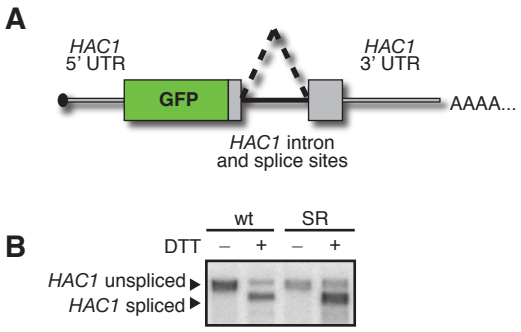
A
HAC1
5' UTR
GFP
HAC1
3' UTR
AAAA...
HAC1 intron
and splice sites
B
wt
SR
DTT
–
+
–
+
HAC1 unspliced
HAC1 spliced

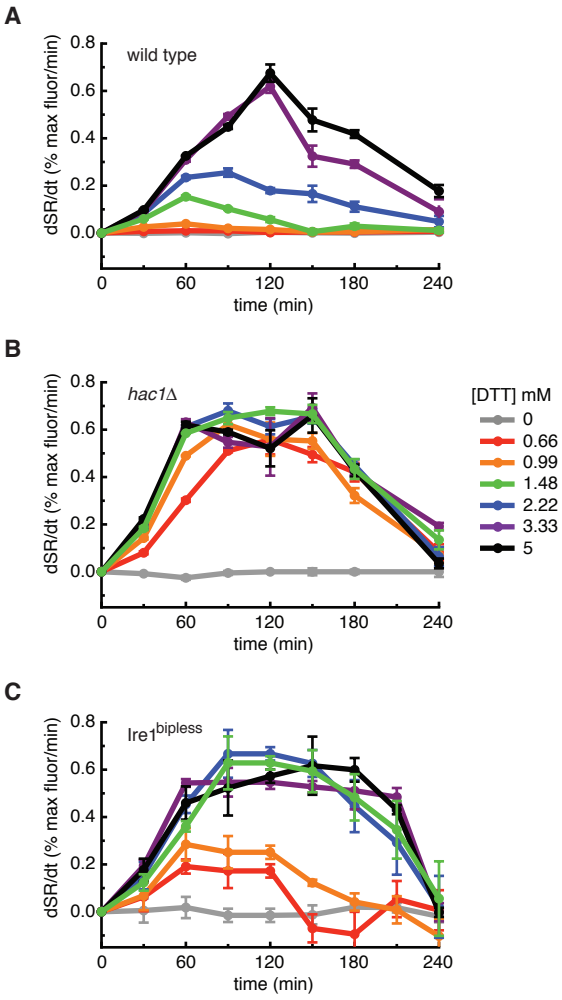
A
wild type
dSR/dt (% max fluor/min)
0.0
0.2
0.4
0.6
0.8
0
60
120
180
240
time (min)
B
hac1Δ
dSR/dt (% max fluor/min)
time (min)
[DTT] mM
0
0.66
0.99
1.48
2.22
3.33
5
C
Ire1bipless
dSR/dt (% max fluor/min)
time (min)

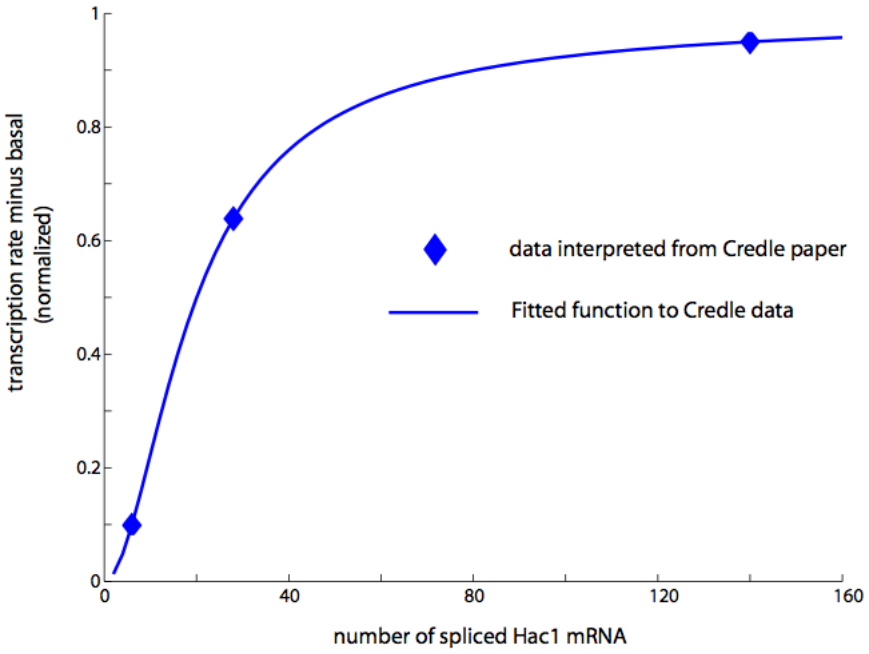
transcription rate minus basal
(normalized)
1
0.8
0.6
0.4
0.2
0
0
40
80
120
160
number of spliced Hac1 mRNA
data interpreted from Credle paper
Fitted function to Credle data

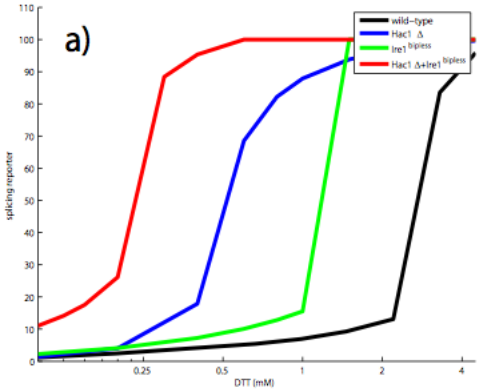
a)
wild−type
Hac1 Δ
Ire1 bipless
Hac1 Δ+Ire1 bipless
splicing reporter
DTT (mM)

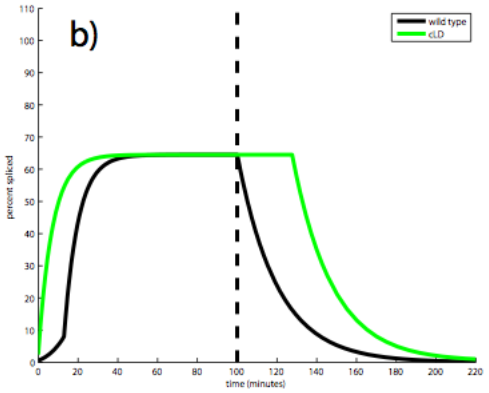
b)
wild type
cLD
percent spliced
time (minutes)

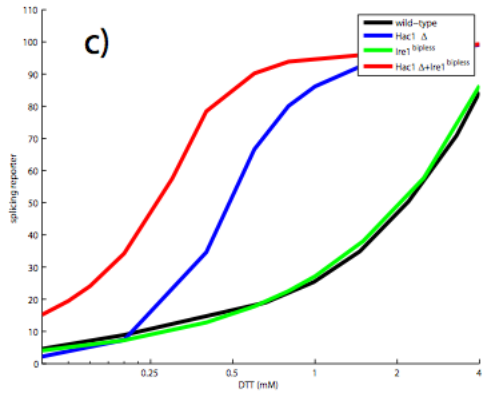
c)
wild−type
Hac1 Δ
Ire1 bipless
Hac1 Δ+Ire1 bipless
splicing reporter
DTT (mM)

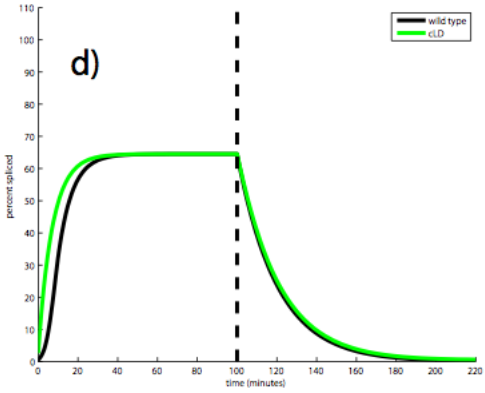
d)
wild type
cLD
percent spliced
time (minutes)

A

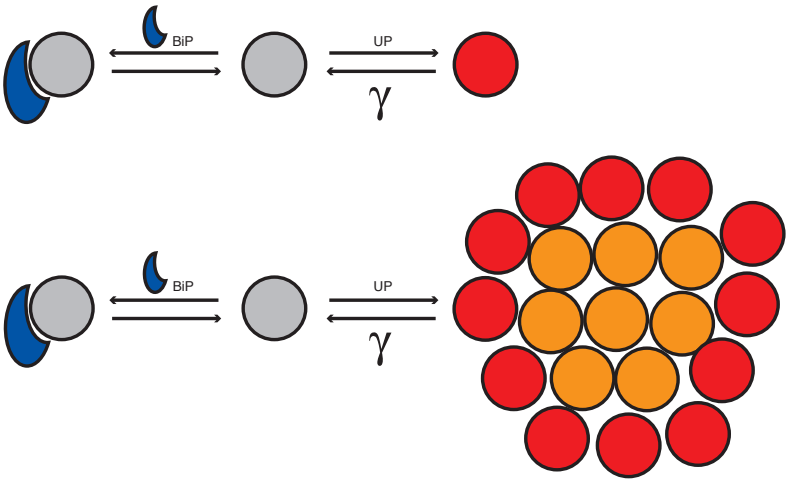
BiP
UP
γ
BiP
UP
γ

B

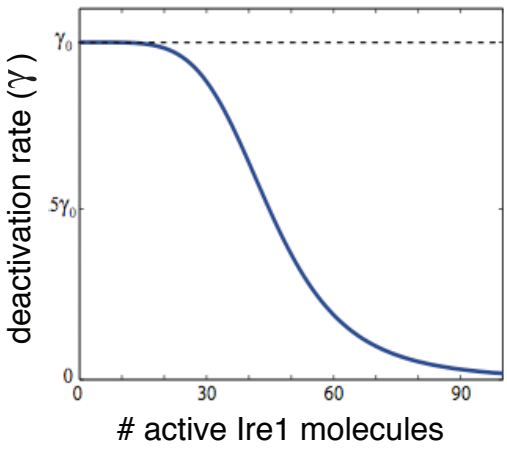
deactivation rate (γ)
γ0
5γ0
0
0
30
60
90
active Ire1 molecules

black–wild type, green – Ire1^{bipless}

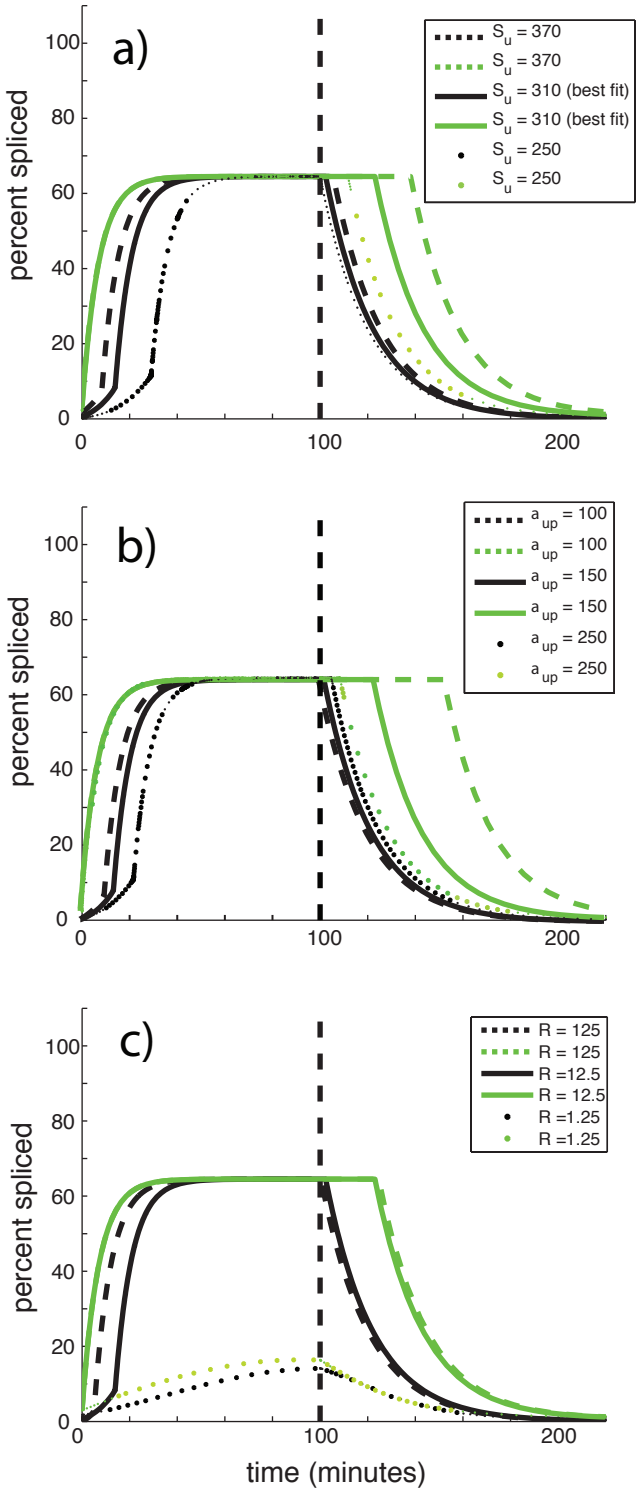

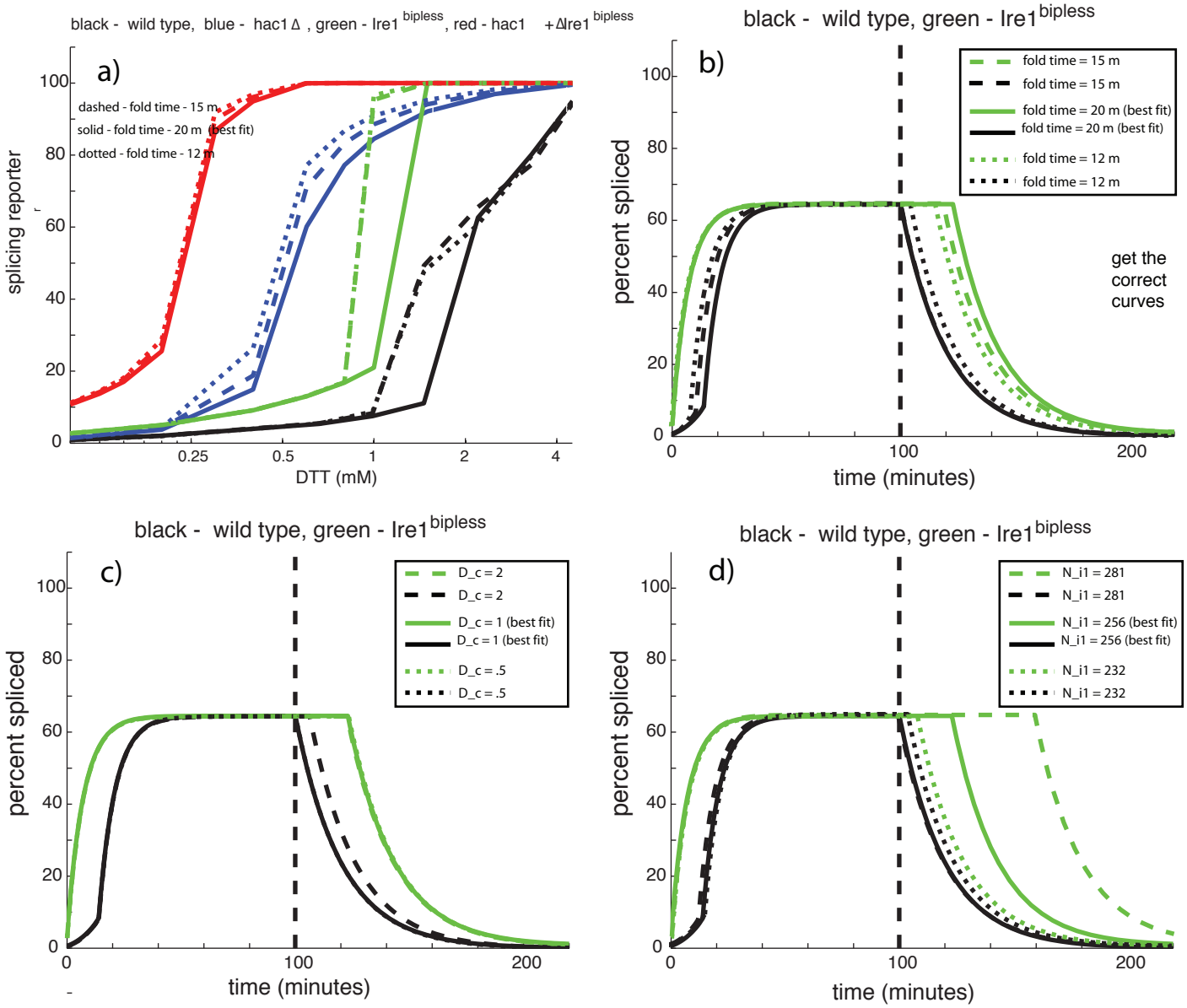
black - wild type, blue - hac1 Δ , green - Ire1 bipless, red - hac1 +ΔIre1 bipless
a)
dashed - fold time - 15 m
solid - fold time - 20 m (best fit)
dotted - fold time - 12 m
splicing reporter
DTT (mM)
black - wild type, green - Ire1 bipless
b)
fold time = 15 m
fold time = 15 m
fold time = 20 m (best fit)
fold time = 20 m (best fit)
fold time = 12 m
fold time = 12 m
get the correct curves
percent spliced
time (minutes)
black - wild type, green - Ire1 bipless
c)
D_c = 2
D_c = 2
D_c = 1 (best fit)
D_c = 1 (best fit)
D_c = .5
D_c = .5
percent spliced
time (minutes)
black - wild type, green - Ire1 bipless
d)
N_i1 = 281
N_i1 = 281
N_i1 = 256 (best fit)
N_i1 = 256 (best fit)
N_i1 = 232
N_i1 = 232
percent spliced
time (minutes)

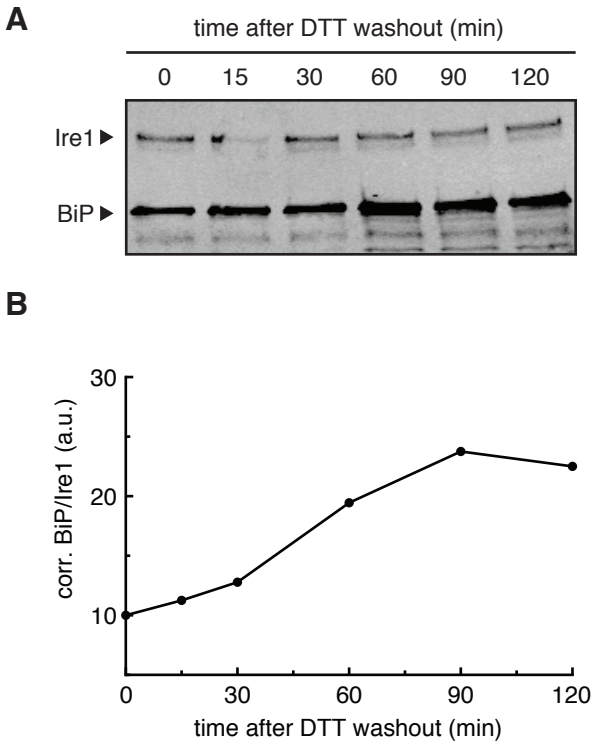
A
time after DTT washout (min)
0
15
30
60
90
120
Ire1
BiP
B
corr. BiP/Ire1 (a.u.)
30
20
10
0
30
60
90
120
time after DTT washout (min)

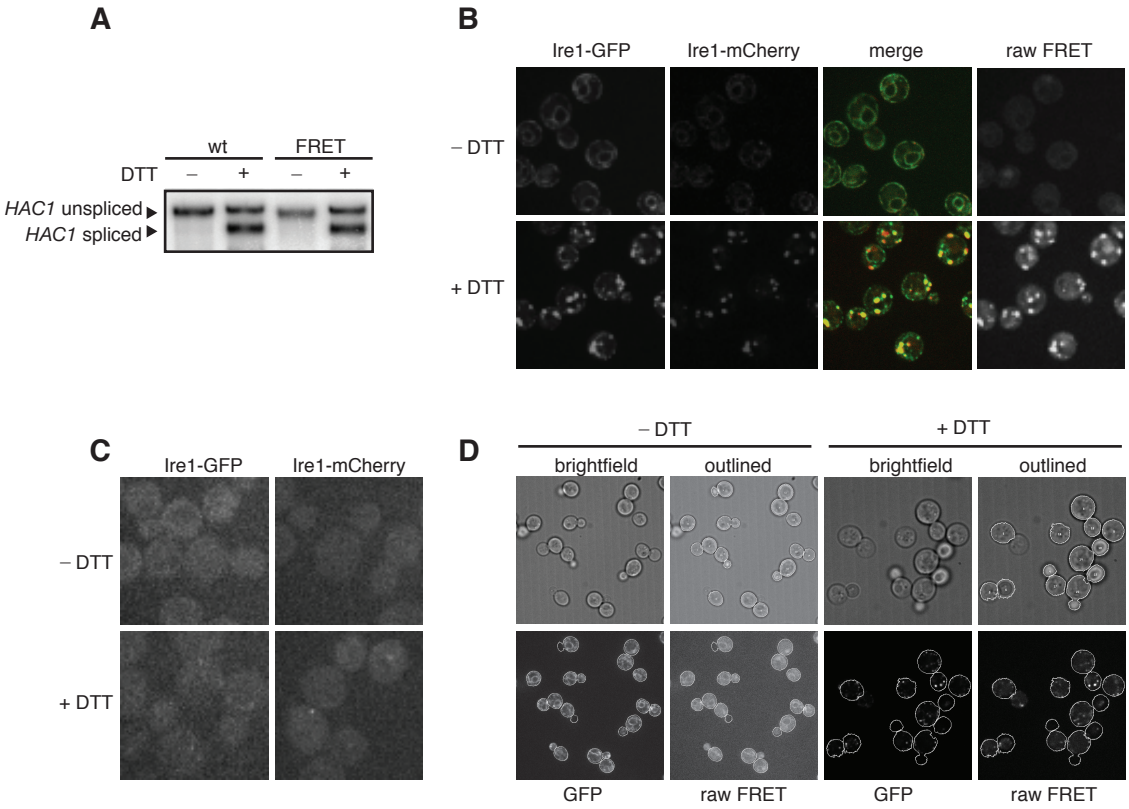
A
wt
FRET
DTT
–
+
–
+
HAC1 unspliced
HAC1 spliced
B
Ire1-GFP
Ire1-mCherry
merge
raw FRET
– DTT
+ DTT
C
Ire1-GFP
Ire1-mCherry
– DTT
+ DTT
D
– DTT
+ DTT
brightfield
outlined
brightfield
outlined
GFP
raw FRET
GFP
raw FRET

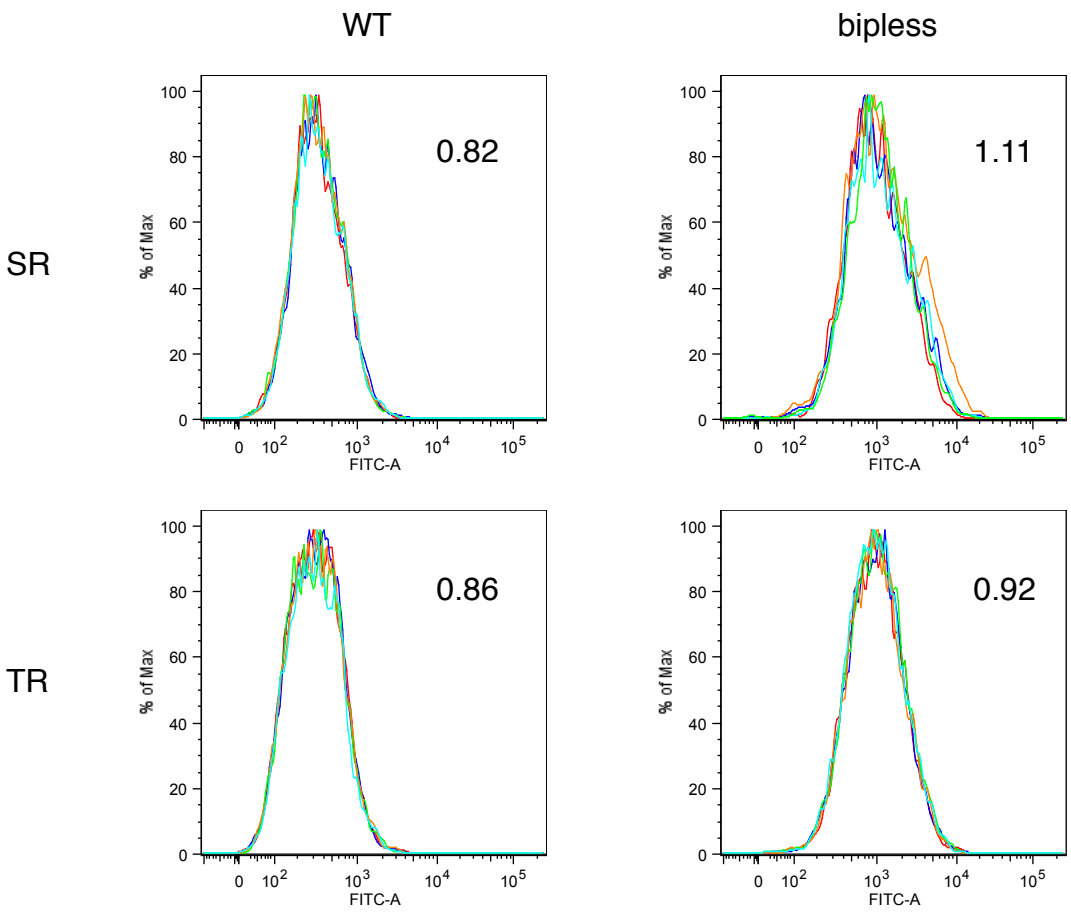
WT
bipless
SR
TR
0.82
1.11
0.86
0.92
% of Max
FITC-A

Computational Model

In this section, we present the computational model developed to capture the salient features of the UPR dynamics. The model we build is based on deterministic mass-action kinetics, resulting in a set of ordinary differential equations.

1 Model Variables

The variables in the model describe the number of molecules rather than concentrations. For ease of notation and clarity of model equations, we will put square brackets around each variable, e.g. $[X]$. A description of the model variables is given in the table below.

variable	description
B_m	BiP messenger RNA
B	BiP protein
E_{1_m}	Ero1 messenger RNA
E_1	Ero1 protein, stabilizes REDOX potential
D_0	dose level of DTT, increases REDOX potential
I_1	Ire1 monomer
$I_1 \cdot B$	Ire1 bound to BiP, inactive Ire1
I_{1A}	Ire1 bound to an unfolded protein, active Ire1,
$H^u_{1_m}$	Unspliced Hac1 messenger RNA
$H^s_{1_m}$	Spliced Hac1 messenger RNA
U	Unfolded protein
$U \cdot B$	folding complex (folding protein with/chaperone)
U_d	Unfolded proteins with broken disulfide bonds
$U_d \cdot B$	misfolded complex (folding protein with broken disulfide bonds/chaperone)

2 Model Assumptions

In building the computational model, we adopted the following biologically motivated assumptions

- Ire1 is activated through contact with unfolded protein that are not in the process of folding properly, that is U, U_d, and $U_d \cdot B$. It is not activated by $U \cdot B$ which is folding properly.
- Only activated Ire1 splices Hac1.
- BiP titrates unfolded proteins, preventing unfolding proteins from interacting with Ire1.
- DTT breaks disulfide bonds in the unfolded protein and folding complexes and this process occurs as an enzymatic reaction. We also assume that there is a constant pool of DTT diffusing in and out of the ER, replenishing the local population.
- Ero1 mends broken disulfide bonds resulting from DTT. The population of unfolded proteins with broken disulfide bonds vs. those without is dependent on the relative populations of Ero1

vs. DTT. In reality, Ero1 is one protein of many that assist in the formation of disulfide bonds, others include oxidoreductases from the PDI family. For simplicity, Ero1 will represent the entire mechanism for disulfide bond formation and will act as an enzyme.

- Ero1 and DTT are equally efficient in their enzymatic reactions. Therefore the competition is 1-to-1.

- Unfolded proteins regulate an allosteric switch in Ire1 from the inactive state to the active state. Ire1 then allosterically deactivates based on the active state's deactivation rate. This model is chosen over the alternate model that unfolded protein activate Ire1 by binding to it and deactivate by dissociating from it. Mathematically, the allosteric model is simpler and because of the small number of Ire1 and the generally large number of unfolded proteins, either scenario would yield essentially the same results.

- The deactivation rate of active Ire1 is non-linearly dependent on the population of active Ire1. The relationship we use is pictorially described in Figure S10a. Ire1 molecules are known to form foci which are correlated with Hac1 mRNA splicing. The nonlinear function we employ in the model is meant to serve as a simple phenomenological description of the deactivation rate of Ire1 from the Ire1 foci, formed during stress. This relationship can describe a variety of underlying mechanistic schemes of Ire1 inactivation

- The population of Ire1 is approximately 256 [*Ghaemmaghami et al.* (2003)].

- The basal population of Hac1 mRNA is 200 [*Walter*].

- The basal population of BiP is approximately 430,000 [*Ghaemmaghami et al.* (2003)].

- We are neglecting the lectin chaperone pathway.

- We are neglecting the ATP/ADP cycle of BiP which is known to switch BiP's affinity (high/ATP and low/ADP) to molecules such as Ire1 and unfolded proteins. In this model we set BiP's affinity constant and equal to both Ire1 and unfolded proteins.

- We are neglecting the contribution of ERAD.

3 Chemical Reactions and Reaction Rate Constants Used in Model

The reaction rate constants we will use in the equations are the traditional reaction rate constant divided by the volume of the space involved (area if on a membrane), e.g. our $c_\mu = k_\mu/V$ where k_μ is the rate constant for some species μ. The model consists of three modules. Below, we provide a description of the chemical reactions modeled and the reactions rates used.

3.1 Protein Folding Module

Reaction	Description
$\emptyset \xrightarrow{S_u} U$	Unfolded protein translocation into ER.
$U + B \xrightarrow{c_{[U\cdot B]}} U \cdot B$	BiP attachment to unfolded protein to form folding complex.
$U \cdot B \xrightarrow{\gamma_{[U\cdot B]}} U + B$	Bip dissociation from folding complex.
$U \cdot B \xrightarrow{\gamma_{fold}} \emptyset + B$	Completion of folding and release of folded protein from folding complex.
$U + D_0 \xrightarrow{c_{D_0}} U_d$	Breakage of unfolded protein's disulfide bonds by DTT.
$U_d + E_1 \xrightarrow{c_{[E_1]}} U$	Formation of disulfide bonds by Ero1 in the unfolded protein with broken disulfide bonds.
$U_d + B \xrightarrow{c_{[U\cdot B]}} U_d \cdot B$	BiP attachment to unfolded protein with broken disulfide bonds to form misfolding complex.
$U_d \cdot B \xrightarrow{\gamma_{[U\cdot B]}} U_d + B$	BiP dissociation from misfolding complex
$U \cdot B + D_0 \xrightarrow{c_{D_0}} U_d \cdot B$	Breakage of disulfide bonds in folding complex by DTT.
$U_d \cdot B + E_1 \xrightarrow{c_{[E_1]}} U \cdot B$	Ero1 forms disulfide bonds in the misfolding complex.
$U \cdot B \xrightarrow{\gamma_{[B]}} U + \emptyset$	BiP's decay from folding complex.
$U_d \cdot B \xrightarrow{\gamma_{[B]}} U_d + \emptyset$	BiP's decay from misfolding complex.

Reaction Rate Constants for Folding Module

S_u - 310 mol s^{-1}. Source rate for protein unfolding. For more details see *Crucial Parameter Fitting* section below.

$c_{[U\cdot B]}$ - .0350 mol^{-2} s^{-1}. Attachment rate of single BiP molecule. Derived using the formula $c_{[U\cdot B]} = 4\pi D_c(2a_p)/V_{er}$ [*Berg and Purcell*(1977)]. $D_c = 1$ μm^2 s^{-1} is a typical cytosolic diffusion coefficient. $a_p = .028$ μm is the typical protein size in the ER. $V_{er} = 2.15$ μm^3 is the approximate volume of the ER.

$\gamma_{[U\cdot B]}$ - 196 mol^{-1} s^{-1}. Dissociation rate of BiP from folding complex. We assume this to be equal to $\gamma_{[I_1\cdot B]}$, the decay rate of the Ire1/BiP complexes. For more details see *Crucial Parameter Fitting* section below.

γ_{fold} - 8.33×10^{-4} mol^{-1} s^{-1}. Folding rate of protein in the folding complex. (20 minute folding time).

c_{D_0} - 1.50×10^{-3} mol^{-2} s^{-1}. Enzymatic rate of disulfide bond breaking. Value is not crucial since we are setting $c_{[E_1]} = c_{D_0}$ for 1-to-1 competition.

$c_{[E_1]}$ - 1.50×10^{-3} mol^{-2} s^{-1}. Enzymatic rate of disulfide bond formation. We have $c_{[E_1]} = c_{D_0}$ since we are assuming 1-to-1 competition.

$\gamma_{[B]}$ - 1.39×10^{-4} mol^{-1} s^{-1}, Decay rate of BiP (2 hour mean decay time). Taken from [*Axelsen and Sneppen*(2004)].

3.2 Ire1 activation, Hac1 splicing, and splicing reporter module

Reaction	Description
$I_1 + B \xrightarrow{c_{[I_1 \cdot B]}} I_1 \cdot B$	BiP binding to Ire1 to form inactive complex.
$I_1 \cdot B \xrightarrow{\gamma_{[I_1 \cdot B]}} I_1 + B$	BiP dissociation from inactive complex
$I_1 + U_g \xrightarrow{c_{up}} I_{1A} + U_g$ where $U_g = U$ or U_d or $U_d \cdot B$	Ire1 activation to enable splicing.
$I_{1A} \xrightarrow{F_{[I_{1A}]}} I_1$	Ire1 deactivation.
$\emptyset \xrightarrow{\beta_{[H^u_{1_m}]}} H^u_{1_m}$	transcription of unspliced Hac1 mRNA.
$H^u_{1_m} \xrightarrow{\gamma_{[H_{1_m}]}} \emptyset$	Decay of unspliced Hac1 mRNA.
$H^s_{1_m} \xrightarrow{\gamma_{[H_{1_m}]}} \emptyset$	Decay of spliced Hac1 mRNA.
$H^u_{1_m} \xrightarrow{\beta_{[H^s_{1_m}]}} H^s_{1_m} + R_{S_m}$	Splicing of Hac1 mRNA and reporter mRNA
$R_{S_m} \xrightarrow{\gamma_{[R_{S_m}]}} \emptyset$	Decay of splicing reporter mRNA.
$\emptyset \xrightarrow{\beta_{R_S}} R_S$	Translation of splicing reporter GFP.
$R_S \xrightarrow{\gamma_{[R_S]}} \emptyset$	Decay of splicing reporter GFP.

Reaction Rate Constants for Ire1 Activation, Hac1 Splicing, and Splicing Reporter Module

$c_{[I_1 \cdot B]}$ - .0350 mol^{-2} s^{-1}. Attachment rate of single BiP molecule to Ire1. For simplicity, we assume $c_{[I_1 \cdot B]} = c_{[U \cdot B]}$.

$\gamma_{[I_1 \cdot B]}$ - 196 mol^{-1} s^{-1}. Dissociation rate of BiP from the inactive complex. For more details see *Crucial Parameter Fitting* section below.

c_{up} - 2.33×10^{-4} mol^{-2} s^{-1}. Attachment rate of Ire1 molecule to an unfolded protein. For more details see *Crucial Parameter Fitting* section below.

$F_{[I_{1A}]}$ - $F_{[I_{1A}]} = \gamma_{[I_{1A}]} \frac{[I_0]^n}{[I_0]^n + [I_{1A}]^n}$ represents a non-linear (active Ire1 cooperative) decay rate as illustrated in Figure S10b. We have set $\gamma_{[I_{1A}]} \approx \gamma_{[I_1 \cdot B]}$ and $n = 4.5, I_0 = 45$. For more details see *Crucial Parameter Fitting* section below.

$\beta_{[H^u_{1_m}]}$ - 0.167 s^{-1} Transcription rate of Hac1 unspliced mRNA. The mean decay time of both spliced and unspliced is assumed to be 20 minutes. Therefore $\beta_{[H^u_{1_m}]}$ is set so that the steady state population of all Hac1 mRNA is equal to 200.

$\gamma_{[H_{1_m}]}$ - 8.33×10^{-4} s^{-1}. Decay rate of Hac1 mRNA corresponding to a mean decay time of 20 minutes as determined from [*Sidrauski et al.*(1996)] (Figure 5c and page 408). We use the same value for both spliced and unspliced.

$\beta_{[H^s_{1m}]}$ - 1.5×10^{-3} mol^{-1} s^{-1}. Splicing rate of Hac1 mRNA corresponding to an 11 minute splicing time inferred from Figure 3 of [*Mori et al.*(1997)], which also shows that the total number of mHac1, spliced and unspliced remains relatively constant, an assumption in our model. The total number of molecules being spliced per second is $\beta_{[H^s_{1m}]}\min([I_{1A}], [H^u_{1m}])$. The function $\min([I_{1A}], [H^u_{1m}])$ is required since the minimum of these quantities will determine the number of molecules being instantaneously spliced.

$\gamma_{[R_{Sm}]}$ 8.33×10^{-4} mol^{-1} s^{-1}. Decay rate of the splicing reporter mRNA. This is assumed to be the same as $\gamma_{[H_{1_m}]}$.

$\beta_{[R_S]}$ 8.33×10^{-3} mol^{-1} s^{-1}. Translation rate of the splicing reporter (2 minutes per translation event).

$\gamma_{[R_S]}$ 3.47×10^{-5}. Decay rate of the splicing reporter GFP (8 hour mean decay time).

3.3 BiP and Ero1 transcription module

Reaction	Description
$\emptyset \xrightarrow{F_{[B_m]}} B_m$	Transcription of BiP mRNA.
$B_m \xrightarrow{\gamma_{[B_m]}} \emptyset$	Decay of BiP mRNA.
$\emptyset \xrightarrow{\beta_{[B]}} B$	Translation of BiP.
$B \xrightarrow{\gamma_{[B]}} \emptyset$	Decay of BiP.
$\emptyset \xrightarrow{F_{[E_{1_m}]}} E_{1_m}$	Translation of Ero1 mRNA.
$E_{1_m} \xrightarrow{\gamma_{[E_{1_m}]}} \emptyset$	Decay of Ero1 mRNA.
$\emptyset \xrightarrow{\beta_{[E_1]}} E_1$	Translation of Ero1.
$E_1 \xrightarrow{\gamma_{[E_1]}} \emptyset$	Decay of Ero1.

$F_{[B_m]}$ - $F_{[B_m]} = \beta_{[B_m]}[1 + N_{[B_m]}f([H^s_{1m}])]$ is a function that relates the transcription rate of BiP mRNA to the amount of spliced Hac1 ($H^s_{1_m}$). $\beta_{[B_m]} = .1625$ mol s^{-1} is the basal transcription rate (see Fitting section below). The function $f([H^s_{1m}]) = [H^s_{1m}]^2/(a_0 + a_1[H^s_{1m}] + [H^s_{1m}]^2)$ is the transcription hill function for the UPRE promoter where $a_0 = 296.5$ and $a_1 = 5.26$. The function is fitted (see Figure S8) to the normalized data in [*Credle et al.*(2005)] where the percent of spliced Hac1 mRNA is related to the LacZ reporter. $N_{[B_m]} = 4$ is used in our model and is within the range of values measured by the transcriptional reporter.

$\gamma_{[B_m]}$ - 6.67×10^{-4} s^{-1}. Decay rate of BiP mRNA corresponding to a 25 minute mean decay time.

$\beta_{[B]}$ - .25 s^{-1}. Translation rate of BiP.

$\gamma_{[B]}$ - 1.39×10^{-4} s^{-1}. Decay rate of BiP corresponding to a 2 hour mean decay time referenced from the modeling paper [*Axelsen and Sneppen*(2004)].

$F_{[E1_m]}$ - $F_{[E1_m]} = \beta_{[E1_m]}[1 + N_{[E1_m]} f([H^s_{1_m}])]$ is the transcription rate for Ero1 mRNA. $\beta_{[E1_m]} = 1.08$ mol s^{-1} is the basal transcription rate. The hill function $f([H^s_{1_m}])$ is the same as that used in $F_{[B_m]}$. $N_{[E1_m]} = 7$ is the value used in the model and is within the range of experimental measurements for the transcriptional reporter.

$\gamma_{[E1_m]}$ - 6.67×10^{-4} s^{-1}. Decay rate of Ero1 mRNA. Assumed to be same as that of BiP mRNA.

$\beta_{[E_1]}$ - .25 s^{-1}. Translation rate of Ero1. For more details see *Crucial Parameter Fitting* section below.

$\gamma_{[E_1]}$ - 1.39×10^{-4} s^{-1}. Decay rate of Ero1. Assumed to be same as that of BiP.

4 Kinetic Model Equations

Module 1: protein folding dynamics

$$
\begin{aligned}
\frac{d[U]}{dt} &= S_U - c_{[U\cdot B]}[U][B] + \gamma_{[U\cdot B]}[U\cdot B] \\
&- c_{D_0} D_0[U] + c_{[E_1]}[E_1][U_d] + \gamma_B[U\cdot B] \\
\frac{d[U\cdot B]}{dt} &= c_{[U\cdot B]}[U][B] - \gamma_{[U\cdot B]}[U\cdot B] \\
&- c_{D_0} D_0[U\cdot B] + c_{[E_1]}[E_1][U_d\cdot B] \\
&- \gamma_B[U\cdot B] - \gamma_{fold}[U\cdot B] \\
\frac{d[U_d]}{dt} &= -c_{[U\cdot B]}[U_d][B] + \gamma_{[U\cdot B]}[U_d\cdot B] \\
&+ c_{D_0} D_0[U] - c_{[E_1]}[E_1][U_d] + \gamma_B[U_d\cdot B] \\
\frac{d[U_d\cdot B]}{dt} &= c_{[U\cdot B]}[U_d][B] - \gamma_{[U\cdot B]}[U_d\cdot B] \\
&+ c_{D_0} D_0[U\cdot B] - c_{[E_1]}[E_1][U_d\cdot B] - \gamma_B[U_d\cdot B]
\end{aligned}
$$

Module 2: Ire1,Hac1 mRNA, and splicing reporter dynamics

$$\begin{aligned}
\frac{d[I_1]}{dt} &= -c_{up}\Big([U]+[U_d]+[U_d\cdot B]\Big)[I_1]+F_{[I_{1A}]}[I_{1A}] \\
&\quad -c_{[I_1\cdot B]}[I_1][B]+\gamma_{[I_1\cdot B]}[I_1\cdot B] \\
\frac{d[I_1\cdot B]}{dt} &= c_{[I_1\cdot B]}[I_1][B]-\gamma_{[I_1\cdot B]}[I_1\cdot B] \\
\frac{d[I_{1A}]}{dt} &= c_{up}\Big([U]+[U_d]+[U_d\cdot B]\Big)[I_1]-F_{[I_{1A}]}[I_{1A}] \\
\frac{d[H^u_{1_m}]}{dt} &= \beta_{[H^u_{1_m}]}-\gamma_{[H^s_{1_m}]}[H^u_{1_m}]-\beta_{[H^s_{1_m}]}\min([I_{1A}],[H^u_{1_m}]) \\
\frac{d[H^s_{1_m}]}{dt} &= -\gamma_{[H^s_{1_m}]}[H^s_{1_m}]+\beta_{[H^s_{1_m}]}\min([I_{1A}],[H^u_{1_m}]) \\
\frac{d[R_{S_m}]}{dt} &= -\gamma_{[R_{S_m}]}[R_{S_m}]+\beta_{[H^s_{1_m}]}\min([I_{1A}],[H^u_{1_m}]) \\
\frac{d[R_S]}{dt} &= -\gamma_{[R_S]}[R_S]+\beta_{[R_S]}[R_{S_m}]
\end{aligned}$$

Module 3: BiP and Ero1 dynamics

$$\begin{aligned}
\frac{d[B_m]}{dt} &= \beta_{[B_m]}[1+N_{[B_m]}f([H^s_{1_m}])]-\gamma_{[B_m]}[B_m] \\
\frac{d[B]}{dt} &= \gamma_{fold}[U\cdot B]+\beta_{[B]}[B_m]-\gamma_{[B]}[B]-c_{[U\cdot B]}[U][B]+\gamma_{[U\cdot B]}[U\cdot B] \\
&\quad -c_{[U\cdot B]}[U_d][B]+\gamma_{[U\cdot B]}[U_d\cdot B]-c_{[I_1\cdot B]}[I_1][B]+\gamma_{[I_1\cdot B]}[I_1\cdot B] \\
\frac{d[E_{1_m}]}{dt} &= \beta_{[E_{1_m}]}[1+N_{[E_{1_m}]}f([H^s_{1_m}])]-\gamma_{[E_{1_m}]}[E_{1_m}] \\
\frac{d[E_1]}{dt} &= \beta_{[E_1]}[E_{1_m}]-\gamma_{[E_1]}[E_1]
\end{aligned}$$

To simulate the various mutants, the equations were adjusted as follows:

strain	alteration to the kinetic equations
wild type	none
hac1Δ	set $N_{[B_m]}=N_{[E_{1_m}]}=0$, i.e. only basal transcription (no feedback).
ire1^{bipless}	set $c_{[I_1\cdot B]}=\gamma_{[I_1\cdot B]}=0$.
hac1Δ + ire1^{bipless}	set $N_{[B_m]}=N_{[E_{1_m}]}=0$. set $c_{[I_1\cdot B]}=\gamma_{[I_1\cdot B]}=0$.

Starting from the equilibrium solution for non-stressed conditions (zero DTT), the DTT levels (represented by D_0 as the molecular number of DTT within the ER) were adjusted as a function of time, simultaneously solving the equations using the ordinary differential equation solver, ODE15s, in MATLAB.

4.1 Crucial Fitted Parameters

In the section, we discuss parameters for which we did not find any quantitative measurements or inferences in the literature. There are seven such parameters. To fit these parameters, we use a subset of the data describing the dose dependent splicing reporter experimental data sampled at 200 minutes after stress induction for the wild type, $hac1\Delta$, $ire1^{bipless}$, and $hac1\Delta$ + $ire1^{bipless}$. Our best fit is shown in Figure S9a. Figure S9b shows the results for the modeled washout experiment based on our fitted model predicting a delay in the ire1^{bipless} mutant, which was also experimentally verified. The details for parameter fitting are listed below.

S_u - The source rate of unfolding proteins, whose value is important relative to the value of total BiP. The best fitted results were obtained when the basal level of total BiP ($\approx 430,000$) was set to be 15-20 percent above the basal level of folding proteins. This value results in the population of free BiP to be around $60,000$. In the model, the larger the amount of free BiP to bound BiP, the slower the onset of splicing in the wild type system in the 5 mM DTT experiment. This is due to the fact free BiP sequesters Ire1 until there is enough unfolded proteins in the ER to titrate free BiP. Therefore, the choice of this parameter was set to match well with the onset of max splicing (20-30 minutes). However, in principle, this value can be changed without affecting the qualitative behavior of the system, especially the delay observed in the washout experiment. Instead, different values for S_u affect the *magnitude* of the delay. Figure S11a illustrates the sensitivity of the model to this parameter by varying the value of S_u. Here we plot the modeled washout experiment for $S_u = 370$ (dashed), 310 (solid), and 250 (dashed). All values produce a delayed response in the ire1^{bipless} case relative to the wild-type, but the delay dependent on the value of S_u.

E_{1_0} - The basal level of Ero1, $E_{1_0} = \beta_{[B_m]}\beta_{[B]}/(\gamma_{[B_m]}\gamma_{[B]})$, was fit to data from hac1Δ and hac1Δ+ ire1^{bipless}. This parameter was especially picked to fit the half maximal induction of the dose response curves for .4 and .25 mM DTT. Since these experiments have no transcriptional feedback, the basal level reaches approximately 1,350,000 molecules per ER volume, keeping in mind that Ero1 in this model represents the full system of molecules combating the effects of a similar number of DTT molecules.

$N_{[B_m]}$ - $N_{[B_m]} = 4$ was found to best fit the dose response data for the transcription feedback response of the wild type and ire1^{bipless} experiments. This value is within the range of the measured transcriptional reporters.

$N_{[E_{1_m}]}$ - $N_{[E_{1_m}]} = 7$ was found to best fit the dose response data for the transcription feedback response of the wild type and ire1^{bipless}. This value is within the range that transcriptional reporters measured.

The constants $c_{[I\cdot B]}$, $\gamma_{[I\cdot B]}$, c_{up} and $\gamma_{[I\cdot U]}$ dictate the system's dynamics, and determine the levels of free BiP and misfolded/unfolded proteins that can compete for free Ire1.

c_{up} - The value of c_{up} relative to $c_{[I\cdot B]}$ is very important. The competition between unfolded proteins and BiP for Ire1 is quantified by the association rate fluxes $c_{up}([U] + [U_d] + [U_d \cdot B])$ for the unfolded protein and $c_{[I\cdot B]}[B]$ for BiP. We found that the ratio $\alpha_{up} = c_{[I\cdot B]}/c_{up} = 150$ works best in fitting the model to data. This value makes intuitive sense since both Ire1 and the unfolded protein (even those with BiP attached) will generally diffuse much slower than

free BiP. Figure S11b shows that the quantitative aspects of the model are dependent on the variation to α_{up} for the values 100 (dashed), 150 (solid), and 250 (dotted). Here the intuition is that the lower the value of α_{up}, the lower the size of the relative population of misfolded proteins that is needed to compete for free Ire1.

$\gamma_{[I_1 \cdot B]}$ - $\gamma_{[I_1 \cdot B]}$ represents the dissociation rate of BiP from the inactive complex. This quantitiy is important since it determines the amount of time that an Ire1 molecule is free versus bound to BiP in a given condition of ER stress. Although no real quantitative measurements have been recorded, there are some estimates based on the work in [*Bertolotti et al.*(2000)] where BiP association to Ire1α in mammalian cells was studied. We will assume similar result for yeast. In the experiments in [*Bertolotti et al.*(2000)] for non-stressed cells, Ire1α/BiP complex and Ire1α were immunoprecipitated. It was found that the majority of Ire1α were in the complex form with BiP. Based on this, we can assume that at equilibrium, the ratio of the "ON" to "OFF" rates are the same as the ratio of the number of Ire1/BiP to free Ire1, neglecting active Ire1 which we'll assume to be zero for this calculation. Thus, we have $\frac{[I_1 \cdot B]}{[I_1]} = \frac{c_{[I_1 \cdot B]}[B]}{\gamma_{[I_1 \cdot B]}} = R$. In our model we set $R = 12.5$. Figure S11c plots the results of the washout experiments for 3 values of R: 125 (dashed), 12.5 (solid), 1.25 (dotted). In this sensitivity test, for a given value of R, we also scaled $\gamma_{[U \cdot B]}$ and $\gamma_{[I_{1A}]}$ by the relative change in R from its best fit value of 12.5, i.e 10 (a), 1 (b), .1 (c), respectively. The results in Figure S11c show that the system is robust for values of $R \geq 12.5$, but at $R = 1.25$, the full splicing response to 5 mM DTT does not occur. An explanation for this is that the basal level of active Ire1 (splicing) are higher in the non-stressed case for $R = 1.25$, thus are preadapted for higher levels of stress.

$\gamma_{[U \cdot B]}$ - There are no known measurements for $\gamma_{[U \cdot B]}$, the dissociation rate of BiP from folding complexes. Setting $\gamma_{[U \cdot B]}$=$\gamma_{[I_1 \cdot B]}$ worked well to fit the model.

$\gamma_{[I_{1A}]}$ - There are no known measurements for $\gamma_{[I_{1A}]}$, the deactivation rate constant of Ire1, where the general deactivation rate in our model is of the form $F_{[I_{1A}]} = \gamma_{[I_{1A}]} \frac{[I_0]^n}{[I_0]^n + [I_{1A}]^n}$ as represented in Figure S10b. The most important assumption of Ire1 deactivation that was crucial for fitting the model to the data was that the active state of Ire1 was stabilized as a function of increasing the active Ire1 population. For our model we were able to fit the data by setting $\gamma_{[I_{1A}]} = \gamma_{[I_1 \cdot B]}$, with a best fit of $n = 4.5, I_0 = 45$. Reasonable fits of the model were obtained over the ranges of $n = 3 - 6, I_0 = 20 - 60$. However, for $n = 1, I_0 = 15$, Figure S9c-d plots the results of the dose dependent splicing reporter sampled at 200 minutes as well the results for the washout experiment. Both the switch-like behavior the $ire1^{bipless}$ dose response and the delay in the $ire1^{bipless}$ washout experiment are lost. That said, we would like to point out that this cooperative function is a simplified representation of the ire1 cooperativity in the foci dynamics.

4.2 Additional Parameter Sensitivity Analysis

The modeling analysis implemented in the paper assumed the mean protein folding time, $1/\gamma_{fold}$, to be 20 minutes. However, the ratio S_u/γ_{fold} dictates the basal unfolded protein population. Therefore, we checked that the qualitative behavior of the model is insensitive to the folding time by varying the mean between 12 and 20 minutes, while keeping the ratio (basal population) constant. Figures S12a-b show the dose response curves at 200 minutes and the washout experiments, respectively, for folding times of 12, 15 and 20 (best fit) minutes. In all cases, the system exhibited the same

qualitative trends seen in the data. We also examined the sensitivity of the model to different values of the cytosolic diffusion coefficient, D_c, which affects many reaction constants simultaneously. We varied D_c over a range of $.5 < D_c < 2.0$ $\mu \mathrm{m}^2 s^{-1}$. Over this range, the model robustly reproduced the trends seen in the data as seen in Figure S12c for the washout experiments. The dose response curves at 200 minutes (not shown) were all very similar as well.

Our model assumes an Ire1 molecular count of 256 molecules/cell [*Ghaemmaghami et al.* (2003)], which is based on an average value over many cells. We varied the range of Ire1 from 232 to 281. A notable feature of the model is that while the deactivation dynamics of the wild type system are still faster than the $ire1^{bipless}$ mutant in the simulation of the washout experiment, a large variability in the shutoff delay was was observed as the number of Ire1 molecules varied for the $ire1^{bipless}$ mutant (Figure S12d). This observation constitutes an interesting experimental prediction.

References

[*Axelsen and Sneppen*(2004)] Axelsen J., Sneppen, K. , (2004) Quantifying the benefits of translation regulation in the unfolded protein response. *Physical Biol.*, 1:159-65.

[*Berg and Purcell*(1977)] Berg H., Purcell, W., (1977) Physics of Chemoreception. *Biophys. Journ.*, 20:193-219.

[*Bertolotti et al.*(2000)] Bertolotti A., Zhang, Y., Hendershot, L., Harding, H., Ron, D., (2000) Dynamic interaction of BiP and ER stress transducers in the unfolded protein response. *Nat. Cell Biol.*, 2(6):326-32.

[*Credle et al.*(2005)] Credle J., Finer-Moore, J., Papa, F., Stroud, R., Walter, P., (2005) On the mechanism of sensing unfolded protein in the endoplasmic reticulum. *Proc. Natl. Acad. Sci. USA*, 102(52):18773-84.

[*Ghaemmaghami et al.* (2003)] Ghaemmaghami S, Huh W-K, Bower K, Howson RW, Belle A, Dephoure N, O'Shea EK, Weissman JS. (2003) Global analysis of protein expression in yeast. *Nature*, 425:737-41.

[*Hebert and Molinari*(2007)] Hebert, D. and Molinari, M. (2007) In and Out of the ER: Protein Folding, Quality Control, Degredation, and Related Human Diseases. *Physiol Rev*, 87:1377-1408.

[*Mori et al.*(1997)] Mori K., Kawahara, T., Hideki, Y., Takashi, Y., (2003) Endoplasmic Reticulum Stress-induced mRNA Splicing Permits Synthesis of Transcription Factor Hac1p/Ern4p That Activates the Unfolded Protein Respsonse. *Mol. Biol. Cell*, 8:1845-62.

[*Sidrauski et al.*(1996)] Sidrauski C., Cox, J., Walter, P., (1996) tRNA Ligase is Required for Regulated mRNA Splicing in the Unfolded Protein Response. *Cell*, 87:405-413.

[*Walter]* Walter, P., Personal Communication.

Chapter 3

Homeostatic Adaptation to Endoplasmic Reticulum Stress depends on Ire1 Kinase Activity

Published March 28, 2011

Homeostatic adaptation to endoplasmic reticulum stress depends on Ire1 kinase activity

Claudia Rubio,[1,2] David Pincus,[1,2] Alexei Korennykh,[1,2] Sebastian Schuck,[1,2] Hana El-Samad,[2] and Peter Walter[1,2]

[1]Howard Hughes Medical Institute and [2]Department of Biochemistry and Biophysics, University of California, San Francisco, San Francisco, CA 94158

Accumulation of misfolded proteins in the lumen of the endoplasmic reticulum (ER) activates the unfolded protein response (UPR). Ire1, an ER-resident transmembrane kinase/RNase, senses the protein folding status inside the ER. When activated, Ire1 oligomerizes and trans-autophosphorylates, activating its RNase and initiating a nonconventional mRNA splicing reaction. Splicing results in production of the transcription factor Hac1 that induces UPR target genes; expression of these genes restores ER homeostasis by increasing its protein folding capacity and allows abatement of UPR signaling. Here, we uncouple Ire1's RNase from its kinase activity and find that cells expressing kinase-inactive Ire1 can regulate Ire1's RNase, splice *HAC1* mRNA, produce Hac1 protein, and induce UPR target genes. Unlike wild-type *IRE1*, kinase-inactive Ire1 cells display defects in Ire1 deactivation. Failure to properly inactivate Ire1 causes chronic ER stress and reduces cell survival under UPR-inducing conditions. Thus, Ire1-catalyzed phosphoryl-transfer aids disassembly of Ire1 signaling complexes and is a critical component of the UPR homeostatic feedback loop.

Introduction

In eukaryotic cells, all proteins that enter the secretory pathway must pass through the ER to be properly folded and modified. When the demand for protein folding in the ER exceeds the capacity of the compartment, misfolded proteins accumulate and activate the unfolded protein response (UPR). Activation of the UPR induces a broad transcriptional program, resulting in increased production of ER-resident protein folding machinery and ER-associated degradation components (Travers et al., 2000), and leading to ER expansion (Bernales et al., 2006; Schuck et al., 2009). As a consequence, the protein folding capacity of the ER is increased and protein folding stress is relieved. The UPR thus serves as a homeostatic feedback loop that monitors the state of the ER and alters gene expression to adjust protein folding capacity according to need, thereby restoring proper function to the ER.

In the yeast *Saccharomyces cerevisiae*, the UPR is initiated by an ER-resident transmembrane sensor, Ire1 (Cox et al., 1993; Mori et al., 1993). When activated by the accumulation of misfolded proteins, Ire1 removes a 252-nucleotide inhibitory intron from the mRNA encoding Hac1, a bZIP transcription factor that up-regulates transcription of UPR target genes (Cox and Walter 1996; Mori et al., 1996; Travers et al., 2000). Removal of this intron and ligation of the severed exons by tRNA ligase produces a spliced form of *HAC1* mRNA that is efficiently translated into the Hac1 transcription factor (Cox and Walter 1996; Rüegsegger et al., 2001). Because unspliced *HAC1* mRNA is not translated before the excision of this intron, Ire1 RNase activation provides the key switch in UPR signaling.

Ire1 is a single-pass transmembrane protein with one domain in the ER lumen and two domains, a kinase and an RNase, in the cytosol (Cox et al., 1993; Sidrauski and Walter 1997). The lumenal domain of Ire1 senses unfolded proteins and, once activated, drives Ire1 oligomerization (Shamu and Walter 1996; Credle et al., 2005). Ire1's lumenal domain resembles the peptide-binding domain of antigen-presenting major histocompatibility complexes. We have proposed that direct binding of unfolded polypeptide chains to a presumed peptide binding groove in this domain provides the activating signal (Credle et al., 2005; Pincus et al., 2010), although more indirect models of Ire1 activation have also been proposed (Bertolotti et al., 2000; Okamura et al., 2000; Kimata et al., 2004). Lateral oligomerization

C. Rubio and D. Pincus contributed equally to this paper.

Correspondence to Peter Walter: peter@walterlab.ucsf.edu

Abbreviations used in this paper: HPL, hyper-phosphorylated loop; SR, splicing reporter; UPR, unfolded protein response; UTR, untranslated region; WT, wild type.

The Rockefeller University Press $30.00
J. Cell Biol.
www.jcb.org/cgi/doi/10.1083/jcb.201007077

Cite by DOI: 10.1083/jcb.201007077 JCB 1 of 14

Published March 28, 2011

brings the cytosolic portion of neighboring Ire1 molecules into proximity, which promotes trans-autophosphorylation of Ire1 kinase and activation of the RNase (Shamu and Walter 1996).

Mutation of essential catalytic residues and phosphorylation sites in the Ire1 kinase domain block *HAC1* mRNA splicing and prevent up-regulation of UPR target genes (Cox et al., 1993; Mori et al., 1993; Shamu and Walter 1996), suggesting that phosphorylation by Ire1 kinase during activation is essential for RNase function. However, if the nucleotide-binding pocket of Ire1 kinase is mutated to specifically accommodate the ATP-competitive drug 1NM-PP1, Ire1 retains RNase activity in response to ER stress, showing that the requirement for phosphorylation can be entirely bypassed (Papa et al., 2003). Occupation of the engineered 1NM-PP1 binding pocket is sufficient to cause the conformational change in Ire1 that activates the RNase. Because phosphorylation sites are necessary for RNase function but phosphorylation by itself appears dispensable, the functional significance of phosphoryl-transfer by Ire1 kinase has remained unclear.

Evidence from studies of Ire1-like enzymes supports the idea that phosphoryl-transfer mediated by the kinase is indeed dispensable for nuclease activation. RNase L, a close homologue of Ire1, is a cytosolic, ligand-activatable RNase that has lost kinase activity but retained a catalytically inactive pseudokinase domain (Dong et al., 2001). In contrast, the kinase activity of Ire1 has been preserved in evolution, suggesting a functional role for Ire1-mediated phosphoryl-transfer. Although previous findings with 1NM-PP1–sensitized Ire1 kinase are in apparent contradiction with this idea, those data show only that Ire1 kinase activity can be bypassed without consequence for RNase activation; they do not rule out a possible role for the kinase in the broader scope of UPR biology.

In this study, we explored the role of the Ire1 kinase function in vitro and in vivo by rationally designed, conservative mutagenesis of central catalytic residues in the Ire1 kinase-active site. Mutations were designed to preserve interactions between ATP cofactor and Ire1 but to selectively disrupt catalytic phosphoryl-transfer. We show that these mutations yield a kinase-inactive Ire1 that retains wild-type (WT) RNase activity in living cells. This variant of Ire1 is activated by unfolded protein accumulation without a requirement for exogenous drugs, such as 1NM-PP1, thereby eliminating potential complications of off-target effects of the drug within the cell. These studies confirmed the view that Ire1's kinase domain regulates its RNase activity, but also revealed a critical role for phosphoryl-transfer in the homeostatic feedback of the UPR.

Results

Mutations in Ire1 kinase abolish phosphoryl-transfer but preserve RNase activity

Based on sequence conservation between Ire1 and related CDK2-like kinases as well as the recently solved crystal structures of the cytosolic portion of Ire1 (Lee et al., 2008; Korennykh et al., 2009), we designed an Ire1 variant with uncoupled kinase and RNase activities. To this end, we identified two catalytic residues, D797 and K799, in the nucleotide-binding pocket of Ire1 kinase. These residues are predicted to coordinate the terminal phosphate of ATP bound to Ire1 kinase (Fig. 1 A), and, by analogy to other kinases, are required to catalyze phosphotransfer (Lee et al., 2008). We reasoned that mutating these residues to asparagines would preserve overall steric packing, hydrophobicity, and hydrogen bonding at the kinase-active site but disable proton transfer and thereby abolish phosphorylation (Fig. S1 A). Thus, we expected that the mutant Ire1(D797N,K799N) would be kinase inactive but still able to activate its RNase via nucleotide binding.

To carry out in vitro studies, we recombinantly expressed and purified the cytosolic portion of Ire1 WT and mutant Ire1. These constructs consisted of kinase and RNase domains preceded at the N terminus by 32 amino acids derived from the linker region that tethers the kinase domain to the transmembrane region. We previously showed that this peptide extension is important, as it enhances Ire1's ability to activate its RNase by up to four orders of magnitude (Korennykh et al., 2009). We term these constructs Ire1KR32 (WT) (Korennykh et al., 2009) and Ire1KR32(D797N,K799N).

MALDI mass spectrometry analyses have shown that WT Ire1KR32 is highly phosphorylated when purified from *Escherichia coli*, likely as a result of autophosphorylation (Korennykh et al., 2009). Phosphorylation is evident in the mass-to-charge ratio (M/z) of WT Ire1KR32, which is higher than expected based on its theoretical molecular weight (Fig. S1 B). The shift of ∼1.3 kD is consistent with the presence of ∼17 phosphates and can be ameliorated by phosphatase treatment (Fig. S1 C). In contrast, purified Ire1KR32(D797N,K799N) has an M/z value that is precisely as expected based on its primary sequence, indicating that this protein is entirely unphosphorylated (Fig. S1 B; and see Fig. S7 in Korennykh et al., 2009). These data suggest that Ire1KR32(D797N,K799N) is kinase inactive.

To confirm that Ire1KR32(D797N,K799N) was indeed kinase inactive, we measured trans-autophosphorylation of the recombinant proteins in an in vitro kinase assay. As expected, WT Ire1KR32 showed robust trans-autophosphorylation (Fig. 1 B, lanes 1–3) whereas Ire1KR32(D797N,K799N) exhibited no detectable kinase activity (Fig. 1 B, lanes 4–6). To show that the kinase-inactive Ire1 mutant is properly folded and is a competent substrate for phosphorylation, we mixed recombinant kinase-inactive Ire1 protein with a shorter WT version, Ire1KR, lacking the 32-amino acid peptide extension (Korennykh et al., 2009). This enzyme retains WT kinase activity (Fig. 1 B, lanes 7–9) and can be distinguished from the Ire1KR32 versions by its lower molecular weight. When we mixed Ire1KR in vitro with Ire1KR32(D797N,K799N), we detected robust phosphorylation of the mutant enzyme (Fig. 1 B, lanes 10–12; top bands). In these mixing reactions, the top bands corresponding to the kinase-inactive variant of Ire1 were more extensively labeled with radioactive phosphate than WT enzyme. This is likely due to the greater number of unphosphorylated residues in kinase-inactive Ire1 available for phosphorylation when introduced to kinase-active enzyme.

Based on the previous observation that occupation of the active site of Ire1 kinase by nucleotide cofactor is sufficient

Published March 28, 2011

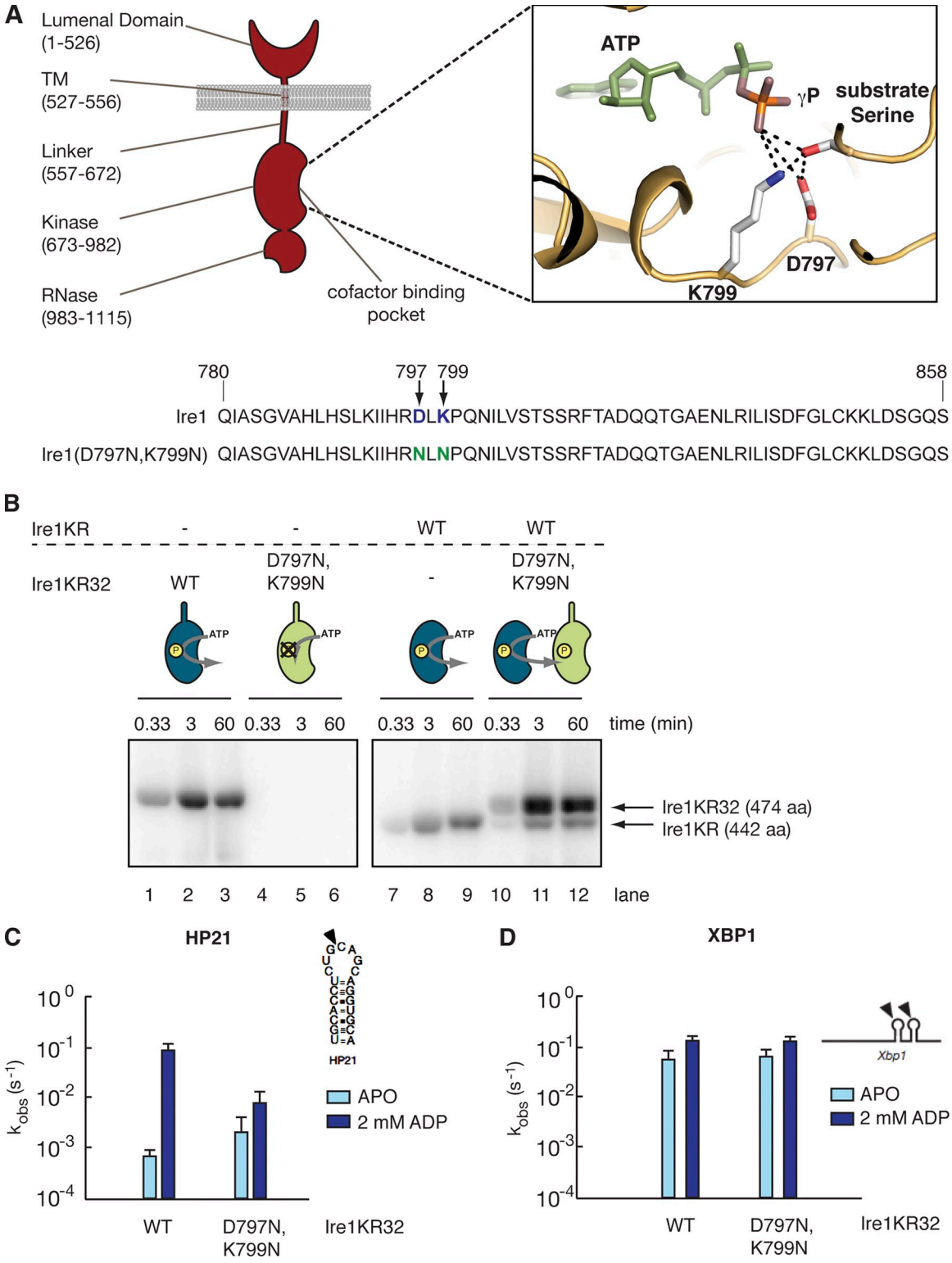

Figure 1. **Mutations in Ire1 kinase abolish phosphate transfer but preserve RNase activity.** (A) A schematic representation of Ire1 depicting the location of each functional domain. Residues D797 and K799 in the nucleotide-binding pocket of the kinase domain hydrogen bond with the terminal phosphate of ATP to catalyze phosphate transfer to the substrate serine. Mutation of D797 and K799 to noncatalytic asparagines is predicted to block phosphate transfer but allow for ATP binding. (B) The kinase activity of recombinant Ire1KR32 (WT, 474 amino acids; lanes 1–3) and Ire1KR32(D797N,K799N) (lanes 4–6) were measured in an in vitro kinase assay. Recombinant Ire1 was mixed with 0.033 μM [γ^{32}]P-ATP and incubated at 30°C for the time indicated. Reactions were stopped in 1% SDS loading buffer and separated by SDS-PAGE. A truncated version of WT Ire1, Ire1KR (442 amino acids; lanes 7–9), was mixed with Ire1KR32(D797N,K799N) (lanes 10–12). (C and D) In vitro RNA cleavage assays were performed using purified substrate RNA, HP21 (C) or *Xbp1* (D), and either WT Ire1KR32 or Ire1KR32(D797N,K799N). Reactions were performed in the presence and absence of 2 mM ADP. The lower sensitivity of the *Xbp1* mRNA cleavage reaction to the ADP cofactor during cleavage suggests that a longer RNA substrate may independently stabilize the Ire1 oligomer, perhaps by bridging between multiple adjacent monomers. Bar values were obtained from single-exponential fitting of time courses. Error bars show standard errors of the single-exponential fitting. The time courses were repeated multiple times and k_{obs} values reproduced within twofold.

Published March 28, 2011

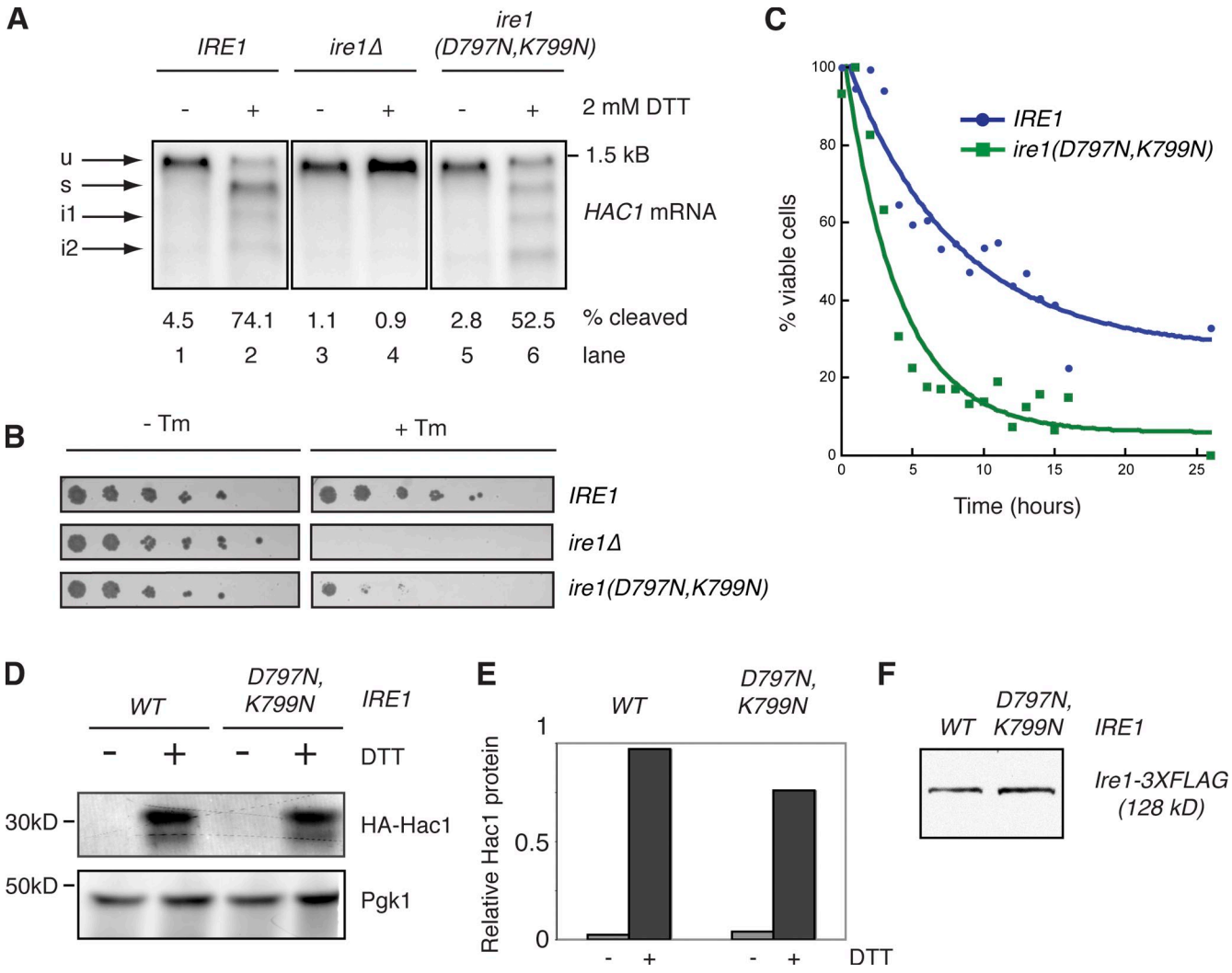

Figure 2. **Ire1 kinase activity, uncoupled from *HAC1* mRNA splicing, is important for cell survival during the UPR.** (A) Cells bearing WT *IRE1* (lanes 1 and 2), a deletion of *ire1* (lanes 3 and 4), or *ire1(D797N,K799N)* (lanes 5 and 6) were left uninduced (−) or induced with 2 mM DTT (+). *HAC1* mRNA splicing was analyzed by Northern blotting. The positions of the unspliced (u; 1449 nucleotides) and spliced (s; 1197 nucleotides) forms of *HAC1* mRNA are indicated with arrows. Splicing intermediate i1 (980 nucleotides) corresponds to the 5′ exon–intron hybrid species, whereas i2 (728 nucleotides) corresponds to the 5′ exon alone. (B) Cells carrying WT *IRE1*, a deletion of *ire1*, or *ire1(D797N,K799N)* were grown in culture, diluted to equal cell number, serially diluted 1:5, and plated onto permissive medium (−Tm) or medium containing 0.25 µg/ml tunicamycin (+Tm). (C) WT *IRE1* or *ire1(D797N,K799N)* cells were grown in culture to OD_{600} 0.2, the UPR was induced by the addition of 2 mM DTT. The value for percent viable cells was determined by measuring the number of colony-forming units over time (see Materials and methods). DTT was refreshed and cells were kept at an OD at or below 0.2 throughout the duration of the experiment. (D) WT or mutant *ire1* cells carrying HA-tagged Hac1 were left uninduced or induced with 2 mM DTT, and total protein was isolated. Samples were separated by SDS-PAGE and subjected to Western blotting using an anti-HA antibody or an anti-PGK1 antibody. (E) Hac1 protein was quantified, normalized to PGK1 levels, and plotted. (F) Total protein was isolated from WT- or *Ire1(D797N,K799N)*- expressing cells, separated by SDS-PAGE, and subjected to Western blotting using an anti-FLAG antibody. Ire1 protein levels are equivalent in WT and *ire1(D797N,K799N)* cells.

to cause activation of the RNase, we expected that Ire1KR32(D797N,K799N) would retain RNase activity and that its activity would be stimulated by the presence of nucleotide. To test this prediction, we measured RNase activity in an in vitro cleavage assay using HP21, a previously characterized small substrate RNA containing a specific Ire1 cleavage site, in the presence or absence of ADP cofactor. In previous experiments, ADP stimulated Ire1KR32's RNase activity by ∼200-fold (Korennykh et al., 2009). Here, in the absence of cofactor, both enzymes exhibited the same basal RNase activity as Ire1KR32 (Fig. 1 C, "APO"), consistent with previous observations (Korennykh et al., 2009). Addition of ADP increased the RNase of Ire1KR32(D797N,K799N) 10-fold (versus ∼100-fold for WT Ire1KR32; Fig. 1 C, "ADP"). These data are consistent with the idea that binding of cofactor stimulates the RNase activity of Ire1 in the absence of phosphorylation (Papa et al., 2003). In in vitro assays using the HP21 substrate, the RNase activity of Ire1KR32(D797N,K799N) was 10-fold lower than that of WT. However, when a larger 443-nt *Xbp1* mRNA-derived RNA fragment was used as a substrate (Korennykh et al., 2009), Ire1KR32(D797N,K799N) cleaved with a rate (k_{obs} = 0.19 s^{-1}) indistinguishable from that of WT Ire1KR32 (k_{obs} = 0.19 s^{-1}; Fig. 1 D). The *Xbp1* mRNA is a 400-nt substrate derived from the mammalian counterpart to *HAC1* mRNA. This substrate is cleaved by Ire1 in vitro with kinetics identical to that of *HAC1* mRNA substrates of comparable length (unpublished data).

Published March 28, 2011

The low ADP sensitivity of the *Xbp1* mRNA cleavage reaction suggests a diminished requirement for cofactor during cleavage of this substrate. Present work in our laboratory is aimed at understanding the molecular mechanism of this phenomenon. This longer substrate RNA more closely resembles the endogenous in vivo substrate of Ire1 RNase, suggesting that kinase-inactive Ire1(D797N,K799N) should retain RNase function in living cells.

Ire1 kinase activity is dispensable for *HAC1* mRNA splicing but enhances cell survival under ER stress

Because our in vitro results showed that we had successfully uncoupled the kinase and RNase functions of Ire1, we used kinase-inactive Ire1(D797N,K799N) to directly investigate the role of Ire1 kinase activity in vivo. This approach afforded the first opportunity to ask this question without requiring the addition of exogenous drug as past studies necessitated.

Our in vitro studies predict that cells expressing Ire1(D797N,K799N) should splice *HAC1* mRNA upon UPR induction. To test this, we constructed a strain carrying a chromosomally integrated mutant *IRE1* allele as the sole copy of *IRE1* in the cell. We then induced the UPR and measured *HAC1* mRNA splicing by Northern blotting. We induced ER stress with DTT, which causes protein misfolding in the ER by disrupting disulfide bond formation. As predicted, spliced *HAC1* mRNA was produced upon DTT treatment in *ire1(D797N,K799N)* cells (Fig. 2 A, lanes 5 and 6). In contrast, *HAC1* mRNA was not spliced in *ire1Δ* cells (Fig. 2 A, lanes 3 and 4). In these experiments, *ire1(D797N,K799N)* proved mildly hypomorphic, as the amount of *HAC1* mRNA cleaved in the mutant cells was reduced compared with WT and *HAC1* splicing intermediates were more abundant at the time point taken. This was not due to differences in the expression levels of Ire1 (Fig. 2 F). Nevertheless, these data reinforce the notion that Ire1 kinase activity is not required for RNA splicing.

We were surprised to discover that splicing of *HAC1* mRNA in *ire1(D797N,K799N)* cells failed to ensure cell survival under ER stress. When plated on medium containing tunicamycin, a drug that induces the UPR by blocking glycosylation in the ER, *ire1(D797N,K799N)* cells displayed a severe growth defect (Fig. 2 B). This resulted from loss of cell viability rather than growth arrest: sustained ER stress killed *ire1(D797N,K799N)* cells significantly earlier than WT cells (Fig. 2 C).

In search of an explanation for this growth defect, we tested whether functional Hac1 protein was produced from spliced *HAC1* mRNA in *ire1(D797N,K799N)* cells. To this end, we measured Hac1 protein production and determined the scope of the transcriptional response by assessing global mRNA expression after UPR induction. WT *IRE1* or *ire1(D797N,K799N)* cells expressing HA-tagged Hac1 were treated with DTT to induce the UPR and probed for HA-Hac1 by Western blotting. *Ire1(D797N,K799N)* cells produced Hac1 protein at nearly WT levels (Fig. 2, D and E). Likewise, the microarray transcriptional profile of UPR-induced *ire1(D797N,K799N)* cells revealed a profile nearly indistinguishable from that of WT cells (Fig. S2 A). Canonical UPR target genes were up-regulated with similar kinetics, and to a comparable extent, in WT and *ire1(D797N,K799N)* cells. Specific UPR target genes are highlighted in Fig. 3 A. Collectively, these data show that the observed reduction in *HAC1* mRNA splicing in *ire1(D797N,K799N)* cells does not lead to impairment of canonical UPR signaling.

One reason that a cell might die despite expression of target genes is that mRNAs are not translated. To confirm that protein products corresponding to UPR targets were also made, we determined Kar2 protein levels by Western blotting and measured global translation rates during the ER stress. The induction of Kar2 mirrored the microarray result for both WT and *ire1(D797N,K799N)* mutant cells (Fig. 3 B), confirming that expression of this canonical UPR target was intact in both strains. Furthermore, general translation rates were equivalent in both WT and *ire1(D797N,K799N)* cells (Fig. S2 B), indicating that global mRNA translation was not impaired in mutant cells. No explanation for the enhanced loss of cell viability of *ire1(D797N,K799N)* mutant cells was evident in these data.

As a consequence of UPR activation, the ER expands to meet the increased need for protein folding capacity (Cox et al., 1997; Bernales et al., 2006; Schuck et al., 2009). To further ensure that UPR signaling downstream of Ire1 was unimpaired, we measured ER expansion. Using a GFP-tagged version of the ER marker Sec63 (Prinz et al., 2000), we quantified expansion of the cortical ER before and after UPR induction in WT and *ire1(D797N,K799N)* cells. In confocal sections through the middle of unstressed cells, the cortical ER marked by Sec63-GFP is visible underneath the plasma membrane as a broken line because the tubular ER network appears in cross section. Upon ER stress, the cortical ER is converted into expanded membrane sheets and appears as a continuous line. Consistent with microarray data showing normal induction of target genes, UPR-mediated ER expansion occurred normally in mutant cells (Fig. 3, C and D). Thus, the slight reduction in Hac1 protein produced in *ire1(D797N,K799N)* cells (Fig. 2 E) did not weaken UPR events downstream of Hac1 protein production. Collectively, the data presented thus far indicate that canonical UPR activation remains intact in *ire1(D797N,K799N)* cells.

Ire1(D797N,K799N) fails to adapt to sustained ER stress

The homeostatic feedback response that is mediated by the UPR is characterized by an activation phase in which Ire1 begins to signal and an adaptive phase that occurs when cells adjust to ER stress and Ire1 is turned off (Pincus et al., 2010). Because our findings indicate that Ire1 activation and induction of its downstream transcriptional targets are normal in *ire1(D797N,K799N)* cells, we set out to examine the dynamics of Ire1 activation and attenuation in *ire1(D797N,K799N)* cells. To this end, we took advantage of a splicing reporter, termed SR, previously developed in our laboratory (Aragón et al., 2009). In the SR, the *HAC1* ORF has been replaced by that of *GFP* (Fig. 4 A), while the intron as well as the 5′ and 3′ untranslated regions (UTRs) of the *HAC1* mRNA are maintained so that translational inhibition of SR mimics that of the *HAC1* mRNA. Ire1-mediated splicing of this reporter produces a GFP signal that can be quantitatively measured by flow cytometry.

Published March 28, 2011

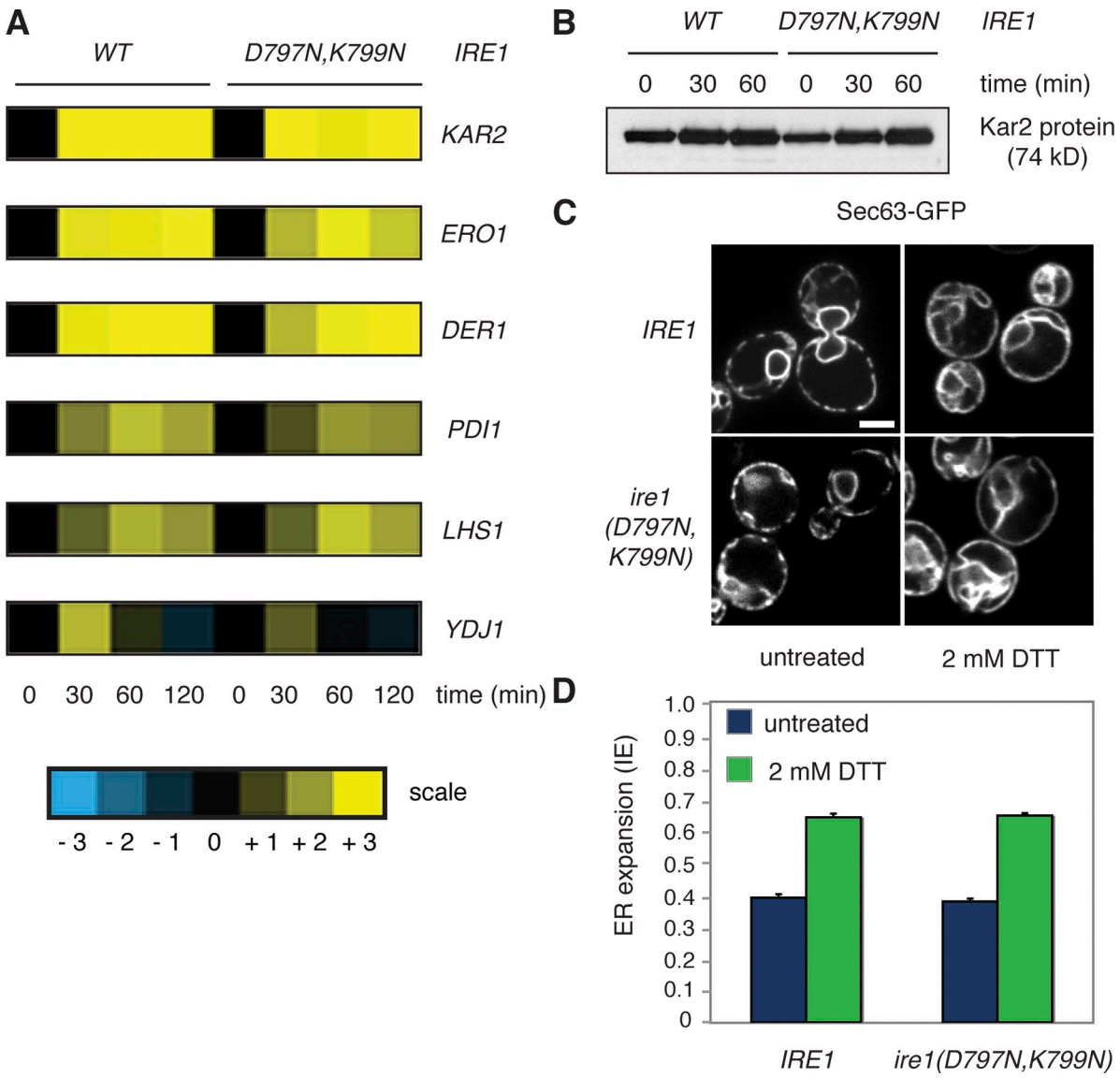

Figure 3. **Downstream events in UPR activation are normal in *ire1(D797N,K799N)* cells.** (A) Microarray analysis was performed to assess the total mRNA expression profiles of WT *IRE1* or *ire1(D797N,K799N)* cells over time after induction with 2 mM DTT. Cells were sampled at 0, 30, 60, and 120 min. Canonical target genes, *KAR2*, *ERO1*, *DER1*, *PDI1*, and *LHS1* were up-regulated and *YDJ1* was down-regulated equally upon UPR induction in both strains. (B) Total protein was isolated from cells bearing WT *IRE1* or *ire1(D797N,K799N)* after 0, 30, or 60 min in 2 mM DTT and analyzed by Western blot for Kar2 protein. Characteristic increase in Kar2 protein upon UPR induction was observed in both strains. (C and D) ER expansion was measured in WT and *ire1(D797N,K799N)* cells. The UPR was induced in WT or mutant *ire1(D797N,K799N)* cells bearing a GFP-tagged version of Sec63 as an ER marker. Images were taken before and after 2 h UPR induction, and cortical ER expansion was quantified as described in Schuck et al. (2009) and expressed as the index of expansion (IE). Error bars indicate SEM. Bar (C), 2 µm.

In WT cells, SR fluorescence increased over time with increasing DTT concentration (Fig. 4 B). At low DTT concentrations (below ~2 mM), GFP levels in WT cells reached a plateau after ~120 min. This plateau, a result of the long half-life of GFP, signifies Ire1 deactivation and is characteristic of an intact homeostatic response that restores the folding capacity of the ER and quells Ire1 signaling.

In *ire1(D797N,K799N)* cells, SR splicing in the first 60–120 min was identical to that observed in WT cells. However, GFP levels continued to rise throughout the time course and its production continued even at doses of DTT to which WT cells adapted (Fig. 4 C). This phenomenon was most evident when reporter activity was plotted as a function of DTT concentration (Fig. 4, D and E). At the 60-min time point, the dose–response curves for both WT and *ire1(D797N,K799N)* cells overlapped, indicating that GFP production during the activation phase was equivalent for both WT and mutant enzymes (Fig. 4 D). In marked contrast, at 240 min the curves deviated substantially (Fig. 4 E), indicating that after prolonged ER stress Ire1(D797N,K799N) continued to signal at low and intermediate doses of DTT. Note that in these experiments both WT Ire1 and Ire1(D797N,K799N) displayed the same basal activity (Fig. 4, D and E; [DTT] = 0.3 mM) and reached the same maximal activity ([DTT] = 3.3 mM), indicating that Ire1 activation by itself was fully intact in the mutant cells (Fig. S3).

Published March 28, 2011

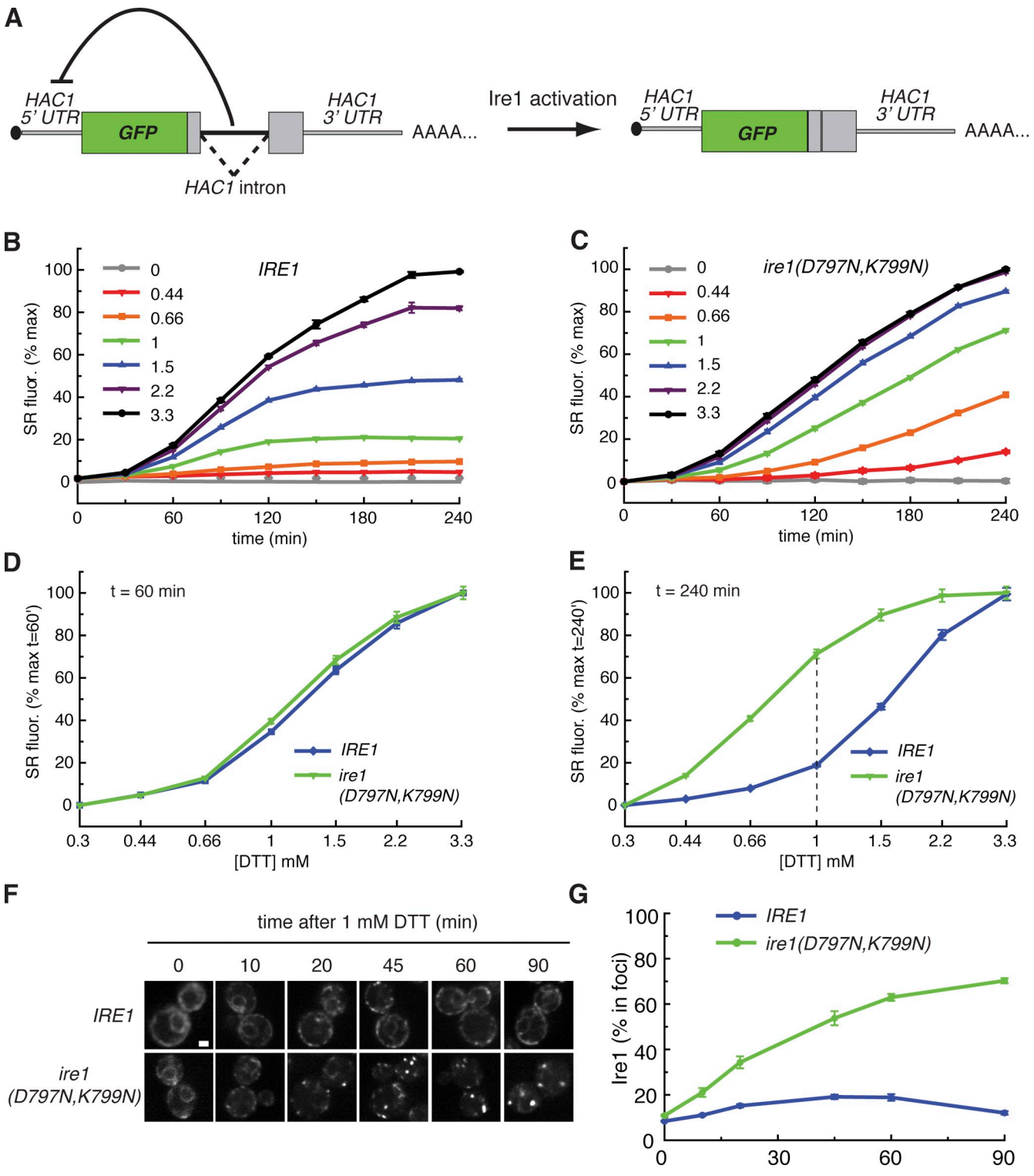

Figure 4. **Activation of Ire1(D797N,K799N) continues after WT activity has plateaued.** (A) A schematic of the fluorescent splicing reporter (SR) in which the *HAC1* ORF was replaced with GFP such that Ire1-mediated splicing of this reporter produces fluorescent GFP. (B and C) A dilution series of DTT, from 0 to 3.3 mM, was added to cells in culture. WT (B) or *ire1(D797N,K799N)* (C) cells were grown at 30°C and sampled at 30-min intervals over a 4-h time course. GFP signal was measured by flow cytometry, normalized to baseline and plotted over time. (D) SR fluorescence was plotted as a function of increasing [DTT] in WT and *ire1(D797N,K799N)* cells at 60 min after DTT addition. (E) The dose–response of SR fluorescence plotted as a function of [DTT] at 240 min after induction reveals that Ire1(D797N,K799N) was significantly more active than WT at all concentrations of DTT. The dotted line indicates the concentration of DTT at which the two curves most deviated. (F) WT or *ire1(D797N,K799N)* cells bearing GFP-tagged Ire1 were treated with 1 mM DTT and formation of Ire1 foci was imaged by confocal microscopy over time. (G) Foci formation measured in F was quantified as percentage of Ire1 in foci and plotted over time. The maximum value, 100%, is reached when all pixels containing Ire1-GFP signal are in foci (see supplementary methods in Aragón et al., 2009 for a detailed description of quantitation).

Published March 28, 2011

As a second measure of Ire1 activity, we monitored Ire1 oligomer formation, which can be observed and quantified by fluorescence microscopy as foci in living cells. Oligomer formation closely correlates with *HAC1* mRNA splicing and therefore is a powerful tool for monitoring Ire1 activation in vivo (Aragón et al., 2009). As in our previous studies, we inserted GFP between the transmembrane linker and kinase domains of WT and mutant forms of Ire1, a location that does not interfere with Ire1 function (Aragón et al., 2009). We measured foci formation of functional WT and mutant Ire1-GFP under conditions at which the adaptation phase dose–response curves of Ire1(D797N,K799N) and WT are most divergent (Fig. 4 E, [DTT] = 1 mM, dotted line). As shown in Fig. 4 F, WT Ire1-GFP formed small, transient foci whereas Ire1(D797N,K799N)-GFP formed foci that persisted to the end of the 90-min experiment (Fig. 4, F and G). This result is consistent with the observation that WT cells adapted to mild ER stress and shut down Ire1 signaling, while Ire1(D797N,K799N)-GFP activation was sustained in the mutant cells. These data indicate that *ire1(D797N,K799N)* cells fail to adapt to prolonged ER stress, suggesting that homeostatic feedback is impaired despite normal induction of UPR target genes.

Ire1(D797N,K799N) cells are able to alleviate ER stress

In principle, the impaired adaptation exhibited in *ire1(D797N,K799N)* cells could be due to a failure of the UPR to fix the problem in the ER or to an inability of Ire1 to deactivate once the stress has been relieved. To test the first possibility, we used a reporter of ER redox potential. DTT induces the UPR by shifting the ER redox potential to become more reducing and causes the accumulation of unfolded proteins by blocking disulfide bond formation; UPR induction, in turn, serves to reoxidize the ER lumen. The level of ER stress can be assessed using an ER-targeted redox-sensitive GFP (ero-GFP) reporter (Hanson et al., 2004; Merksamer et al., 2008). To test whether *ire1(D797N,K799N)* cells restore the oxidizing environment to the ER during sustained UPR insult, cells were treated with 0, 1, or 2 mM DTT (Fig. 5, A and B) and the ratio of reduced/oxidized ero-GFP ("r/o ratio") was measured by flow cytometry. In WT cells, the ero-GFP r/o ratio increased upon DTT treatment and then gradually decreased as ero-GFP became reoxidized over the course of the experiment (Fig. 5 A).

In *ire1(D797N,K799N)* cells the basal r/o ratio of ero-GFP was elevated relative to that in WT cells (Fig. 5 B, 0 mM DTT) and resulted in a relatively smaller fold increase. Despite the diminished dynamic range of the reporter, reoxidation was evident in *ire1(D797N,K799N)* cells at both concentrations of DTT (Fig. 5 D), indicating that UPR induction restored the oxidative potential of the ER. By contrast, the ero-GFP r/o ratio in *ire1Δ* cells showed normal baseline levels and plateaued after DTT addition (Fig. 5 C). Because these cells are unable to activate the UPR, these data are consistent with the requirement for UPR target gene induction to restore the oxidative environment of the ER.

Deactivation of Ire1(D797N,K799N) is impaired

An unexpected explanation for the elevated baseline of the ero-GFP r/o ratio in *ire1(D797N,K799N)* cells was provided by observing the intracellular localization of ero-GFP by fluorescence microscopy. In untreated WT cells, ero-GFP was localized to the ER as expected, whereas in *ire1(D797N,K799N)* cells ero-GFP was partially localized to the cytoplasm both before and after UPR induction (Fig. 5 E). The cytosolic ero-GFP likely accounts for the higher basal ero-GFP r/o ratio measured in Fig. 5 B because the cytosol is a reducing environment.

The cytosolic mislocalization of ero-GFP seen in *ire1(D797N,K799N)* cells was puzzling because our preceding data revealed no differences between WT and *ire1(D797N,K799N)* cells in the absence of stress. Most relevantly, mislocalization was not observed for Sec63-GFP, which properly localized to the ER in *ire1(D797N,K799N)* cells (Fig. 3 C). To confirm that translocation of endogenous ER-targeted proteins was normal, we analyzed the translocation of the ER chaperone Kar2. No difference in Kar2 translocation between untreated WT and *ire1(D797N,K799N)* cells was observed (unpublished data). We therefore conclude that the high expression levels of the ero-GFP reporter are responsible for its own localization defect in *ire1(D797N,K799N)* cells. We hypothesize that sustained expression of ER-targeted ero-GFP from a strong constitutive promoter causes chronic ER stress that, in *ire1(D797N,K799N)* cells, interferes with proper ero-GFP import into the ER.

To understand the nature of this ER translocation impairment, we turned to *ire1Δ* cells. These cells, which are unable to mount a productive UPR, properly localized ero-GFP to the ER (Fig. 5 E). The lack of cytosolic ero-GFP signal in *ire1Δ* cells demonstrates that loss of Ire1 activity is not sufficient to impair ER translocation. Rather, a productive UPR is additionally required to cause the translocation defect observed in *ire1(D797N,K799N)* cells.

One possibility is that *ire1(D797N,K799N)* cells fail to adapt to the chronic burden imposed on the ER by ero-GFP expression and do not properly deactivate Ire1. The resulting prolonged UPR signaling would create an overload of ER-targeted proteins, which might overwhelm the capacity of the translocation machinery and cause a back-up of ER client proteins in the cytoplasm. To address this hypothesis, we monitored the abatement of *HAC1* mRNA splicing and resolution of Ire1 foci after removal of ER stress. Northern blot analysis revealed that *HAC1* mRNA splicing in WT cells declined within 45 min of removing DTT and reset by 90 min after DTT removal (Fig. 6 A, top). In contrast, *ire1(D797N,K799N)* cells continued to splice *HAC1* mRNA even 120 min after ER stress had been removed (Fig. 6 A, bottom), indicating that loss of Ire1 kinase activity profoundly delayed Ire1 shut-off. The same trend was observed when we measured Ire1 foci formation: the dissolution of foci in WT cells was noticeable as early as 30 min after DTT washout, whereas Ire1(D797N,K799N) foci were still detectable 120 min after DTT removal (Fig. 6 B). These data are consistent with the hypothesis that the mechanism of Ire1(D797N,K799N) deactivation is impaired despite the fact that protein folding problems inside the ER are alleviated in these cells.

Hyper-phosphorylation of Ire1 is required for rapid de-oligomerization

Mass spectrometry data of the purified cytosolic portion of Ire1 suggest that a 28-amino acid loop (residues 864–892) in the

Published March 28, 2011

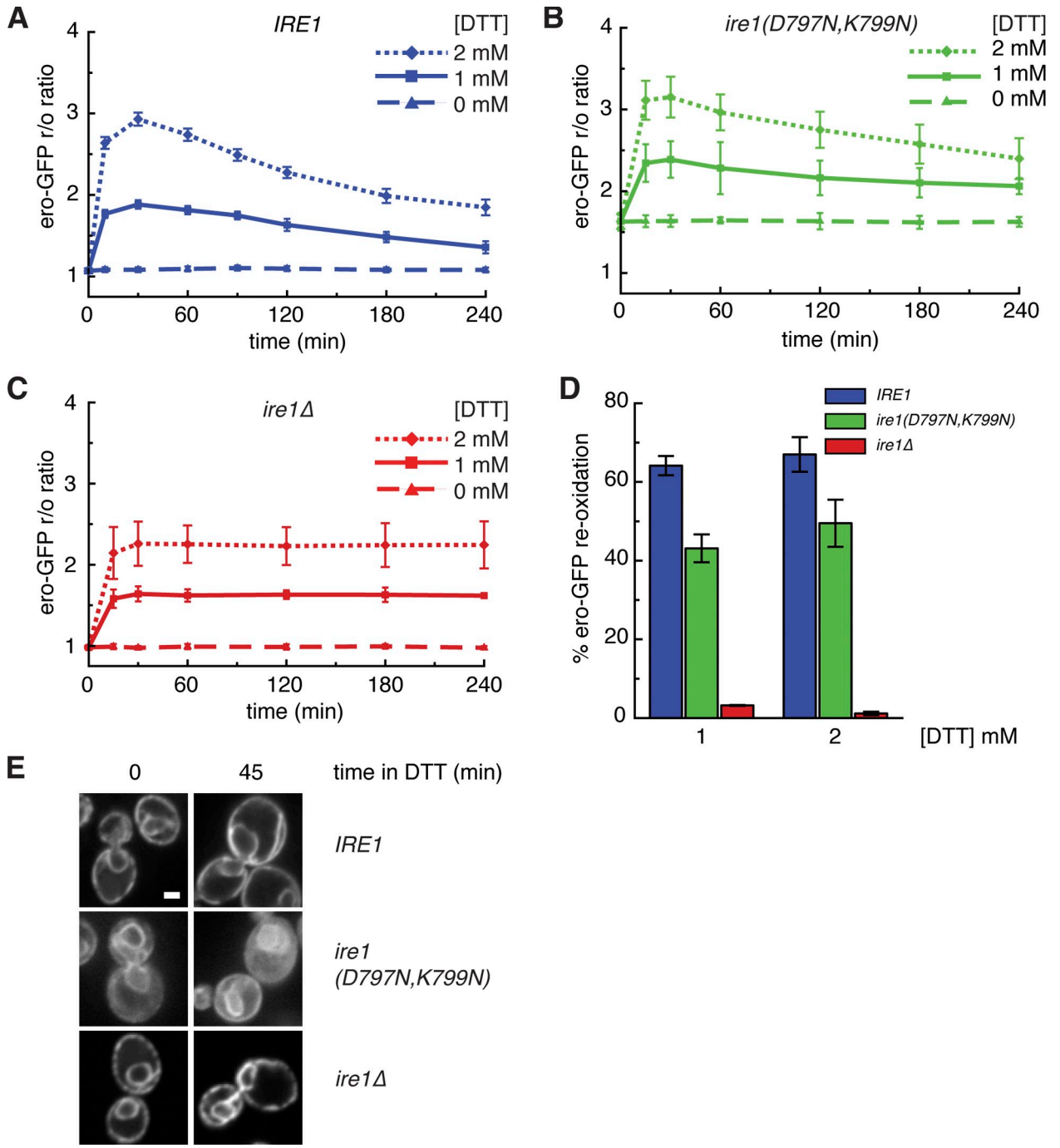

Figure 5. **The oxidation potential of the ER is restored in *ire1(D797N,K799N)* cells.** (A–D) Re-oxidation of the ero-GFP reporter occurs in the absence of kinase activity. (A) WT, (B) *ire1(D797N,K799N)* and (C) *ire1Δ* cells bearing the ER-targeted redox reporter, ero-GFP, were treated with 0, 1, or 2 mM DTT. The ratio of reduced-to-oxidized signal (r/o ratio) was measured by flow cytometry and plotted over time. (D) Percent reoxidation of ero-GFP was calculated for WT, *ire1(D797N,K799N)*, and *ire1Δ* cells in 0, 1, and 2 mM DTT (see Materials and methods). (E) Cells expressing ero-GFP were analyzed by spinning disk confocal microscopy before and after treatment with 2 mM DTT for 45 min.

C-terminal end of the kinase domain is highly phosphorylated (unpublished data). We propose that trans-autophosphorylation of this loop (termed HPL for hyper-phosphorylated loop) by Ire1 might contribute to quenching Ire1 activity. If this were true, deletion of HPL in WT *IRE1* would mimic the sustained signaling observed in *ire1(D797N,K799N)* cells, whereas deletion of HPL in Ire1(D797N,K799N) would have no effect on the deactivation phenotype of the mutant protein. To test this possibility, we created *ire1ΔHPL-GFP* and *ire1(D797N,K799N)ΔHPL-GFP* cells and monitored attenuation of Ire1 foci after ER stress removal. As shown in Fig. 6 B, foci in *ire1ΔHPL-GFP* cells formed readily upon treatment with 5 mM DTT and were sustained substantially longer than in WT control cells after DTT was removed. In contrast, the persistence of foci in *ire1(D797N,K799N)ΔHPL-GFP* cells mirrored that in *ire1(D797N,K799N)-GFP* cells (Fig. 6 C, orange and green

Published March 28, 2011

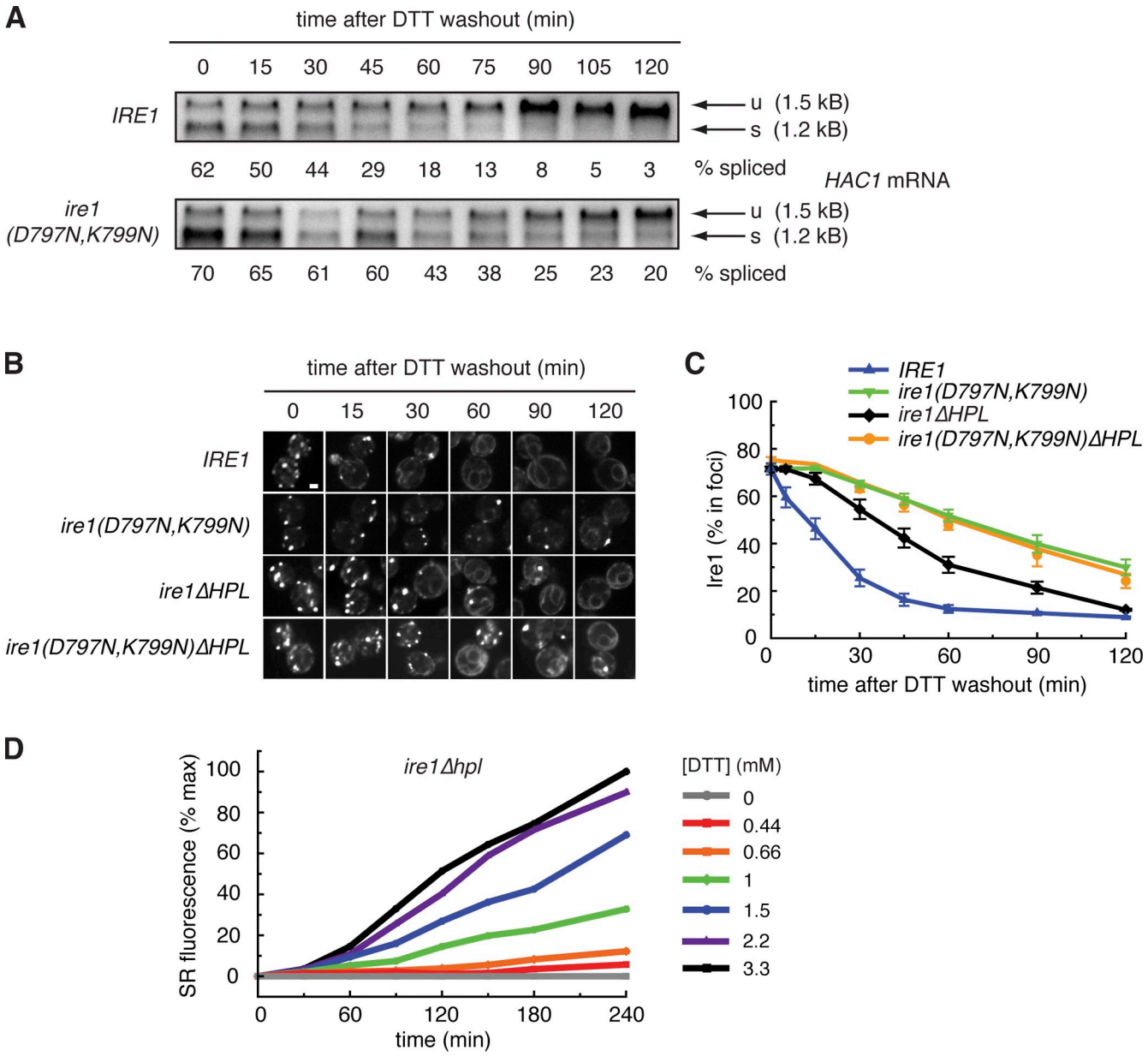

Figure 6. **Shut-off of Ire1(D797N,K799N) is delayed after removal of ER stress.** (A) WT or *ire1(D797N, K799N)* cells were treated with 5 mM DTT for 60 min before DTT washout. Cell samples were taken after DTT washout and total RNA was analyzed by Northern blot for *HAC1* mRNA. Unspliced (u) and spliced (s) forms of *HAC1* mRNA are indicated by arrows. (B and C) GFP-tagged variants of Ire1 were visualized by fluorescence microscopy after washout of 5 mM DTT. Quantitation of Ire1 foci is displayed in the bottom panel. (D) *Ire1ΔHPL* cells retain RNase activity. A dilutions series of DTT, from 0 to 3.3 mM, was added to *ire1ΔHPL* cells bearing the splicing reporter, SR. Cells were grown at 30°C and sampled at 30-min intervals over a 4-h time course. GFP signal was measured by flow cytometry and plotted over time.

lines), indicating that deletion of HPL had no effect on deactivation of Ire1 in the absence of phosphoryl-transfer. Importantly, *ire1ΔHPL-GFP* cells retained RNase activity as measured by SR splicing (Fig. 6 D), indicating that activation of Ire1ΔHPL-GFP was intact. Interestingly, the SR splicing phenotype of *ire1ΔHPL-GFP* cells resembled that of *ire1(D797N,K799N)* cells, indicating that Ire1ΔHPL has a deactivation defect similar to kinase-inactive Ire1 (compare Figs. 4 C and 6 D). The kinetics of foci disappearance in *ire1ΔHPL* cells resembled that in *ire1(D797N,K799N)* cells (Fig. 6 B), supporting the hypothesis that the HPL contributes to the regulation of Ire1 shut-off. Notably, however, the phenotype in *ire1ΔHPL* cells was not as strong as that seen in *ire1(D797N,K799N)* cells, indicating that phosphorylation of regions outside the HPL must also contribute to Ire1 deactivation.

Discussion

Ire1 provides the central gate in the information flow from the ER lumen during UPR induction. In response to sensing excessive concentrations of mis- or unfolded proteins in the ER lumen, Ire1 undergoes oligomerization and activation of its RNase function, which initiates the nonconventional splicing of *HAC1* mRNA. The role of Ire1's kinase domain has remained mysterious.

Published March 28, 2011

The paradox primarily derives from the observation that phosphoryl-transfer can be entirely bypassed in drug-sensitized Ire1 mutants while splicing and the downstream transcriptional program remain active, yet other mutations in the kinase domain, such as K702R, which abolishes kinase activity, impair the UPR. Here we used a rationally designed mutation in the kinase-active site that blocks phosphoryl-transfer activity but preserves nucleotide binding. The mutant retains Ire1's activation potential in vivo. Despite activating the canonical set of UPR target genes, however, the mutation prevents cells from restoring homeostasis. We trace this physiological defect to a defect in Ire1 shut-off, revealing a role of Ire1-mediated phosphoryl-transfer in regulating the homeostatic feedback of the UPR that is important for cell survival. A recent independent study (see Chawla et al. in this issue) showed that kinase-inactive Ire1(D828A) was able to bind nucleotide cofactor but was likewise unable to shut down Ire1 signaling in the absence of kinase activity. These data lend further support to the notion that Ire1 kinase plays an important role in the attenuation of Ire1 signaling.

Ire1 mutations allow uncoupling of kinase and RNase activities

Occupancy of the nucleotide-binding pocket in the Ire1 kinase domain renders the cytosolic portion of Ire1 prone to oligomerization by stabilizing the kinase module in the open conformation (Korennykh et al., 2009). Oligomerization in turn causes activation of Ire1's RNase, as interactions between neighboring Ire1 molecules in the ordered oligomer stabilize essential structural elements in the RNase-active site (Korennykh et al., 2009). Conformational control of the Ire1 kinase domain therefore regulates RNase activation.

In the ER membrane, oligomerization of Ire1 lumenal domains triggers activation of Ire1's cytosolic kinase/RNase modules by increasing their local concentration. In this manner, Ire1's RNase activity is subservient to events in the ER lumen, and cofactor binding to the kinase domain adjusts the activation threshold of the enzyme. Despite being kinase inactive, we found that Ire1(D797N,K799N) preserves activation of the UPR. The RNase activity of Ire1KR32(D797N,K799N) is responsive to the addition of nucleotide in vitro and Ire1(D797N,K799N) retains ER stress-responsive RNase activity in vivo, suggesting that nucleotide binding is a key step in Ire1 activation. Recent work showed that the nucleotide-binding pocket of Ire1 kinase was highly conserved in a sequence comparison of yeast Ire1 species, further supporting the notion that this binding module is an essential component of Ire1 (Poothong et al., 2010).

Sustained production of ER-targeted proteins is detrimental

We found that Ire1(D797N,K799N) activity is sustained well beyond the time when WT Ire1 activity shuts off, illustrating a loss in the quality of the UPR homeostatic feedback regulation. While ER stress properly activates Ire1(D797N,K799N) and induces a canonical transcriptional response, the mutant enzyme continues to signal as though the response were ineffective. Thus, the kinase activity of Ire1 plays a crucial role in completing the negative feedback loop of the UPR.

In WT cells, ero-GFP is localized to the ER and can serve as a reporter of the ER environment. Despite inducing the canonical UPR transcriptional program, *ire1(D797N,K799N)* cells exclude a portion of ero-GFP from the ER. In this context, a fraction of the reporter is retained in the reducing environment of the cytosol and ero-GFP returns a misleading signal that does not properly report on the condition of the ER lumen. Results obtained with this reporter must therefore be interpreted with caution. We believe that despite the increased baseline r/o ratio measured in *ire1(D797N,K799N)* cells, oxidative folding conditions are restored in the ER lumen. We surmise that the increase in cytosolic signal of ero-GFP is due to impaired ER translocation of the reporter.

The simplest explanation for this translocation block is that an increased load of ER-targeted proteins resulting from sustained activation of the UPR overloads the import machinery. In accordance with this view, long-term, acute ER stress leads to the appearance of preKar2 protein in WT cells as well, where it was previously observed as a higher molecular weight band (e.g., see Fig. 5 A in Schuck et al., 2009). Thus, it appears that the capacity of a cell to adapt to the increased ER load on the ER translocation machine may be inherently limited, leading to protein mislocalization under conditions of extreme stress. In this scenario, an ER-translocation defect would be a symptom of severe ER stress and may be coupled to a plethora of pleiotropic defects that could explain the severe growth defect observed in UPR-induced *ire1(D797N,K799N)* cells.

In mammalian cells, activation of the PERK-branch of the UPR serves to down-regulate translation and thereby to reduce the overall load of newly synthesized proteins entering the ER. In *S. cerevisae* no analogous pathway exists. The PERK pathway might have evolved as a solution to the impairment in ER translocation observed in yeast and therefore serves a physiologically desirable function: to slow the influx of protein into the secretory pathway under conditions of ER stress.

Phosphorylation of Ire1 is important for deactivation

A compelling finding in this work is that phosphoryl-transfer by Ire1 kinase, although largely dispensable for its activation, plays an important role in Ire1 shut-off. Abatement of *HAC1* mRNA splicing and dispersal of foci are delayed in *ire1(D797N,K799N)* mutant cells, both under mild ER stress where the UPR in WT cells can restore homeostasis and under massive ER stress followed by washout of the inducing agent. Here we postulate that phosphorylation of Ire1 contributes significantly to its deactivation. We propose that without phosphorylation to aid in Ire1 de-oligomerization, Ire1(D797N,K799N) shut-off occurs by diffusional dispersion upon oligomer dissociation. Although the molecular mechanism by which phosphorylation promotes Ire1 shut-off is currently not understood, we have shown that a 28-amino acid surface loop (HPL) on the Ire1 kinase domain is important for efficient shut down of Ire1 signaling. Because deletion of the HPL from Ire1 only partially phenocopies the *D797N,K799N* mutation, it is likely that other regions in Ire1 also contribute. The HPL contains seven serine and two threonine residues that could be phosphorylated. Peptides corresponding

Published March 28, 2011

to this loop are selectively missing from mass spectrometry analyses of recombinant, phosphorylated Ire1KR32, yet can be detected after phosphatase treatment (unpublished data). Because phosphopeptides are notoriously difficult to detect by mass spectrometry, these data suggest that peptides in this loop are phosphorylated. Deletion of the HPL from a recombinant Ire1 construct, Ire1KR32Δ28, was necessary in order to yield a high-resolution crystal structure of active oligomeric Ire1 (Korennykh et al., 2009). These observations lead us to speculate that the HPL is highly phosphorylated and destabilizes oligomerization of the cytosolic portion of Ire1 in vitro, perhaps by charge repulsion. A similar mechanism might operate in vivo, with phosphorylation of the HPL contributing to dissolution of Ire1 oligomers and thereby to Ire1 deactivation. Alternatively, some still-unknown UPR-modulating protein might bind the phosphorylated HPL and, akin to arrestin binding to G protein–coupled receptors, coordinate timely shut-off of Ire1 signaling. In addition, it remains possible that Ire1 kinase has other, yet-unidentified, targets that promote cell survival when phosphorylated.

Demonstrating a role of Ire1 phosphorylation in its shut-off does not contradict the notion that phosphorylation events also play a role in its activation. In particular, we have previously shown that phosphorylated residues in Ire1's activation loop form salt bridges to adjacent Ire1 subunits in the active oligomer (Korennykh et al., 2009). The mild hypomorphic effects on *HAC1* mRNA splicing observed in *ire1(D797N,K799N)* cells may result from a lack of such positive feedback that enhances oligomer stability initially through phosphorylation.

Destabilization of Ire1 oligomers by phosphorylation of the HPL and other sites may be temporally delayed and serve as a molecular timer that balances oligomer assembly and disassembly. In this scenario, both forward and reverse reactions would remain responsive to changing conditions in the ER lumen and the Ire1 signal transmitted via the oligomerization state of the lumenal domain. Longer Ire1 activity would lead to the accumulation of a greater number of phosphates and an Ire1 oligomer would be increasingly destabilized. In this way, phosphorylation may aid the rapid disassembly even of large oligomers that are held together through multiple, mutually reinforcing intramolecular interactions. The lumenal domain of Ire1 would thus remain empowered as the sole driver of activation and de-activation, thereby rendering Ire1 highly sensitive to changes in the ER lumen.

Materials and methods

Yeast strains and growth conditions

Cells were grown in 2x synthetic complete medium supplemented with 100 µg/ml inositol. Over the course of this study, we noticed that Ire1 kinase-inactive cells were sensitive to saturation in culture. Thus, cells grown in culture were kept at subsaturating conditions for at least 12 h before beginning any experiment. The yeast strains and plasmids used in this study are listed in Tables I and II, respectively.

In vitro assays

Recombinant Ire1 proteins were purified from *E. coli* as described previously (Korennykh et al., 2009).

Kinase assays were performed using 10 µM of purified Ire1 in kinase buffer (20 mM Hepes, pH 7.0 at 30°C, 70 mM NaCl, 2 mM $Mg(OAc)_2$, 5 mM DTT, and 5% glycerol) supplemented with 0.033 µM [γ^{32}]P-ATP (Perkin-Elmer). Reactions were performed at 30°C. In reactions containing two distinct versions of recombinant Ire1 protein, 5 µM of each was added. Phosphorylated proteins were separated on a 12% denaturing polyacrylamide gel and detected with a phosphorimager screen (Molecular Dynamics).

MALDI mass spectrometry and in vitro RNA cleavage assays were performed as described by Korennykh et al. (2009). In vitro cleavage reactions were started by adding 1 µl of ^{32}P-labeled RNA to 9 µl of premixture containing 20 mM Hepes, pH 7.4, 70 mM NaCl, 2 mM $MgCl_2$, 4 mM DTT, 5% glycerol, and 2 mM ADP. Reactions were performed at 30°C, contained ≤1 pM radioactively ^{32}P-labeled RNA, 3 µM purified Ire1, and were conducted under single turnover conditions. Reactions were quenched at time intervals with 6 µl stop solution (10 M urea, 0.1% SDS, 0.1 mM EDTA, 0.05% xylene cyanol, and 0.05% bromophenol blue). Samples were analyzed by 10–20% PAGE, gels were scanned by Typhoon (Molecular Dynamics), and quantified using ImageQuant and GelQuant.NET programs. The data were plotted and fit to exponential curves using SigmaPlot to determine observed rate constants.

Isolation of total RNA and Northern blot analysis

Total RNA was isolated from yeast cells using hot acid phenol chloroform extraction (Rüegsegger et al., 2001). Unless otherwise indicated, the UPR was induced by the addition of 2 mM DTT (Gold Biotechnology) for 40 min.

Table I. **Yeast strains**

Yeast strain	Genotype
YCR200	*ireΔ::TRP1, his3::UPRE-LACZ-HIS3,* W303a derivative
YCR201	as YCR200, except *ura3::IRE1-3xFLAG-URA3*
YCR202	as YCR200, except *ura3::ire1(D797N, K799N)-3xFLAG-URA3*
YCR203	as YCR200, except *ura3::ire1(D828A)-3xFLAG-URA3*
YDP002	*cry1a, ire1::KanMX6* [23]
YCR204	as YDP002, except *ura3::IRE1-3xFLAG*
YCR205	as YDP002, except *ura3::ire1(D797N, K799N)-3xFLAG*
YCR206	as YDP002, except *ura3::IRE1-3xFLAG, his3::HA-HAC1-HIS3*
YCR207	as YDP002, except *ura3::ire1(D797N, K799N)-3xFLAG, his3::HA-HAC1-HIS3*
YCR208	as YDP002, except *IRE1-3xFLAG, leu2::SR-LEU2*
YCR209	as YDP002, except *ire1(D797N, K799N)-3xFLAG, leu2::SR-LEU2*
YCR210	as YCR201, except *TDH3::ero-GFP-kanMX6-4xUPRE-mCherry*
YCR211	as YCR202 except *TDH3::ero-GFP-kanMX6-4xUPRE-mCherry*
YCR212	as YDP002, except *leu2::IRE1-GFP-LEU2*
YCR213	as YDP002, except *leu2::ire1(D797N, K799N)-GFP-LEU2*
YCR214	as YDP002, except *leu2::ire1(D828A)-GFP-LEU2*
YCR215	as YDP002, except *leu2::ire1ΔHPL-GFP-LEU2*
YCR216	as YDP002, except *leu2::ire1(D797N,K799N)ΔHPL-GFP-LEU2*

Published March 28, 2011

Northern blot analysis was performed using 15 µg of total RNA separated on a 1.5% (wt/vol) denaturing agarose gel and transferred to a supported nitrocellulose membrane (GE Water & Press Technologies). The *HAC1* mRNA was detected using a radiolabeled 500-bp DNA probe directed against the 5′ exon of the transcript (Cox and Walter 1996).

Cell viability assays

To score the plate phenotype, yeast cells were grown to an OD_{600} of 0.3 or lower and diluted to equal cell numbers. Cell suspensions were serially diluted 1:5 and transferred to plates using a pin tool. UPR-inducing plates contained 0.25 µg/ml tunicamycin (EMD). To analyze cell viability in culture, cells were grown in the presence of 2 mM DTT at 30°C for 26 h. At each time point, cells were counted, the OD_{600} was measured, and 300 cells were plated onto permissive media. Colony forming units (CFUs) were counted from the plates after 3 d at 30°C. Viability was calculated by dividing the number of CFUs by the number of cells plated. Cells were kept below an OD_{600} of 0.2 and the DTT was refreshed throughout the course of the experiment.

Isolation of protein and Western blot analysis

Total protein was isolated from cells by vortexing in the presence of glass beads in 8 M urea, 50 mM Hepes, pH 7.4, and 1% SDS. Samples were boiled then cleared by centrifugation at 16,000 *g* for 10 min. 25 µg total protein was separated by SDS-PAGE (NuPAGE; Invitrogen), transferred to nitrocellulose, and probed with antibody. For HA-epitope detection, the monoclonal HA.11 (Covance) was used at a dilution of 1:3,000. Pgk1 protein was detected using Pgk1-specific antibody at a 1:5,000 dilution (Invitrogen). For detection of the Kar2 protein, a Kar2-specific antibody (Walter laboratory, University of California, San Francisco, San Francisco, CA) was used at a 1:5,000 dilution.

Microarray analysis

Cultures were inoculated to an OD_{600} of 0.05 and grown at 30°C in 2x synthetic media supplemented with 100 µg/ml inositol. Upon reaching an OD_{600} of 0.3, the UPR was induced by the addition of 2 mM DTT. Cells were harvested at 0, 30, 60, and 120 min from 500 ml of culture (150 ODs) by filtration onto a nitrocellulose membrane (Millipore). Membranes were frozen in liquid nitrogen and stored at −80°C before RNA isolation.

Total RNA was isolated using hot acid phenol chloroform extraction (Sarver and DeRisi 2005). cDNA was reverse transcribed from 15 µg of total RNA using Superscript III (Invitrogen) and a 1:1 mixture of oligo(dT) and random hexamers. Reverse transcription was performed in the presence of amino-allyl dUTP (aa-dUTP) (Invitrogen) at a ratio of 2:3 aa-dUTP/dTTP. A fraction of each cDNA sample was pooled to create a reference sample; the pooled reference was labeled with Cy3 dye (GE Healthcare). The remaining sample cDNA from each time point was labeled with Cy5 dye (GE Healthcare). Each Cy5-labeled sample was mixed with an equal amount of Cy3-labeled pooled reference cDNA and hybridized to oligonucleotide microarrays representing the full yeast genome (DeRisi et al., 1997). Microarray data were extracted and analyzed using the methods described in Sarver and DeRisi (2005). Before clustering, data were compressed such that all data corresponding to identical gene products were averaged.

Yeast oligonucleotide arrays were printed using primers for each predicted or known gene supplied by Operon. Two primer sets, AROS and YBOX, were combined to create these arrays. Oligonucleotide arrays were printed at the UCSF Center for Advanced Technology (San Francisco, CA).

Measuring global translation rates and ER expansion

Global translation rates were measured by monitoring [^{35}S]methionine incorporation during UPR induction. Cells were grown to an OD_{600} of 0.3, harvested by filtration, and resuspended in media lacking methionine. Starvation was performed for 30 min at 30°C. The UPR was induced by the addition of 2 mM DTT. At the time of UPR induction, 1 µCi/ml [^{35}S]methionine (PerkinElmer) plus 50 µM cold methionine was added to cells. The OD_{600} was measured and samples were harvested every 15 min for 3 h after UPR induction. Cells were lysed, total protein was isolated by TCA precipitation, and scintillation counts were measured. To graph the results, total scintillation counts were normalized to the OD_{600} and plotted over time.

To assay ER expansion, WT or mutant *ire1* cells bearing *SEC63-GFP* on a centromeric plasmid were left untreated or treated with 2 mM DTT for 2 h and imaged. Expansion of the cortical ER was quantified as described previously (Schuck et al., 2009). In brief, we first measured the Sec63-GFP signal along the cell cortex for at least 40 cells per condition and calculated its coefficient of variation (CV). The cortical ER of untreated cells appears as a broken line with large signal fluctuations, giving a high CV. In DTT-treated cells, Sec63-GFP is more evenly distributed along the cell cortex as part of expanded ER sheets, resulting in a low CV. We then derived the index of expansion (IE) by dividing the CV of the Sec63-GFP signal from the nuclear envelope, which represents maximally expanded ER and yields the smallest possible CV, by the CV of the cortical signal. Hence, the IE increases as the ER expands.

Splicing reporter (SR) assays

WT or mutant cells bearing SR integrated at the *URA3* locus were induced with DTT as indicated and flow cytometry was performed as described previously (Pincus et al., 2010). Cells were cultured at 30°C in 2x SDC in 96-well deep-well plates in a plate shaker (Innova) at 900 rpm. 1 M DTT stocks were made fresh from powder and stored at 4°C for each experiment. Fresh 5x working stocks were prepared at the start of the experiment by diluting DTT in 1 step into 2x SDC to 37.5 mM (5x 7.5 mM) in 10 ml. This 37.5-mM working stock was serially diluted by 1.5-fold increments (6 ml + 3 ml SDC) 10 times to span the range. To initiate the experiment, 200 µl of each 5x stock was added to 800 µl cells in the 96-well plates at time 0. Cells were incubated at 30°C and sampled every 30 min by 12-channel pipetting 100 µl of each culture into a 96-well microtiter plate. 10 µl of each 100 µl was sampled to flow cytometry analysis using a flow cytometer (model LSR-II; BD) equipped with a high throughput sampler, a 488-nm 100-mW laser, FITC emission filter, and FACS DIVA software to compile .fcs files. Files were analyzed in MatLab and/or FloJo. No cuts or gates were applied to cell distributions. Median FITC-A values were calculated for each dose-time point and plotted in ProFit. Errors were calculated from the standard deviation of the median for three biological replicates.

Measuring the redox potential of the ER using the ero-GFP reporter

To measure the ER redox potential the ero-GFP reporter (pPM56; Merksamer et al., 2008) was integrated into the *TDH3* locus of WT or mutant cells. The UPR was induced with 1 mM or 2 mM DTT. GFP fluorescence at 405 nm and 488 nm was measured by flow cytometry and the ratio of the 405-nm and 488-nm signal (r/o ratio) was plotted as a function of time. Percent ero-GFP reoxidation was calculated using the equation: $\%\ reoxidation = 1 - ((F - I)/(M - I))$ where I = initial ero-GFP r/o ratio (at t = 0), M = maximum ero-GFP r/o ratio (at t = 30 min), and F = final ero-GFP r/o ratio (at t = 240 min).

Ire1 foci formation and quantitative fluorescence microscopy

IRE1 was tagged with *GFP* as described previously (Aragón et al., 2009) and integrated at the *LEU2* locus to create strains YCR212, YCR213, and YCR214. Cells were grown in an Erlenmeyer flask at 30°C and transferred to a 96-well glass-bottom plate coated with concanavalin A. Ire1-GFP was imaged by confocal microscopy and images were processed and quantified as described by Pincus et al. (2010). Microscopy was performed

Table II. **Yeast plasmids**

Plasmid	Description	Marker
pCR100	*IRE1-3xFLAG*, pRS306	URA3
pCR101	*ire1(D797N, K799N)-3xFLAG*, pRS306	URA3
pCR102	*ire1(D828A)-3xFLAG*, pRS306	URA3
pCR103	*IRE1-3xFLAG*, pRS303	HIS3
pCR104	*ire1(D797N, K799N)-3xFLAG*, pRS303	HIS3
pPM56	*TDH3-ero-GFP*, 4x*UPRE-mCherry* (Merksamer et al., 2008)	URA3, kanMX6
pJK59	*Sec63-GFP*, CEN (Prinz et al., 2000)	URA3

using a spinning disk confocal unit (CSU-22; Yokogawa) on a TI inverted microscope (Nikon) equipped with a 150-mW, 491-nm laser and an EMCCD camera (Evolve; Photometrics). Cells were grown in 2x SDC to mid-log phase, diluted to OD_{600} = 0.1, gently sonicated, and 80 µl was added to 96-well glass-bottom plates coated with concanavalin A. Cells were allowed to settle for 20 min before imaging. DTT was prepared as 5x working stocks as in flow cytometry SR assays, and 20 µl added to wells at time 0. For washout experiments, cells were incubated with 5 mM DTT for 1 h in Eppendorf tubes and washed 2x with fresh media before transferring to 96-well plates for imaging. Cells were imaged at each time point using a 100x oil objective with 5-s exposures of 491-nm excitation. Images were acquired using the open source MicroManager v1.2 software, processed by identifying cell boundaries and assigning the 16-bit fluorescence images to individual cells using the open source Cell-ID software. Background was calculated from the mean intensity of areas in each fluorescent image not assigned to cells, and subtracted from the cellular mean intensities to obtain corrected single-cell values. For each time point at each dose, images of three different fields of cells were obtained and quantified. Thus, a total of 30–100 cells were analyzed per time point. Mean values were plotted in ProFit and error bars represent the standard error of the mean.

Online supplemental material

Fig. S1 shows that mutations in Ire1 kinase abolish phosphoryl-transfer. Fig. S2 shows that the transcriptional response and global translation rates are normal in *ire1(D797N,K799N)* cells. Fig. S3 shows that the fold change of SR splicing in WT and *ire1(D797N,K799N)* cells are comparable. Online supplemental material is available at http://www.jcb.org/cgi/content/full/jcb.201007077/DC1.

The authors wish to thank Joe DeRisi, the UCSF Center for Advanced Technology (CAT), and Philipp Kimmig for reagents and assistance with the microarray hybridization experiments; and Kurt Thorn and the Nikon Imaging Center (NIC) as well as the Consortium for Frontotemporal Dementia Research (CFR) for assistance with and access to spinning disk confocal microscopes. We are grateful to Christopher Patil, Shannon Behrman, and Saskia Neher for critical reading of the manuscript and to Jonathan Weissman, Joe DeRisi, and members of the Walter Laboratory for expert advice and valuable discussion throughout the course of the project. We thank Will Prinz and Phillip Merksamer for providing plasmids.

C. Rubio was supported by the National Science Foundation and the UC President's Dissertation Year Fellowship; D. Pincus was supported by the National Science Foundation; A. Korennykh was supported by the Jane Coffin Childs Memorial Fund for Medical Research Fellowship; and S. Schuck was supported by the Human Frontier Science Program. Research was additionally funded by grants from the National Institutes of Health to P. Walter and H. El-Samad, and the Howard Hughes Medical Institute. P. Walter is an Investigator of the Howard Hughes Medical Institute.

The authors declare no conflicts of interest.

Submitted: 15 July 2010
Accepted: 1 February 2011

References

Aragón, T., E. van Anken, D. Pincus, I.M. Serafimova, A.V. Korennykh, C.A. Rubio, and P. Walter. 2009. Messenger RNA targeting to endoplasmic reticulum stress signalling sites. *Nature*. 457:736–740. doi:10.1038/nature07641

Bernales, S., K.L. McDonald, and P. Walter. 2006. Autophagy counterbalances endoplasmic reticulum expansion during the unfolded protein response. *PLoS Biol.* 4:e423. doi:10.1371/journal.pbio.0040423

Bertolotti, A., Y. Zhang, L.M. Hendershot, H.P. Harding, and D. Ron. 2000. Dynamic interaction of BiP and ER stress transducers in the unfolded-protein response. *Nat. Cell Biol.* 2:326–332. doi:10.1038/35014014

Chawla, A., S. Chakrabarti, G. Ghosh, and M. Niwa. 2011. Attenuation of the yeast UPR response is essential for survival and is mediated by IRE1 kinase. *J. Cell Biol.* 193:■■■–■■■. doi:10.1083/jcb.201008071

Cox, J.S., and P. Walter. 1996. A novel mechanism for regulating activity of a transcription factor that controls the unfolded protein response. *Cell*. 87:391–404. doi:10.1016/S0092-8674(00)81360-4

Cox, J.S., C.E. Shamu, and P. Walter. 1993. Transcriptional induction of genes encoding endoplasmic reticulum resident proteins requires a transmembrane protein kinase. *Cell*. 73:1197–1206. doi:10.1016/0092-8674(93)90648-A

Cox, J.S., R.E. Chapman, and P. Walter. 1997. The unfolded protein response coordinates the production of endoplasmic reticulum protein and endoplasmic reticulum membrane. *Mol. Biol. Cell*. 8:1805–1814.

Credle, J.J., J.S. Finer-Moore, F.R. Papa, R.M. Stroud, and P. Walter. 2005. On the mechanism of sensing unfolded protein in the endoplasmic reticulum. *Proc. Natl. Acad. Sci. USA*. 102:18773–18784. doi:10.1073/pnas.0509487102

DeRisi, J.L., V.R. Iyer, and P.O. Brown. 1997. Exploring the metabolic and genetic control of gene expression on a genomic scale. *Science*. 278:680–686. doi:10.1126/science.278.5338.680

Dong, B., M. Niwa, P. Walter, and R.H. Silverman. 2001. Basis for regulated RNA cleavage by functional analysis of RNase L and Ire1p. *RNA*. 7:361–373. doi:10.1017/S1355838201002230

Hanson, G.T., R. Aggeler, D. Oglesbee, M. Cannon, R.A. Capaldi, R.Y. Tsien, and S.J. Remington. 2004. Investigating mitochondrial redox potential with redox-sensitive green fluorescent protein indicators. *J. Biol. Chem.* 279:13044–13053. doi:10.1074/jbc.M312846200

Kimata, Y., D. Oikawa, Y. Shimizu, Y. Ishiwata-Kimata, and K. Kohno. 2004. A role for BiP as an adjustor for the endoplasmic reticulum stress-sensing protein Ire1. *J. Cell Biol.* 167:445–456. doi:10.1083/jcb.200405153

Korennykh, A.V., P.F. Egea, A.A. Korostelev, J. Finer-Moore, C. Zhang, K.M. Shokat, R.M. Stroud, and P. Walter. 2009. The unfolded protein response signals through high-order assembly of Ire1. *Nature*. 457:687–693. doi:10.1038/nature07661

Lee, K.P., M. Dey, D. Neculai, C. Cao, T.E. Dever, and F. Sicheri. 2008. Structure of the dual enzyme Ire1 reveals the basis for catalysis and regulation in nonconventional RNA splicing. *Cell*. 132:89–100. doi:10.1016/j.cell.2007.10.057

Merksamer, P.I., A. Trusina, and F.R. Papa. 2008. Real-time redox measurements during endoplasmic reticulum stress reveal interlinked protein folding functions. *Cell*. 135:933–947. doi:10.1016/j.cell.2008.10.011

Mori, K., W. Ma, M.J. Gething, and J. Sambrook. 1993. A transmembrane protein with a cdc2+/CDC28-related kinase activity is required for signaling from the ER to the nucleus. *Cell*. 74:743–756. doi:10.1016/0092-8674(93)90521-Q

Mori, K., T. Kawahara, H. Yoshida, H. Yanagi, and T. Yura. 1996. Signalling from endoplasmic reticulum to nucleus: transcription factor with a basic-leucine zipper motif is required for the unfolded protein-response pathway. *Genes Cells*. 1:803–817. doi:10.1046/j.1365-2443.1996.d01-274.x

Okamura, K., Y. Kimata, H. Higashio, A. Tsuru, and K. Kohno. 2000. Dissociation of Kar2p/BiP from an ER sensory molecule, Ire1p, triggers the unfolded protein response in yeast. *Biochem. Biophys. Res. Commun.* 279:445–450. doi:10.1006/bbrc.2000.3987

Papa, F.R., C. Zhang, K. Shokat, and P. Walter. 2003. Bypassing a kinase activity with an ATP-competitive drug. *Science*. 302:1533–1537. doi:10.1126/science.1090031

Pincus, D., M.W. Chevalier, T. Aragón, E. van Anken, S.E. Vidal, H. El-Samad, and P. Walter. 2010. BiP binding to the ER-stress sensor Ire1 tunes the homeostatic behavior of the unfolded protein response. *PLoS Biol.* 8:e1000415. doi:10.1371/journal.pbio.1000415

Poothong, J., P. Sopha, R.J. Kaufman, and W. Tirasophon. 2010. Domain compatibility in Ire1 kinase is critical for the unfolded protein response. *FEBS Lett.* 584:3203–3208. doi:10.1016/j.febslet.2010.06.003

Prinz, W.A., L. Grzyb, M. Veenhuis, J.A. Kahana, P.A. Silver, and T.A. Rapoport. 2000. Mutants affecting the structure of the cortical endoplasmic reticulum in *Saccharomyces cerevisiae*. *J. Cell Biol.* 150:461–474. doi:10.1083/jcb.150.3.461

Rüegsegger, U., J.H. Leber, and P. Walter. 2001. Block of HAC1 mRNA translation by long-range base pairing is released by cytoplasmic splicing upon induction of the unfolded protein response. *Cell*. 107:103–114. doi:10.1016/S0092-8674(01)00505-0

Sarver, A., and J. DeRisi. 2005. Fzf1p regulates an inducible response to nitrosative stress in *Saccharomyces cerevisiae*. *Mol. Biol. Cell*. 16:4781–4791. doi:10.1091/mbc.E05-05-0436

Schuck, S., W.A. Prinz, K.S. Thorn, C. Voss, and P. Walter. 2009. Membrane expansion alleviates endoplasmic reticulum stress independently of the unfolded protein response. *J. Cell Biol.* 187:525–536. doi:10.1083/jcb.200907074

Shamu, C.E., and P. Walter. 1996. Oligomerization and phosphorylation of the Ire1p kinase during intracellular signaling from the endoplasmic reticulum to the nucleus. *EMBO J.* 15:3028–3039.

Sidrauski, C., and P. Walter. 1997. The transmembrane kinase Ire1p is a site-specific endonuclease that initiates mRNA splicing in the unfolded protein response. *Cell*. 90:1031–1039. doi:10.1016/S0092-8674(00)80369-4

Travers, K.J., C.K. Patil, L. Wodicka, D.J. Lockhart, J.S. Weissman, and P. Walter. 2000. Functional and genomic analyses reveal an essential coordination between the unfolded protein response and ER-associated degradation. *Cell*. 101:249–258. doi:10.1016/S0092-8674(00)80835-1

Published March 28, 2011

Rubio et al., http://www.jcb.org/cgi/content/full/jcb.201007077/DC1

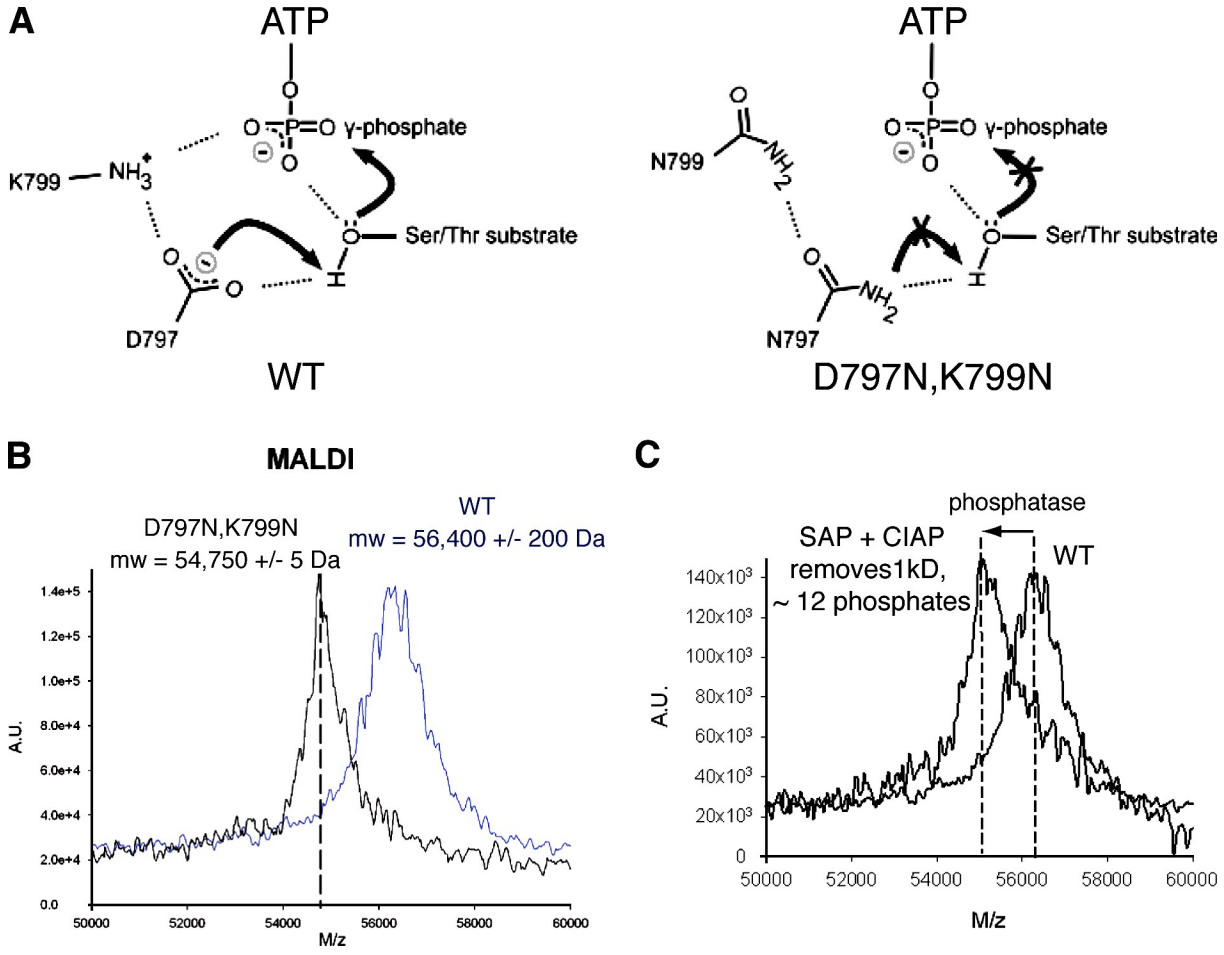

Figure S1. **Mutations in Ire1 kinase abolish phosphoryl-transfer.** (A) Schematic diagram depicting predicted hydrogen bonding and proton transfer between key residues in the nucleotide-binding pocket of Ire1 kinase. (B) Recombinant Ire1(D797N,K799N) is unphosphorylated. MALDI mass spectrometry of purified recombinant Ire1KR32 reveals that the mass-to-charge ratio of WT Ire1KR32 (observed molecular weight (mw_{obs}): 56,400 ± 200 D; calculated mw: 54,767.22 D) is ~1.3 kD higher than expected from its amino acid composition. A 1.3-kD shift in molecular weight corresponds to ~17 phosphates. The mw_{obs} of Ire1KR32(D797N,K799N) was 54,750 ± 5 D, consistent with the calculated mw: 54,752.15 D. (C) Phosphatase treatment of recombinant Ire1KR32 reduces its M/z value to its true molecular weight + 0.2 kD. This reduction in molecular weight is consistent with the removal of ~12 phosphates. Phosphatase-treated Ire1KR32 has a mw_{obs} = 55,050 ± 50 D and a calculated mw = 54,767.22 D.

Published March 28, 2011

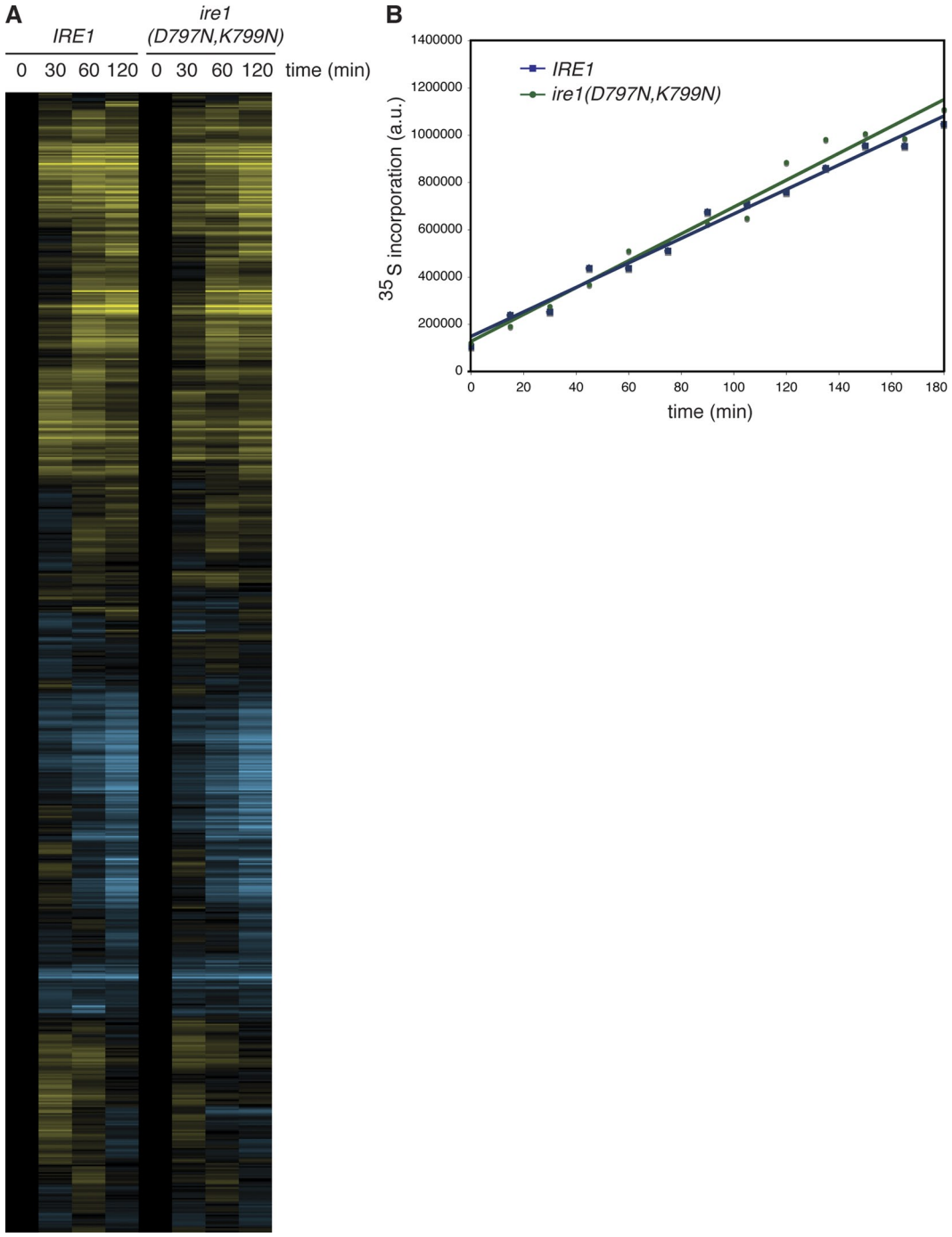

Figure S2. **The transcriptional response and global translation rates are normal in *ire1(D797N,K799N)* cells.** (A) Microarray analysis of genome-wide mRNA abundance. Total mRNA expression profiles of WT and *ire1(D797N,K799N)* cells were determined over a 2-h time course of UPR induction. (B) Global translation rates were measured by [^{35}S]-methionine incorporation over a 3-h time course of UPR induction. [^{35}S]-scintillation counts were normalized to cell number and plotted over time (P = 0.12).

Published March 28, 2011

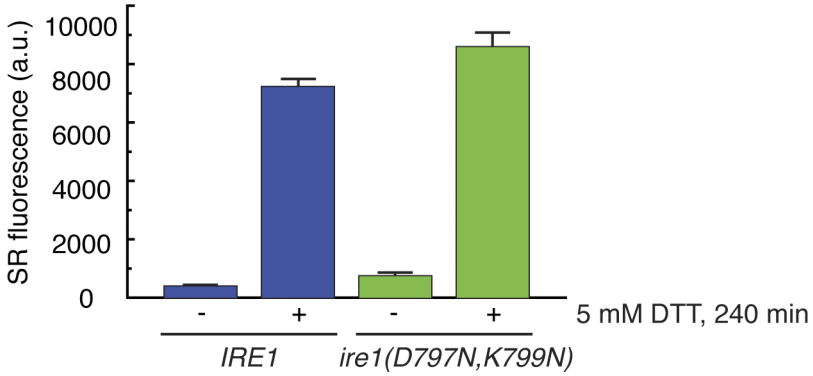

Figure S3. **The fold change of SR splicing in WT and *ire1(D797N,K799N)* cells is comparable.** Minimum (0% or −DTT) and maximum (100% or +DTT) values were taken from SR splicing assays using 5 mM DTT at times 0 and 240 min, respectively.

Chapter 4

Constitutive Activation of the Unfolded Protein Response Impairs Cellular Fitness by Causing Oxidative Stress

Constitutive Activation of the Unfolded Protein Response Impairs Cellular Fitness by Causing Oxidative Stress^

David Pincus[1], Andres Aranda[1], Peter Walter[1,2] and Hana El-Samad[1,*]

[1] Department of Biochemistry and Biophysics, University of California, San Francisco 94122

[2] Howard Hughes Medical Institute, University of California, San Francisco 94122

[*] Corresponding author: hana.el-samad@ucsf.edu (415) 514-4242

^ This work was incomplete at the time this thesis was written. In fact, there was not yet enough data to verify the claim made in the title. This chapter of the thesis serves only to reflect the thinking at the time it was written. As such all analysis and conclusions are subject to change. This draft only contains an abstract, figure legends and figures.

Abstract

The unfolded protein response (UPR) is an intracellular signaling pathway that transmits information about protein folding conditions in the endoplasmic reticulum (ER) to the nucleus to regulate the expression of genes involved in secretory processes. Cells have evolved to tightly regulate both activation of the UPR when unfolded proteins accumulate in ER, a condition known as ER stress, and deactivation once the response is sufficient. While the UPR is thought to be cytoprotective, the existence of mechanisms that prevent unnecessary activation and ensure efficient deactivation suggests that UPR activity imposes fitness costs to the cell. To explore the detrimental effects of UPR activation we decoupled UPR activity from ER stress by placing the active form of the UPR-specific transcription factor Hac1 under inducible and titratable control. We found that growth rate is inversely proportional to the concentration of active Hac1, slowing by nearly 50% at levels comparable to activation by ER stress. RNA sequencing from cells treated across a dose response of Hac1 showed that in addition to UPR target genes, activation in the absence of ER stress induces genes involved combating oxidative and cytoplasmic stress. Reporter time courses revealed that these other stress responses are activated an hour after direct UPR targets are induced, suggesting that UPR target gene upregulation causes oxidative stress. Supporting this notion, overexpression of the UPR target gene *ERO1*, an essential ER-resident oxidase involved in disulfide bond formation, to the level reached by Hac1 overexpression accounts for XX% of the Hac1-mediated growth impairment. Moreover, removing the Hac1 binding site from the *ERO1* promoter rescues XX% of the growth rate upon

Hac1 overexpression. These results indicate that responding to stress can be inherently stressful and provide rationale for the evolution of mechanisms that tightly control activation and deactivation of stress response pathways.

Figure Legends

Figure 1: Decoupling UPR Activation from ER Stress Impairs Cellular Fitness

A) Overexpression of Hac1 impairs cell growth. Yeast cells bearing either a control gene (*YFP*) or intronless *HAC1* under the control of the galactose-inducible *GAL1* promoter were diluted and spotted on media with either glucose or galactose as the carbon source. B) Titratible expression of Hac1 with estradiol. Cells bearing Hac1 under the control of the *GAL1* promoter and expressing the estradiol-responsive, chimeric GEM transcription factor were treated across a dose response of estradiol. Protein extracts were probed with anti-HA antibody followed by fluorescent secondary antibody and visualized using the Li-Cor system. C) Growth rate is inversely proportional to Hac1 levels. Average growth rate of cells grown in log phase over 12 hours in media containing different concentrations of estradiol plotted. Relative Hac1 levels quantified from immunoblots normalized to 0 and 500 nM estradiol.

Figure 2: The Hac1-Mediated Transcriptional Landscape

A) Venn diagram of the number of transcripts upregulated by at least 2-fold in cells treated with 100 nM estradiol (Est), 5 μg/ml tunicamycin (Tm) or 5 mM DTT. B) RNA seq reads from control cells and cells treated with Est, Tm or DTT aligned to ORFs representative of 3 classes of UPR target genes (*KAR2* has a "UPRE1" in its promoter; *ERO1* has a "UPRE2" in its promoter; *INO1* is activated by a Hac1-dependend de-repression mechanism) and a non-target gene (*PGK1*). C) GO term enrichment for regions of the Venn diagram. Bar colors correspond to colors in the

Venn diagram. D) Black bars: Number of target genes induced between 2-4 fold, between 4-8 fold or greater than 8 fold. Gray bars: Percent of target genes in each category with recognizable UPREs in their promoters. UPREs were recognized if the promoter had a UPRE score in the top 10% genome wide (Fordyce et al. 2012). E) Target genes without UPREs include genes involved in other stress responses. *HSP12* and *PGM2* are targets of the general cytoplasmic stress response pathway and are highly induced by DTT and Tm, and moderately induced by Est. *HOR2* and *GPD1* are targets of the high-osmolarity response pathway and are only induced by DTT and Tm. *TSA1*, *DDR48*, *RAD50* and *AIM24* are all involved in the response to oxidative stress and are induced equally by DTT, Tm and Est. Targets of the heat shock factor, *SSA1* and *HSP82* are not induced in any condition. *MLP1* and *PRM5*, targets of the cell wall integrity pathway, are induced by DTT and Tm but not Est.

Figure 3: Primary and Secondary Hac1 Target Genes

A) Fold change of primary Hac1 target genes – genes with UPREs in the promoter or that are known targets of de-repression – as a function of estradiol concentration. Fold change varies more than affinity. B) Fold change of secondary target genes – genes under the control of other stress responsive transcription factors – as a function of estradiol concentration. Genes involved in the oxidative stress response are dose-dependently upregulated.

Figure 4: ER Stressors and Hac1 Induce Secondary Stress Responses

Flow cytometry time courses of cells bearing fluorescent reporters for various stress response pathways (GFP fused to a promoter of a target gene, except the

splicing reporter) after being treated with 100 nM Est, 5 μg/ml Tm or 5 mM DTT. A. Table of the reporters, the pathways they report on and the transcriptional activator of each pathway. B) *ERO1*, a direct Hac1 target promoter, is induced by Est, Tm and DTT with similar kinetics. C) Splicing reporter (SR) is induced strongly by Tm and DTT and weakly by estradiol. D) *HSP12*, a target of the general stress response pathway, is induced strongly by Tm and DTT but with significantly delayed kinetics compared to *ERO1*. E) *SSA1*, a target of Hsf1, is weakly induced in all conditions. F) *HOR2*, a target of the response to high osmolarity, is strongly induced by Tm and DTT. G) *TSA2*, a target of the oxidative stress response, is induced in all conditions. H) *MLP1*, a target of the cell wall integrity pathway, is significantly induced by Tm. I) Time courses of all reporters in response to estradiol. J) Time courses of all reporters in response to Tm. K) Time courses of all reporters in response to DTT.

Figure 5: Ero1 Overexpression Inhibits Growth

Control cells or cells bearing *ERO1* under the control of the galactose-inducible *GAL1* promoter were diluted and spotted on media with either glucose or galactose as the carbon source.

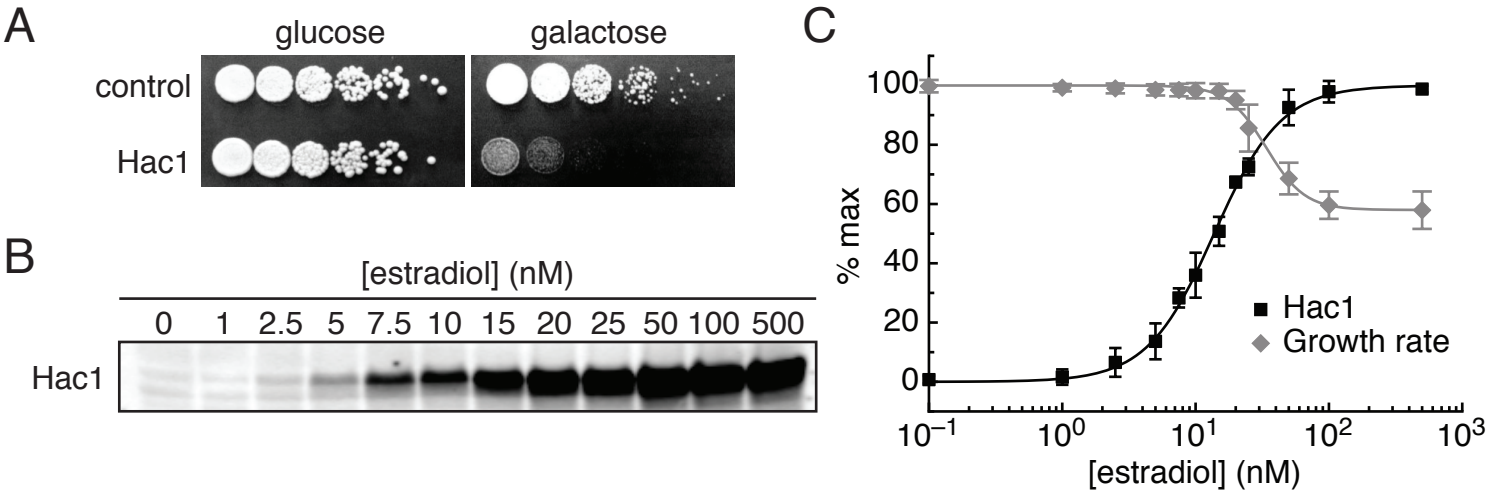
A
glucose
galactose
control
Hac1
B
[estradiol] (nM)
0 1 2.5 5 7.5 10 15 20 25 50 100 500
Hac1
C
100
80
60
40
20
0
% max
Hac1
Growth rate
10^{-1} 10^{0} 10^{1} 10^{2} 10^{3}
[estradiol] (nM)

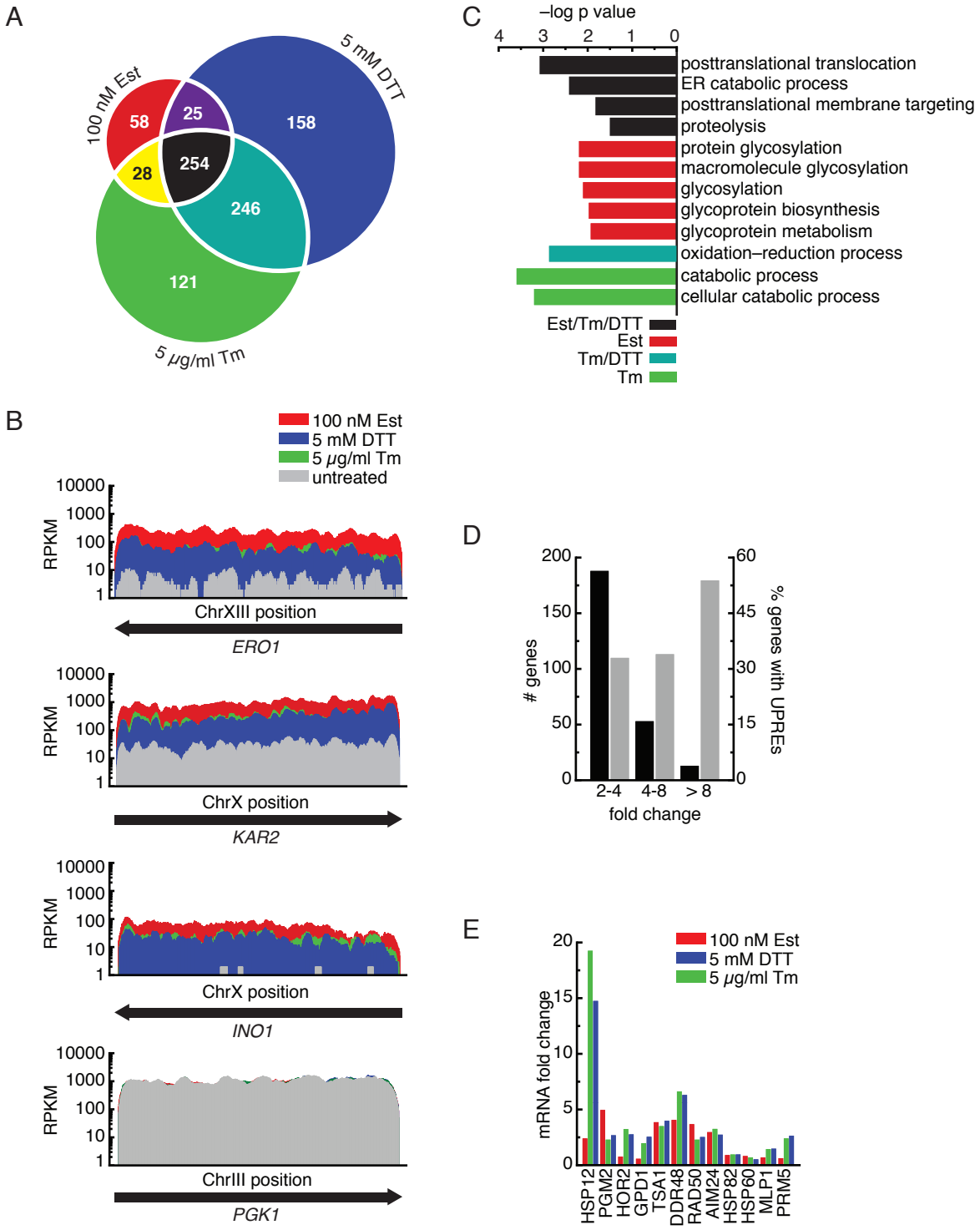
A
100 nM Est
5 mM DTT
5 μg/ml Tm
58
25
158
254
28
246
121
B
100 nM Est
5 mM DTT
5 μg/ml Tm
untreated
RPKM
ChrXIII position
ERO1
ChrX position
KAR2
ChrX position
INO1
ChrIII position
PGK1
C
–log p value
posttranslational translocation
ER catabolic process
posttranslational membrane targeting
proteolysis
protein glycosylation
macromolecule glycosylation
glycosylation
glycoprotein biosynthesis
glycoprotein metabolism
oxidation–reduction process
catabolic process
cellular catabolic process
Est/Tm/DTT
Est
Tm/DTT
Tm
D
genes
% genes with UPREs
2-4
4-8
> 8
fold change
E
100 nM Est
5 mM DTT
5 μg/ml Tm
mRNA fold change
HSP12
PGM2
HOR2
GPD1
TSA1
DDR48
RAD50
AIM24
HSP82
HSP60
MLP1
PRM5

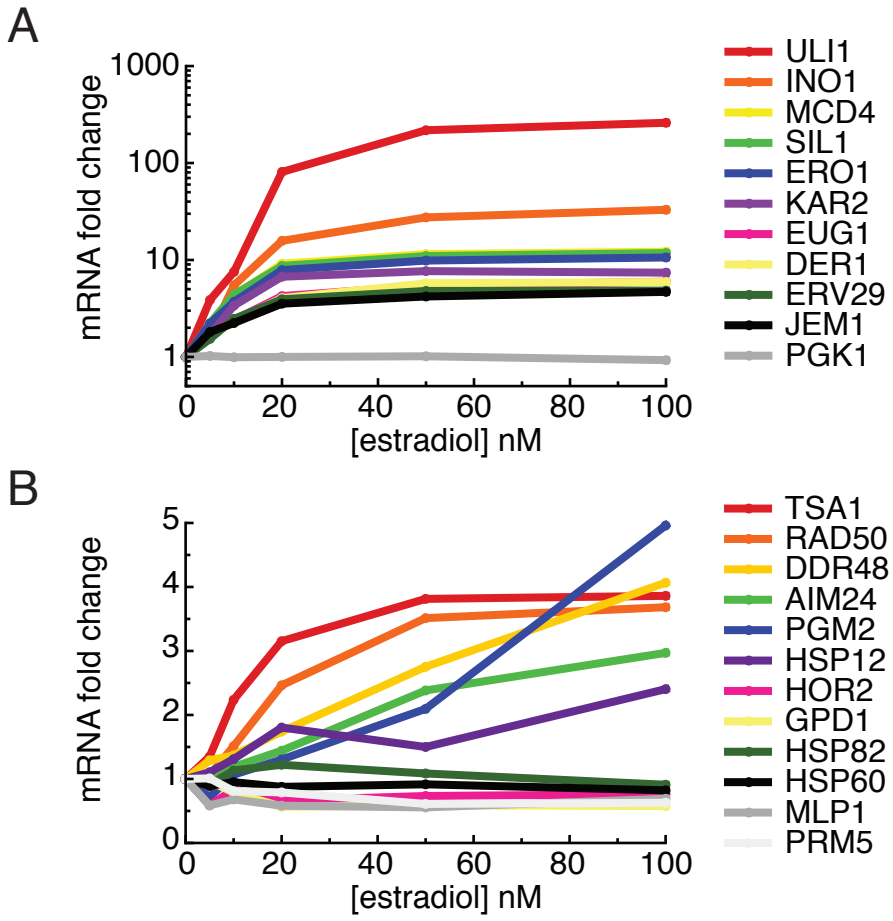
A
1000
100
10
1
mRNA fold change
0
20
40
60
80
100
[estradiol] nM
ULI1
INO1
MCD4
SIL1
ERO1
KAR2
EUG1
DER1
ERV29
JEM1
PGK1
B
5
4
3
2
1
0
mRNA fold change
0
20
40
60
80
100
[estradiol] nM
TSA1
RAD50
DDR48
AIM24
PGM2
HSP12
HOR2
GPD1
HSP82
HSP60
MLP1
PRM5

A

reporter	pathway	activator
ERO1	UPR	Hac1
SR	UPR	Ire1
HSP12	general stress	Msn2/4
SSA1	heat shock	Hsf1
HOR2	hyper-osmotic stress	Hog1/Hot1
TSA2	oxidative stress	Yap1-7
MLP1	cell wall stress	Slt2/Rlm1

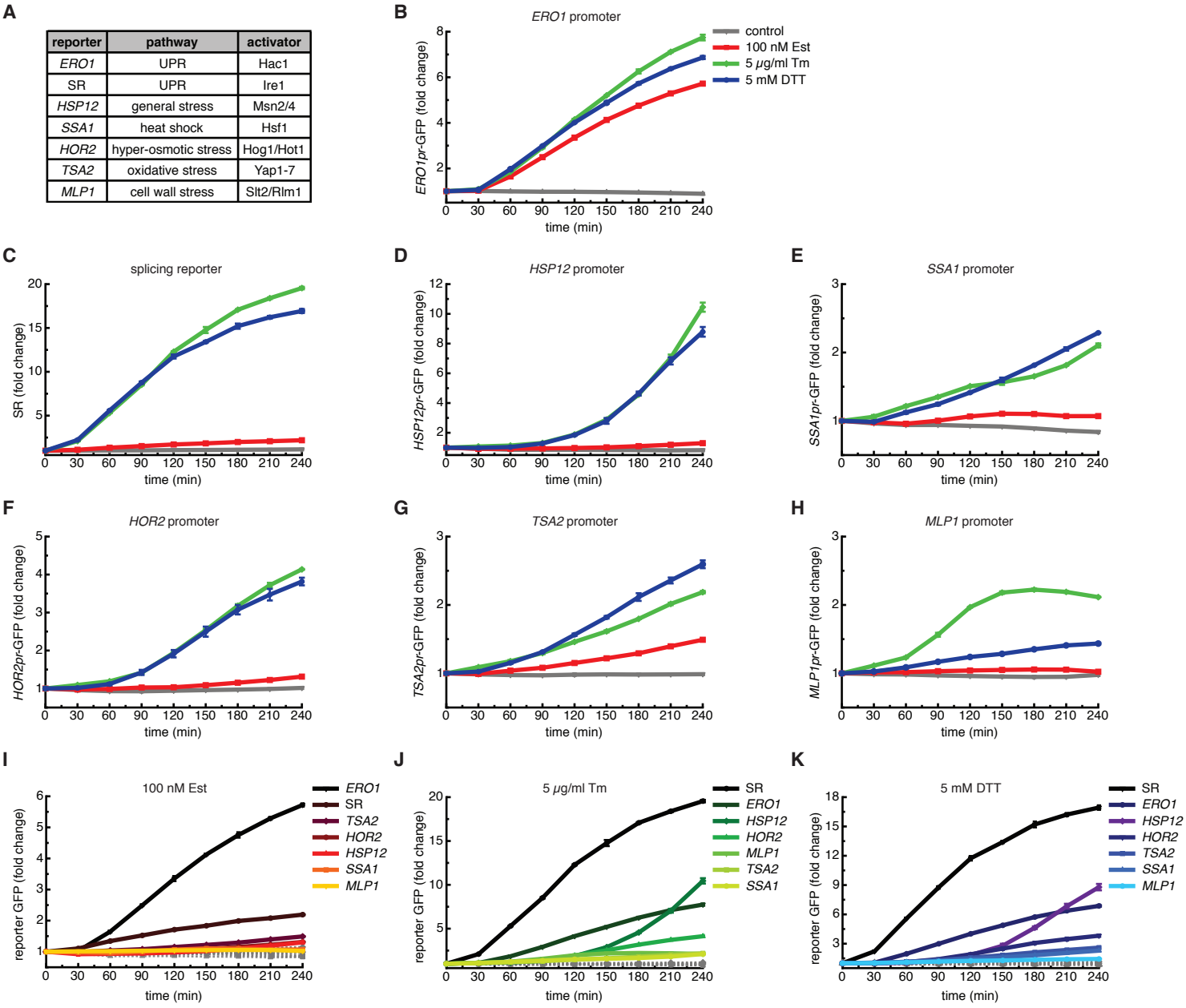

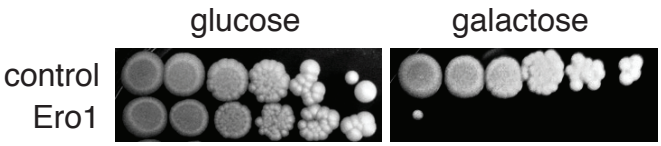
glucose
galactose
control
Ero1

Appendix A

Comment: The First Line of Defense Against ER Stress

Published August 6, 2012

A first line of defense against ER stress

David Pincus[1] and Peter Walter[1,2]

[1]Department of Biochemistry and Biophysics and [2]Howard Hughes Medical Institute, University of California at San Francisco, San Francisco, CA 94158

BiP is the predominant DnaK/Hsp70-type chaperone protein in the ER. It is required for folding and assembling newly synthesized ER client proteins, yet having too much BiP inhibits folding. In this issue, Chambers et al. (2012. *J. Cell Biol.* doi:10.1083/jcb.201202005) report that ADP ribosylation of BiP provides a reversible switch that fine tunes BiP activity according to need.

Too much of a good thing can be bad. Just as an overzealous parent can impede a child's development, so can overactive molecular chaperones slow protein folding. Chaperones are ancient and universally conserved machines that are required at nearly every stage of a protein's life: they assist in the initial folding of polypeptides, assembly of protein complexes, inhibition of toxic aggregation, and stabilization of unfolded states so that they can be degraded (Bukau et al., 2006). Perhaps counterintuitive, a too-high concentration of chaperones inhibits protein folding (Dorner et al., 1992). This effect is a result of overstabilization of the unfolded state and results in increased degradation (Otero et al., 2010). Accordingly, translational efficiency of chaperones can be feedback regulated (Gülow et al., 2002).

In eukaryotes, transmembrane and secreted proteins are folded and assembled in the ER. Cells confront the challenge of a variable flux of proteins entering the ER. Perturbations in protein flux can result from rapid environmental changes, such as fluctuating nutrients that vary with feeding and fasting cycles, or long-term physiological programs, such as differentiation. To meet fluctuating demands and maintain optimal homeostasis of protein maturation, the ER must continually monitor and adjust its protein folding capacity.

Chaperone proteins and enzymes that add posttranslational modifications assist in the folding and maturation processes in the ER (Sitia and Braakman, 2003). When the flux of unfolded proteins entering the ER surpasses the capacity of the folding machinery, a condition termed ER stress arises. In response, ER resident transmembrane sensors activate a network of intracellular signaling pathways, collectively called the unfolded protein response (UPR; Walter and Ron, 2011). The UPR induces a comprehensive transcriptional program that leads to enhanced expression of genes encoding machinery to increase the folding capacity of the organelle. Additionally, the UPR inhibits protein translation and initiates the degradation of some ER-bound mRNAs, thus decreasing the load of unfolded proteins entering the compartment. The increase of the folding capacity of the ER mediated by the transcriptional response, however, takes hours to take appreciable effect, and the reduction in load afforded by translational attenuation and mRNA degradation has no effect on the accumulated unfolded proteins already present in the ER. Thus, a need exists for mechanisms allowing rapid fine tuning of the ER's folding capacity.

In this issue, Chambers et al. (2012) report a mechanism that acts to respond quickly to changing conditions in the ER lumen before the UPR takes effect. It was noticed in the 1980s that a fraction of the major ER resident chaperone BiP, a DnaK/Hsp70 family member, exists in an ADP-ribosylated form and that this fraction is inversely proportional to the folding load in the ER (Carlsson and Lazarides, 1983; Ledford and Jacobs, 1986; Hendershot et al., 1988; Leno and Ledford 1989). Though it had been proposed that ADP ribosylation could serve as a rapid regulator of BiP activity, only correlative evidence was reported. Now, in the current work, Chambers et al. (2012) characterize the physiology of BiP-ADP ribosylation, map the modification sites, provide insight into the biophysical mechanism by which ADP ribosylation can inactivate BiP, and lend compelling quantitative support for the notion that this modification provides a mechanism of regulating BiP activity. The results of the study lead to the working model that partitioning BiP between an active and a latent ADP-ribosylated pool allows the cell to adapt quickly (Fig. 1).

To assess the physiological regulation of BiP-ADP ribosylation, the authors monitored the modification state of BiP in extracts from mouse pancreas after periods of feeding or fasting. After feeding, when secretory demand on the pancreas is high, ADP-ribosylated BiP was below the limit of detection. In contrast, after fasting, when the secretory load in the pancreas is low, ~50% of BiP was ADP ribosylated. Moreover, the ADP-ribosylated form of BiP was depleted from a high–molecular weight multichaperone complex in which the unmodified form was enriched, suggesting that the modified form is not engaged in folding substrates.

After mapping two potential ADP ribosylation sites, the authors took an in vitro approach to understand the effect of the modification on BiP function. The crystal structure of the

Correspondence to Peter Walter: peter@walterlab.ucsf.edu

Published August 6, 2012

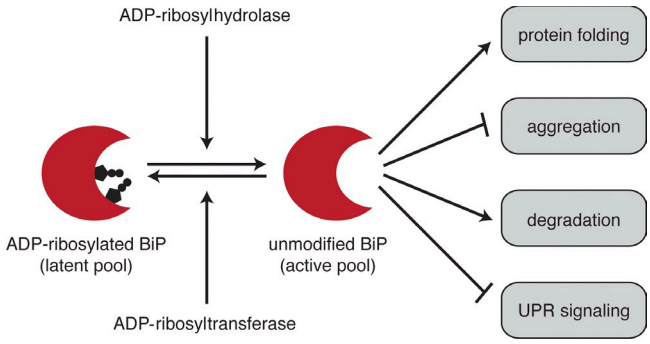

Figure 1. **ADP ribosylation provides a reversible switch that fine tunes BiP activity.** The unmodified active pool of BiP contributes to protein folding and degradation and inhibits aggregation and UPR signaling. If too much unmodified BiP is present, then folding is inhibited as the unfolded state is stabilized and degradation is increased. To improve efficiency of protein folding, excess BiP is ADP ribosylated by an unknown ADP-ribosyltransferase. This pool of inactive BiP can be reactivated by removal of the modification by an unknown ADP-ribosylhydrolase.

substrate-binding domain of the BiP homologue DnaK provided some hints: one of the mapped ADP ribosylation sites is predicted to make an intramolecular ionic interaction with the lid domain involved in substrate engagement and in the allostery underlying the chaperone's cycle of substrate binding and release (Schlecht et al., 2011). Thus, the authors hypothesized that ADP ribosylation would destabilize the closed-lid conformation of BiP, thereby diminishing its ability to bind to substrates. To test this idea, the authors designed an ADP ribosylation mimetic. Though the mimetic lacks the bulk of the true ADP-ribosyl moiety, it mimics the negative charge of the modification and, hence, is likely to underestimate the destabilizing effect that ADP ribosylation would have on the closed-lid conformation.

Nevertheless, the mimetic mutant BiP displayed a 40-fold decrease in the stability of the substrate-bound complex compared with the wild type, supporting the idea that ADP ribosylation would impair substrate binding. Furthermore, in the presence of ATP and substrate peptide, both the mutant and the ADP-ribosylated form of BiP were resistant to the specific BiP protease SubA (which preferentially cleaves the closed-lid, substrate-bound form of wild-type BiP), suggesting that both mostly populate the open-lid, unbound conformation.

To gain quantitative insight into the potential benefits of the modification, the authors built a mathematical model based on kinetic theory. The model reports on protein folding, aggregation, and degradation as a function of fluctuations in secretory load from feeding and fasting cycles. The model compared the consequences of BiP up-regulation through the UPR alone or in combination with reversible ADP ribosylation. Importantly, including ADP ribosylation resulted in 10% less aggregation and 25% less degradation. The predicted reduction in protein aggregation resulted from the quick recruitment of the inactive pool of BiP through removal of the ADP-ribose, whereas the predicted decrease in degradation resulted from a rapid inactivation of BiP by modification after it was no longer required. The model reveals the value of sequestering excess BiP from the active pool, which otherwise impairs protein folding by wasteful degradation. This result underscores the importance of the often-overlooked facet of homeostasis, the deactivation of the response.

As is the case for all advances in our understanding, many more questions arise. What are the enzymes responsible for adding and removing the ADP-ribose? Once we know the enzymes that regulate BiP, it will be important to understand their regulation that must reflect conditions in the ER. How universal is this mechanism? It will be valuable to delineate the scope of cell types and organisms in which BiP-ADP ribosylation occurs. How important is the transcriptional activity of the UPR during normal physiological fluctuations? In light of the quick and acute response afforded by BiP modification, the role of the UPR may need to be recast primarily as a longer-term adaptation process. What are the limits of the response? How much of an increase in unfolded protein load can the pool of latent BiP cope with? What are the physiological consequences of removing the ability for BiP to be ADP ribosylated (i.e., what is the fitness cost of the predicted 10% increase in aggregation and the 25% increase in degradation)? What is the role, if any, of ADP ribosylation in regulating BiP's interaction with the UPR sensor proteins? BiP binds to the ER stress sensors, so ADP-ribosylated BiP may be ideally suited to tune UPR activity. Do inactive pools of other chaperones exist in the ER or other compartments in the cell?

Finally, this work epitomizes the power of multidisciplinary and multiscale approaches to distill functional insight from complex biological systems. It provides an elegant example of a synergistic combination of in vivo, in vitro, and in silico techniques, connecting a descriptive physiological correlate to a molecular mechanism and embedding the interpretation of the results in a formal theoretical framework.

Submitted: 12 July 2012
Accepted: 16 July 2012

References

Bukau, B., J. Weissman, and A. Horwich. 2006. Molecular chaperones and protein quality control. *Cell.* 125:443–451. http://dx.doi.org/10.1016/j.cell.2006.04.014

Carlsson, L., and E. Lazarides. 1983. ADP-ribosylation of the Mr 83,000 stress-inducible and glucose-regulated protein in avian and mammalian cells: Modulation by heat shock and glucose starvation. *Proc. Natl. Acad. Sci. USA.* 80:4664–4668. http://dx.doi.org/10.1073/pnas.80.15.4664

Chambers, J.E., K. Petrova, G. Tomba, M. Vendruscolo, and D. Ron. 2012. ADP ribosylation adapts an ER chaperone response to short-term fluctuations in unfolded protein load. *J. Cell Biol.* 198: 371–385.

Dorner, A.J., L.C. Wasley, and R.J. Kaufman. 1992. Overexpression of GRP78 mitigates stress induction of glucose regulated proteins and blocks secretion of selective proteins in Chinese hamster ovary cells. *EMBO J.* 11:1563–1571.

Gülow, K., D. Bienert, and I.G. Haas. 2002. BiP is feed-back regulated by control of protein translation efficiency. *J. Cell Sci.* 115:2443–2452.

Hendershot, L.M., J. Ting, and A.S. Lee. 1988. Identity of the immunoglobulin heavy-chain-binding protein with the 78,000-dalton glucose-regulated protein and the role of posttranslational modifications in its binding function. *Mol. Cell. Biol.* 8:4250–4256.

Ledford, B.E., and D.F. Jacobs. 1986. Translational control of ADP-ribosylation in eucaryotic cells. *Eur. J. Biochem.* 161:661–667. http://dx.doi.org/10.1111/j.1432-1033.1986.tb10491.x

Leno, G.H., and B.E. Ledford. 1989. ADP-ribosylation of the 78-kDa glucose-regulated protein during nutritional stress. *Eur. J. Biochem.* 186:205–211. http://dx.doi.org/10.1111/j.1432-1033.1989.tb15196.x

Published August 6, 2012

Otero, J.H., B. Lizák, and L.M. Hendershot. 2010. Life and death of a BiP substrate. *Semin. Cell Dev. Biol.* 21:472–478. http://dx.doi.org/10.1016/j.semcdb.2009.12.008

Schlecht, R., A.H. Erbse, B. Bukau, and M.P. Mayer. 2011. Mechanics of Hsp70 chaperones enables differential interaction with client proteins. *Nat. Struct. Mol. Biol.* 18:345–351. http://dx.doi.org/10.1038/nsmb.2006

Sitia, R., and I. Braakman. 2003. Quality control in the endoplasmic reticulum protein factory. *Nature*. 426:891–894. http://dx.doi.org/10.1038/nature02262

Walter, P., and D. Ron. 2011. The unfolded protein response: From stress pathway to homeostatic regulation. *Science*. 334:1081–1086. http://dx.doi.org/10.1126/science.1209038

Appendix B

Reconstitution of Ire1 Oligomerization Dynamics on a Supported Lipid Bilayer

Reconstituting Ire1 Oligomerization Dynamics on a Supported Lipid Bilayer^

David Pincus[1], Benjamin Heineke[1], Hana El-Samad[1], Peter Walter[1,2]

[1] Department of Biochemistry and Biophysics, University of California, San Francisco 94122

[2] Howard Hughes Medical Institute, University of California, San Francisco 94122

^ This work remains in progress. All data included here is preliminary.

Abstract

To transmit information about the folding conditions in the ER to regulate gene expression in the nucleus, the ER-resident sensor protein Ire1 oligomerizes in the plane of the ER membrane in the presence of accumulated unfolded proteins. While Ire1 oligomerization has been observed *in vivo* with fluorescent microscopy and *in vitro* via analytical ultracentrifugation, analysis of quantitative and dynamic properties of Ire1 oligomerization has remained elusive. Here, we report the use of TIRF microscopy to study the behavior of purified, recombinant Ire1 lumenal domain at the single molecule level when incorporated into a supported lipid bilayer. We find that we can observe single particles of Ire1 diffuse in the plane of the bilayer and that particles transiently interact with one another. As a snap-shot, Ire1 predominately distributed between monomers and dimers, with a few higher-order species. The goals are to 1) shift this distribution toward oligomers by adding peptide to mimic unfolded proteins and monitor oligomerization dynamics, and 2) determine the effects the chaperone protein BiP in the distribution of Ire1 and its dynamics.

Figure Legends

Figure 1: Expression, Purification and Labeling of Ire1-bLD

Ire1-bLD is the core lumenal domain of Ire1 (cLD) with the additions of the 50 aa juxtamembrane BiP-binding segment and a 10x-HIS tag at the C-terminus. It was purified as a fusion to maltose binding protein (MBP). After purification by Ni-NTA and Amylose, the MBP domain was cleaved with factor Xa and Ire1 bLD was labeled with Cy3 at C263 (a surface exposes cysteine engineered in place of a serine). A) Coomassie gel is initial purification over Ni-NTA column and elution with imidazole. B) Coomassie and fluorescent scan of protein before and after cleavage with factor Xa.

Figure 2: Construction and Characterization of Supported Lipid Bilayers with Ni-NTA-DOGS

Lipid bilayers were formed in 96-well glass bottom microscope plates. Small unilamellar vesicles (SUVs) were prepared consisting of 94% PC, 5% Ni-NTA-DOGS and 1% 488-DHPE by extruding resuspended, sonicated lipid mixture through a 50 nm pore filter. SUVs were added to helmanex-treated wells, were incubated and washed immediately before imaging. A) Images from a FRAP experiment demonstrating bilayer fluidity. B) Quantification of many FRAP experiments showing consistent fluidity.

Figure 3: Dynamic Ire1 Oligomerization on a Supported Lipid Bilayer

Cy3-labeled Ire1-bLD-HIS was added to bilayers at various concentrations. Between 10-100 pM Ire1 in the solution above the bilayer gave the best single particle tracking. A) Snapshot of single Cy3-Ire1-bLD-HIS particles by TIRF microscopy. B) Quantification of snapshots of Cy3-Ire1-bLD-HIS compared to Cy3-ubiquitin-HIS. Ire1 shows broader distribution suggesting the presence of dimers and higher order species. C) Time series of transient interactions between Ire1 particles. Yellow arrows point to interactions and apparent dimers.

A

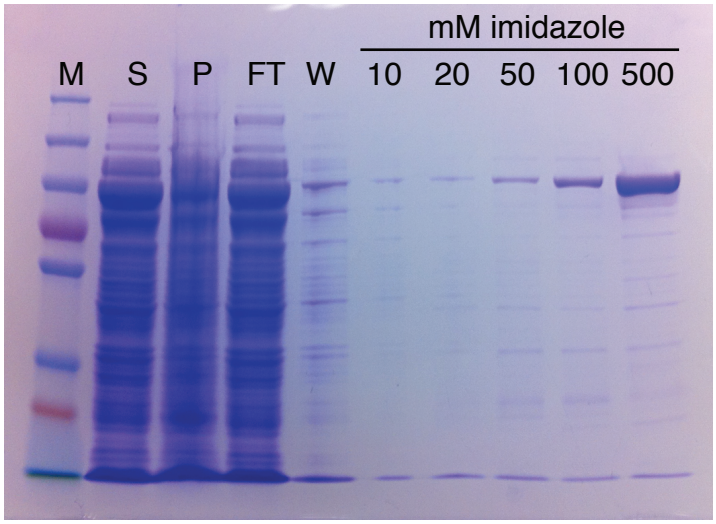

MBP-Ire1-bLD-10xHis

B

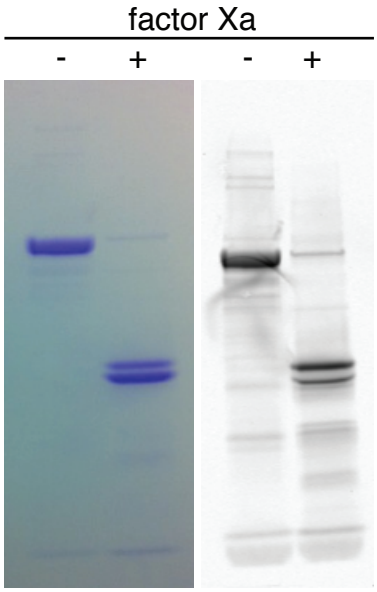

MBP-Ire1-bLD-10xHis

Ire1-bLD-10xHis
MBP

A

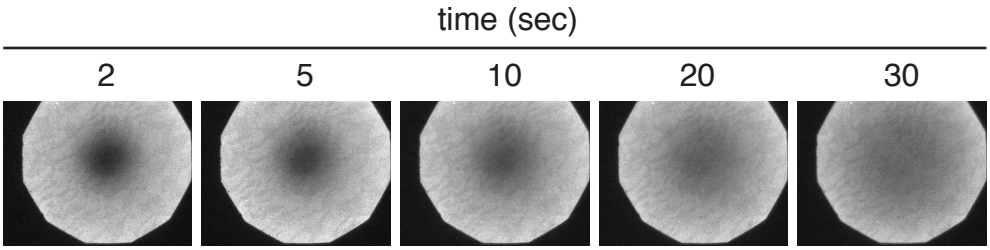
time (sec)
2
5
10
20
30

B

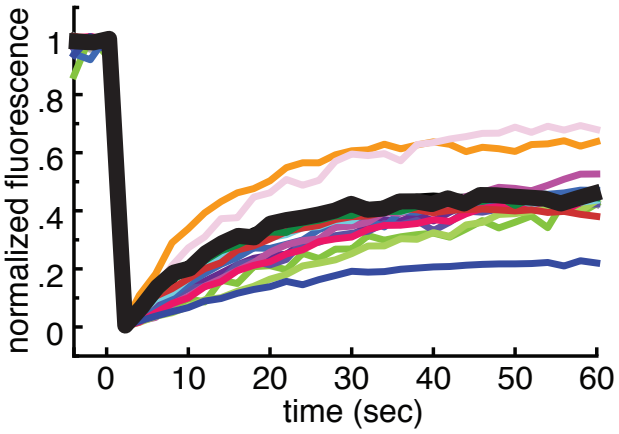
normalized fluorescence
1
.8
.6
.4
.2
0
0
10
20
30
40
50
60
time (sec)

A

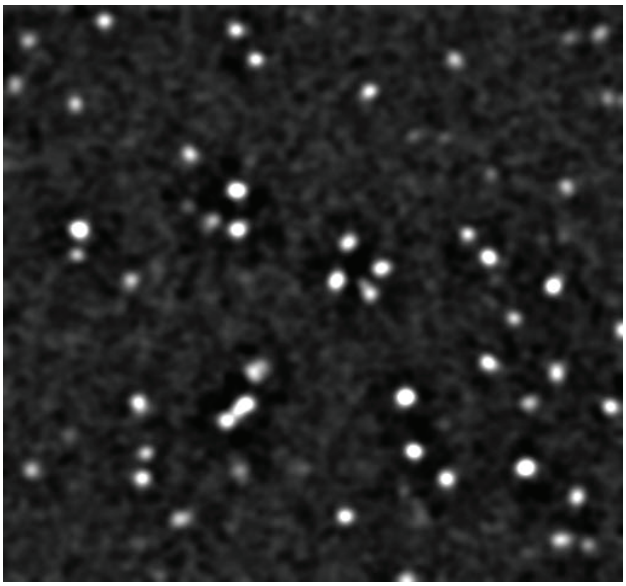

B

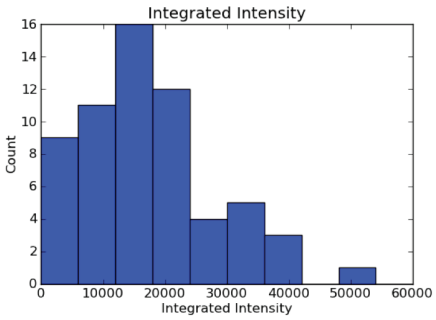
Integrated Intensity
Count
Integrated Intensity
0
2
4
6
8
10
12
14
16
0
10000
20000
30000
40000
50000
60000

C

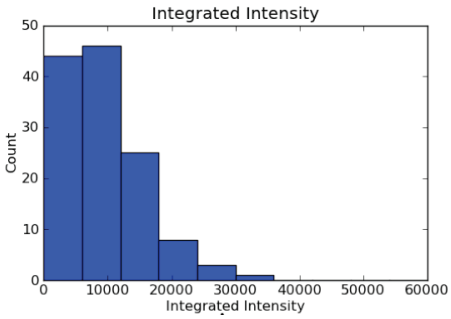
Integrated Intensity
Count
Integrated Intensity
0
10
20
30
40
50
0
10000
20000
30000
40000
50000
60000

D

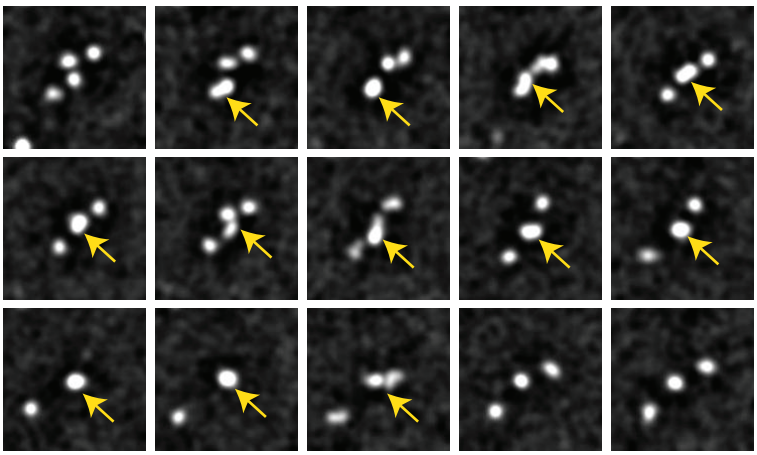

Publishing Agreement

It is the policy of the University to encourage the distribution of all theses, dissertations, and manuscripts. Copies of all UCSF theses, dissertations, and manuscripts will be routed to the library via the Graduate Division. The library will make all theses, dissertations, and manuscripts accessible to the public and will preserve these to the best of their abilities, in perpetuity.

Please sign the following statement:

I hereby grant permission to the Graduate Division of the University of California, San Francisco to release copies of my thesis, dissertation, or manuscript to the Campus Library to provide access and preservation, in whole or in part, in perpetuity.

Author Signature

9/11/2012

Date